

DEVELOPMENT OF EXPLOSIVE-FREE METHOD FOR THE BREAKAGE OF HARD
ROCK USING SOUNDLESS CHEMICAL DEMOLITION AGENTS

By

Kelly-Meriam Habib

Department of Mining and Materials Engineering

McGill University

Montreal, Quebec, Canada

December 2022



A thesis submitted to McGill University in partial fulfillment of the degree of Doctor of
Philosophy

© Copyright (2022)

Table of Contents

Table of Contents	i
List of Figures	v
List of Tables	xi
Abstract.....	xiii
Résumé	xvi
Acknowledgements	xix
Contributions of Authors.....	xxi
List of Abbreviations	xxii
Chapter 1: Introduction	1
1.1 Background.....	1
1.2 Study Problem.....	2
1.3 Scope of Work.....	3
1.4 Research Objectives	3
1.5 Thesis Outline.....	4
Bridging text between manuscripts.....	6
Chapter 2.....	7
Evaluating the application of rock breakage without explosives in underground construction- a critical review of chemical demolition agents	7
Abstract.....	7
2.1 Introduction	8
2.2 Explosive-Free Specialized Methods.....	12
2.2.1 Thermal Fragmentation.....	12
2.2.2 Plasma Blasting Technology	14
2.2.3 Controlled Foam Injection	16
2.2.4 Radial-Axial Splitter	18

2.2.5 Supercritical Carbon Dioxide.....	20
2.3 Soundless Chemical Demolition Agents (SCDAs).....	21
2.3.1 Types of SCDA.....	23
2.4 Challenges Associated with SCDA Application to Underground Construction.....	26
2.5 Conclusions	30
References	32
Bridging text between manuscripts.....	44
Chapter 3.....	45
Methodology for the estimation of expansive cement borehole pressure.....	45
Abstract.....	45
3.1 Introduction	46
3.2 Materials and Methods.....	53
3.2.1 Setup.....	53
3.3 Test Identification.....	54
3.4 Tested configurations	55
3.5 Experimental Results and Discussion.....	56
3.5.1 Effect of Borehole Size.....	56
3.5.2 Effect of host medium rigidity.....	57
3.5.3 Direct Pressure Measurement.....	59
3.6 Finite element model.....	63
3.7 Conclusions	66
References	67
Bridging text between manuscripts.....	67
Chapter 4.....	71
Laboratory investigation into the use of soundless chemical demolitions agents for the breakage of hard rock.....	72

Abstract.....	72
4.1 Introduction	73
4.2 Experimental Program	76
4.3 Results and Discussion.....	78
4.3.1 Rock Characterization.....	78
4.3.2 The influence of borehole size on granite.....	79
4.3.3 Effect of SCDA on rock breakage under load.....	87
4.4 Conclusions	95
References	96
Chapter 5: Effectiveness of Soundless Chemical Demolition Agents for rock breakage under uniaxial loading condition.....	98
5.1 Introduction	98
5.2 Single SCDA hole under uniaxial condition.....	100
5.2.1 Data	100
5.2.2 XFEM Model.....	103
5.2.3 Modeling Results: Single SCDA Hole	106
5.3 Hole Shielding.....	108
5.3.1 Experimental Program	108
5.3.2 Experimental Results and Discussion	110
5.3.3 XFEM Model.....	113
5.3.4 Numerical Modeling Results	114
5.4 Estimation of SCDA Hole Spacing.....	115
5.5 Conclusions	118
Chapter 6: The influence of different environmental conditions on SCDA	120
6.1 Introduction	120
6.2 Experimental Program	121

6.3 Results and Discussion.....	123
6.3.1 Effect of cold temperature	125
6.3.2 Effect of hot conditions	128
6.3.3 Effect of humid conditions	132
6.4 Conclusions	136
Chapter 7: Field Applications	138
7.1 Introduction	138
7.2 Experimental Program	139
7.2.1 Hoyle Pond Mine Site (Surface).....	139
7.2.2 Éléonore Mine Site (Underground).....	140
7.2.3 Loading of SCDA.....	144
7.2.4 Monitoring Tools	145
7.3 Results and Discussion.....	146
7.3.1 Boulder Test at Hoyle Pond	146
7.3.2 Boulder Test at Éléonore.....	148
7.3.3 Slash Test #1 at Éléonore.....	149
7.3.4 Slash Test #2 at Éléonore.....	150
7.4 Summary of Test Results.....	153
7.5 Conclusions	153
Chapter 8: Conclusions.....	155
8.1 Research Summary	155
8.2 Research Conclusions	165
8.3 Contribution to original knowledge	166
References.....	168

List of Figures

Chapter 2

Figure 2.1 Typical Drill and Blast Cycle	10
Figure 2.2 Thermal fragmentation machinery, (a) Nippon Dragon Machine; (b) Mounted drill of the thermal fragmentation method (reprinted from (Poirier et al., 2003)).....	13
Figure 2.3 Components of the plasma blasting method (reprinted from [18]).	15
Figure 2.4 Controlled Foam Injection Components (reprinted from (Pickering & Young, 2017))	17
Figure 2.5 Radial-axial splitter (adapted from Paraszczak & Planeta, 2003).....	19
Figure 2.6 Soundless chemical demolition agents. (a) Fracture propagation around a pressurized borehole (adapted from Harada et al. 1989). (b) Broken rock with the use of SCDA (reprinted from Betonamit).....	22
Figure 2.7 Proposed continuous, drill, and SCDA cycle for tunnel face advance.....	29

Chapter 3

Figure 3.1 Sphere model for expansive pressure of calcium hydroxide. a) free lime b) critical degree of hydration, c) restrained and unrestrained conditions of calcium hydroxide crystals (Bentur & Shalom, 1974; De Silva et al., 2016).....	46
Figure 3.2 Fractural propagation in a borehole [modified after 4].	47
Figure 3.3 Steel cylinder configurations tested in this research	55
Figure 3.4 Expansive pressure of expansive cement with varying borehole size and constant rigidity (R)	57

Figure 3.5 Expansive pressure evolution for varying host medium rigidity and a constant borehole size 38.1 mm (1.5").....	58
Figure 3.6 Direct pressure measurement in specimen S-C-150-275-S with (a) Side view of XPM6-1KBG Miniature Pressure Sensor (b) Top view of XPM6-1KBG miniature pressure sensor threaded into wall cylinder (c) Expansive cement filled cylinder with embedded temperature...	60
Figure 3.7 Measured Expansive Pressure of varying borehole size	61
Figure 3.8 Expansive Cement heat of hydration with time of varying borehole size.....	62
Figure 3.9 Measured peak pressure (Pa) vs. calculated peak pressure (Pc)	62
Figure 3.10 Model of axisymmetric steel cylinder (a) Geometry (b) Out-of-plane strain with scaled deformations	64
Figure 3.11 Iterative procedure to determine SCDA modulus of elasticity of expansive cement at peak pressure.....	65

Chapter 4

Figure 4.1 Location of strain gauges.....	76
Figure 4.2 Test set-up for loaded specimens a) 200-tonne uniaxial compressive rig b) greased top surface of rock specimen c) metal loading plate placed on rock specimen	77
Figure 4.2 Brazilian test set-up on Stanstead granite core.....	78
Figure 4.4 Slab G-SL1-100-500-M-01 a) At time t_0 b) Initial breakage at time t_{18} c) Complete breakage at time t_{24}	80
Figure 4.5 G-SL1-100-500-M-02 a) At time t_0 b) Initial breakage at t_{15} c) Complete breakage at t_{21}	81
Figure 4.6 G-SL1-100-500-M-03 a) At time t_0 b) Initial breakage at t_{23} c) Complete breakage at t_{27}	81

Figure 4.7 Measured strains in specimen G-SL1-100-500-M-02.....	82
Figure 4.8 Measured strains in specimen G-SL1-100-500-M-03.....	82
Figure 4.9 G-SL2-125-625-M-01 a) At time t_0 b) Initial breakage at $t_{11.5}$ c) Complete breakage at t_{17}	83
Figure 4.10 G-SL2-125-625-M-02 a) At time t_0 b) Initial breakage at t_{16} c) Complete breakage at t_{20}	83
Figure 4.11 Measured strains in specimen G-SL2-125-625-M-01	84
Figure 4.12 Measured strains in G-SL2-125-625-M-02.....	84
Figure 4.13 G-SL2-150-600-M-01 a) At time t_0 b) Initial breakage $t_{7.5}$ c) Complete breakage t_{10}	85
Figure 4.14 G-SL2-150-600-M-02 a) At time t_0 b) Initial breakage t_{11} c) Complete breakage at t_{13}	85
Figure 4.15 Measured strains of specimen G-SL2-150-600-M-01.....	86
Figure 4.16 Measured strains in specimen G-SL2-150-600-M-02.....	86
Figure 4.17 G-SL2-150-600-UT-L a) At time t_0 b) TFC at t_7 C) Breakage at $t_{7.5}$ d) Complete breakage at t_{10}	89
Figure 4.18 Measured strains in specimen G-SL2-175-700-M-L	90
Figure 4.19 G-SL2-175-700-M-L a) At time t_0 b) Initial breakage $t_{6.8}$ c) Breakage at t_9 d) Complete breakage $t_{9.73}$	91
Figure 4.20 Measured strains in specimen G-SL2-175-700-M-L	92
Figure 4.21 G-SL2-175-700-LT-L a) At time t_0 b) Initial breakage c) Breakage at t_7 at d) Complete breakage at t_{12}	92
Figure 4.22 Measured strains in specimen G-SL2-175-700-LT-L	93

Chapter 5

Figure 5.1 Specimen configuration with strain gauge locations for a single SCDA-injected hole subjected to uniaxial loading	101
Figure 5.2 Fracturing of tested specimen under 5 MPa load.	102
Figure 5.3 Measured SCDA-induced strains (Refer to Figure 5.1 for strain gauge location)	103
Figure 5.4 Model loading steps and boundary conditions	106
Figure 5.5 Model of specimen G-SL2-175-700-M.....	107
Figure 5.6 Experimental setup for hole shielding experiment.....	109
Figure 5.7 Complete Breakage of specimens a) G-SL2-100-400-M-L b) G-SL2-SH-1.5-1D c) G-SL2-SH-2.0-1D.....	111
Figure 5.8 Specimen G-SL1-100-400-M-01,02 measured strain	112
Figure 5.9 Specimen G-SL2-HS-1.5-1D-01,02 measured strain.....	112
Figure 5.10 Specimen G-SL2-HS-2-1D-01,02 measured strain.....	113
Figure 5.11 XFEM model for hole shielding test	114
Figure 5.12 Typical XFEM model results	117

Chapter 6

Figure 6.1 Microclimate benchtop chamber (Model #: MCB (H)-1.2).....	121
Figure 6.2 Strain gauge configurations.....	122
Figure 6.3 G-C-150-600-25-30 a) t_0 b) TFC at $t_{4.5}$ c) MDT at $t_{5.5}$	124
Figure 6.4 Measured strains and SCDA heat of hydration of specimen G-C-150-600-25-30 ...	125
Figure 6.5 Sample G-C-150-600-(-5)-30 a) t_0 b) TFC at t_{39} c) MDT at t_{45}	126
Figure 6.6 Measured strains and SCDA heat of hydration of specimen G-C-150-600-(-5)-30 .	126

Figure 6.7 G-C-150-600-(5)-30 a) t_0 b) TFC at t_{18} c) MDT at t_{22}	127
Figure 6.8 Measured strains and SCDA heat of hydration of specimen G-C-150-600-(5)-30....	127
Figure 6.9 G-C-150-600-(5)-30 a) t_0 b) TFC at t_{14} c) MDT at t_{18}	128
Figure 6.10 Measured strains and SCDA heat of hydration of specimen G-C-150-600-(5)-30.	128
Figure 6.11 G-C-150-600-(20)-30 a) t_0 b) TFC at $t_{6.75}$ c) MDT at $t_{7.25}$	129
Figure 6.12 Measured strains and SCDA heat of hydration of specimen G-C-150-600-(20)-30	129
Figure 6.13 G-C-150-600-(20)-30 a) t_0 b) TFC at t_3 c) MDT at $t_{3.5}$	130
Figure 6.14 Measured strains and SCDA heat of hydration of specimen G-C-150-600-(30)-30	130
Figure 6.15 G-C-150-600-(40)-30 a) t_0 b) TFC at $t_{0.7}$ c) MDT at $t_{1.7}$	131
Figure 6.16 Measured strains and SCDA heat of hydration of specimen G-C-150-600-(40)-30	131
Figure 6.17 G-C-150-600-(35)-30 a) t_0 b) TFC at $t_{1.5}$ c) MDT at t_2	132
Figure 6.18 Measured strains and SCDA heat of hydration of specimen G-C-150-600-(35)-30.	133
Figure 6.19 G-C-150-600-(35)-30 a) t_0 b) TFC at $t_{1.5}$ c) MDT at $t_{2.5}$	133
Figure 6.20 Measured strains and SCDA heat of hydration of specimen G-C-150-600-(35)-70	134
Figure 6.21 G-C-150-600-(35)-90 a) t_0 b) TFC at $t_{1.5}$ c) Time of Complete Fracturing t_2	134
Figure 6.22 Measured strains and SCDA heat of hydration of specimen G-C-150-600-(35)-90	135
Figure 6.23 Summary TFC and MDT in different ambient conditions	136

Chapter 7

Figure 7.1 Greywacke boulder tested at Hoyle Pond mine site	139
Figure 7.2 Rock Temperature Greywacke boulder at Hoyle Pond	140
Figure 7.3 Plan view of Level 530 with locations of test performed at Éléonore Mine Site.....	140

Figure 7.4 Wacke Boulder Test at Éléonore.....	141
Figure 7.5 Rock Temperature of Boulder at Éléonore.....	141
Figure 7.6 Slash Test #1 at Éléonore Mine Site.....	143
Figure 7.7 Rock temperature of Slash #1.....	143
Figure 7.8 Slash Test #2 at Éléonore Mine Site.....	144
Figure 7.9 Rock Temperature of Slash #2	144
Figure 7.10 Plastic Cartridge used for horizontal loading of slash tests.....	145
Figure 7.11 Fragmented Boulder at Hoyle Pond	146
Figure 7.12 Fragmented Boulder with forklift at Hoyle Pond.....	147
Figure 7.13 SCDA Temperature of SCDA for boulder test at Hoyle Pond.....	147
Figure 7.14 Fragmented Boulder at Éléonore.....	148
Figure 7.15 SCDA Temperature of SCDA for boulder test at Hoyle Pond.....	149
Figure 7.16 Minimal cracking around bottom left hole of Slash #1	150
Figure 7.17 Loaded Holes of Slash #2.....	150
Figure 7.18 Cracking Coalescing between SCDA holes of Slash #2	151
Figure 7.19 SCDA Temperature of SCDA for Slash #2.....	151
Figure 7.20 Front View of Slash #2.....	151

List of Tables

Chapter 3

Table 3.1 Reported expansive pressure of different commercially available expansive cement (Betonamit, n.d; Bristar, n.d; Dexpan, n.d; Expando,n.d; Ecobust, n.d).	49
Table 3.3 Abbreviations for test identification.	56
Table 3.3 Summary of tested steel cylinder configurations.....	56
Table 3.4 Material Properties for the FE model	64
Table 3.5 The modulus elasticity of expansive cement with varying borehole size.....	65

Chapter 4

Table 4.1 Description of tested specimens	78
Table 4.2 Summary of test results under no load.....	87
Table 4.3 Summary of L_f/Φ	94

Chapter 5

Table 5.1 Description of tested specimens (extracted from Chapter 4).....	101
Table 5.2 Material, interface, and crack properties	105
Table 5.3 Critical Strain of specimens (extracted from Figure 3)	107
Table 5.4 SCDA pressure at Crack Initiation and Complete Breakage	108
Table 5.5 Description of tested specimens for hole shielding	110
Table 5.6 Summary of test results for Hole Shielding.....	111
Table 5.7 Critical Strain of specimens (extracted from Figure 5.8-10).....	114
Table 5.8 SCDA Pressure at Crack Initiation and Complete Breakage.....	115
Table 5.9 Summary of initialized stress in SCDA and length of fracture	116

Chapter 6

Table 6.1 Description of tested specimen 123
Table 6.2 Summary of Test Results 135

Chapter 7

Table 7.1 Summary conditions for each test..... 145
Table 7.2 Summary of test results..... 145

Abstract

Drilling and blasting with explosives is a widely used technique for rock fragmentation in the mining industry for mine development and ore production. However, the use of explosives is associated with rigorous safety and environmental constraints as blasting generates greenhouse gas emissions, ground vibrations and dust. As a result, interest in developing explosive-free technologies as safer alternatives for rock fragmentation in underground mines has emerged. This thesis focuses on Soundless Chemical Demolitions Agents (SCDA) as an environmentally friendly method for rock breakage and a potential replacement of explosives. SCDA, also commonly known as expansive cement, are cementitious powdery substances with quicklime (CaO) as a primary ingredient that expands during the moist curing process which results in high expansive pressure if this hydration reaction happens in a confined condition such as in a borehole. SCDA are commercially available and are being used for block splitting in dimension stone quarries and rehabilitation projects for the demolition of concrete foundations. Although, expansive cement has been on the market for 30 years, it has not been implemented in underground hard rock mines. This is primarily due to the presence of high in-situ stress which would highly limit the initiation and propagation of rock fractures.

This thesis is part of a multi-phase project which aims to develop a sound methodology for rock fragmentation in underground mines. More specifically, it is the first phase of the project which focuses on laboratory tests to investigate and optimize the mechanical performance of SCDA in various conditions. A comprehensive state-of-the-art critical review is first conducted to situate the importance and feasibility of SCDA with respect to other explosive-free rock breakage technologies which include thermal fragmentation, plasma blasting, controlled foam injection,

radial-axial splitter, and supercritical carbon dioxide. The merits and limitations of each technology are discussed in detail to emphasize the potential of using SCDA as an alternative to blasting with explosives in underground excavation applications. Following the literature review, a series of laboratory tests was conducted on thick-walled steel cylinders filled SCDA to quantify its expansive pressure. Various steel configurations were built to examine expansive pressure variation with borehole size and radial rigidities of the host medium. An axisymmetric finite element model was developed and validated with the steel cylinder experimental results, then used to discern the evolution of elastic modulus of the SCDA with time. A second series of experiments was conducted on prismatic blocks of Stanstead granite with a central horizontal borehole. The blocks are 152.4 mm (6'') wide x 406.44 mm (16'') high x 203.2 mm (8'') thick. The first set investigates the effect of SCDA on breakage of granite under no load. The influence of borehole size on the time to fracturing with SCDA for borehole sizes of 25.4 mm (1''), 31.75 mm (1.25''), and 38.1 mm (1.5'') is examined. The second set investigates the effect of confinement by applying a uniaxial stress of 5 MPa to the block whereby the time to and length of fracture was monitored. Based on test results, a suitable borehole spacing-to-diameter ratio is suggested to ensure block fracturing for practical applications. An Extended Finite Element Method (XFEM) in Abaqus was used to build a numerical model to validate the suggested spacing between SCDA holes under uniaxial conditions. These results should serve as a basis for hole pattern design for applications involving uniaxial compression. Additional tests were then conducted on granite Stanstead specimens to study the effect of shielding a single SCDA hole with relief holes under the uniaxial compression. The experimental results were validated with XFEM model. The tests show that shield holes around the SCDA hole do not improve the time nor the length of fracturing.

The effect of ambient conditions on the performance of SCDA is then investigated in the laboratory using a Microclimate benchtop test chamber (Model #: MCB(H)-1.2). Granite specimens of 152.4 mm x 152.4 mm x 203.2mm (6'' x 6'' x 8'') with a single 38.1 mm (1.5'') SCDA hole were placed in the chamber and subjected to various humidity levels (30%, 70%, 90%), hot conditions (30°C, 40°C) and cold conditions (-5°C, 5°C, 20°C) to simulate a range of possible conditions in underground mines. The study shows that temperature plays a key role on the heat of hydration of SCDA as well as the time of fracture. Finally, field tests were conducted at two mine sites: Hoyle Pond and Éléonore mine site. The goal of these tests was to assess SCDA effectiveness in real mining applications. The first set of tests included the fragmentation of large boulders while the second set involved excavation intersections (slashing).

Résumé

Le forage et le dynamitage avec des explosifs est une technique largement utilisée pour la fragmentation de la roche dans l'industrie minière pour le développement minier et la production de minerai. Pourtant, l'utilisation d'explosifs est associée à des risques sécuritaires et contraintes environnementales rigoureuses tel que le dynamitage génère des émissions de gaz à effet de serre, des vibrations du sol et de la poussière. En conséquence, l'intérêt pour le développement de technologies sans explosifs comme alternatives a augmenté pour la fragmentation de la roche dans les mines souterraines. Cette thèse se concentre sur les agents de démolitions chimique silencieux (SCDA) en tant que méthode sûre de l'environnement pour la fragmentation de roche et un remplacement potentiel des explosifs. Les SCDA également connus sous le nom de ciment expansif sont des substances pulvérulentes cimentaires avec la chaux vive (oxyde de calcium ou CaO) comme ingrédient principal qui se dilate pendant le processus de durcissement humide ce qui entraîne une pression expansive élevée si cette réaction d'hydratation se produit dans un état confiné comme e.g. trou de forage. Les SCDA sont disponibles dans le commerce et sont utilisés pour la fragmentation de roche dans les carrières de pierre de taille et les projets de réhabilitation pour la démolition des fondations en béton. Malgré que le ciment expansif ait été mis en œuvre dans les mines souterraines de roche dure. Cela est principalement dû à la présence de fortes contraintes in-situ qui limiteraient fortement l'initiation et la propagation des fractures de la roche. Cette thèse fait partie d'un projet en plus phases qui vise à développer une méthodologie solide pour la fragmentation des roches dans les mines souterraines. Plus précisément, il s'agit de la première phase du projet qui se concentre sur des essais en laboratoire pour étudier et optimiser les performances mécaniques du SCDA dans diverses conditions. Une revue de littérature complet

de l'état de l'art est d'abord effectuée pour situer l'importance et la faisabilité de la SCDA par rapport à d'autres technologies de rupture de roche sans explosifs notamment la fragmentation thermique, le sablage au plasma, l'injection de mousse contrôlée, le séparateur radial-axial et dioxyde de carbon supercritique. Les mérites et les limites de chaque technologie sont discutés en détail pour souligner le potentiel de l'utilisation de SCDA comme alternative au dynamitage avec des explosifs dans les applications d'excavation souterraine. Pour donner suite à la revue de la littérature, une série d'essais en laboratoire a été menée sur des cylindres en acier à paroi épaisse remplis de SCDA pour quantifier la pression expansive. Diverses configurations en acier ont été construites pour examiner la pression expansive avec la taille de trou de forage et les rigidités radiales du milieu hôte. Un modèle d'éléments finis axisymétrique a été développé et validé avec les résultats expérimentaux du cylindre en acier, puis utilisé pour discerner l'évolution du module d'élasticité du SCDA avec le temps. Une deuxième série de tests a été réalisée sur des blocs prismatiques de granite de *Stanstead* avec un trou de forage centrale. Les blocs mesurent 152.4 mm de large x 404.44 mm de haut x 203.2 mm d'épaisseur. La première série étudie l'effet du SCDA sur la rupture du granite sans charge. L'influence de la taille du trou de forage sur le temps de fragmentation avec SCDA pour les tailles de trous de forage de 25,4 mm (1"), 31,75 mm (1,25") et 38,1 mm (1,5") sont examinées. Le deuxième ensemble étudie l'effet du confinement en appliquant une contrainte uniaxiale de 5 MPa au bloc, le temps et la longueur de la fracture étant surveillés. Sur la base des résultats des tests, un rapport espacement/diamètre du trou de forage approprié est suggéré pour assurer la fracturation en blocs pour les applications pratiques. Une méthode étendue des éléments finis (XFEM) dans Abaqus a été utilisée pour construire un modèle numérique afin de valider l'espacement suggéré entre les trous SCDA dans des conditions uniaxiales. Ces résultats devraient servir de base à la conception du modèle de trous pour les

applications impliquant une compression uniaxiale. Des tests supplémentaires ont ensuite été effectués sur des spécimens de granit de Stanstead pour étudier l'effet de blindage d'un seul trou SCDA avec des trous de décharge sous la compression uniaxiale. Les résultats expérimentaux ont été validés avec le modèle XFEM. Les tests montrent que les trous de blindage autour du trou SCDA n'améliorent pas le temps ni la durée de fracturation. L'effet des conditions ambiantes sur les performances du SCDA est ensuite étudié en laboratoire à l'aide d'une chambre d'essai de paillasse Microclimate (Modèle # : MCB(H)-1.2) Cubes de granit de 152.4 mm x 152.4 mm x 203.2mm (6'' x 6'' x 8'') avec un seul trou SCDA de 38,1 mm (1,5") ont été placés dans la chambre et soumis à divers niveaux d'humidité (30 %, 90 %), des conditions chaudes (30 °C, 40 °C) et des conditions froides (-5°C, 5 °C, 10 °C) pour simuler une gamme de conditions possibles dans mines souterraines. L'étude montre que la température joue un rôle clé sur la chaleur d'hydratation des SCDA ainsi que sur le temps de rupture. Enfin, un essai sur le terrain a été effectué sur un site minier au cours duquel un gros bloc de Graywacke a été fragmenté avec du SCDA en utilisant le rapport suggéré entre l'espacement des trous de forage et le diamètre. Le bloc a été testé à une température ambiante de 8-10°C. Enfin, des essais sur le terrain ont été effectués sur deux sites miniers : Hoyle Pond et Éléonore. L'objectif de ces tests est d'évaluer l'efficacité du SCDA dans des applications minières réelles. La première série de tests comprenait la fragmentation de gros rochers avec une série de trous SCDA tandis que la deuxième série de tests impliquait l'excavation d'intersection (entaille ou slash).

Acknowledgements

I would like to thank first and foremost my supervisor Professor Hani Mitri. Thank you for your constant support, guidance, and technical advice for these past few years. I am grateful for your dedication and patience with our project ensuring there was continuous progress. I would also like to thank you for giving me opportunities to present at conferences and allow me to grow my confidence with public speaking. I have learned great lessons of perseverance, patience, and good work ethics. I would also like to highlight your great leadership during the pandemic.

This thesis is dedicated to my dad, Dr. Magdi Habib. You have always been an inspiration to me, and I always hoped to earn a Ph.D. like you and a long-standing career in mining. Thank you for being my support and motivation to keep me going. I would also like to dedicate this thesis to my late mother, Mona Morcos, whom I hope I've made proud. Many thanks brother, Kevin Habib, for his support by making sure I had a comfortable lifestyle during my Ph.D. I also extend my thanks to my family members and friends for their support.

I would also like to give a big thanks to Dr. Isaac Vennes for his technical advice and friendship. I am thankful for your thorough technical advice, helping me with the lab work and teaching me numerical modeling in Abaqus with patience

I would like to thank my colleagues Dr. Shahe, Shnorhokian, Tuo Chen, and Yizhuo Li who have made these 3.5 years a great experience. I am thankful for their team efforts, work ethics, support during this project.

I would like to thank Ramnarine Harihar and Andreas Hofmann from the Faculty of Engineering Machine Shop for their excellent machining work for my lab investigation. I would like to extend

my thanks to John Bartczak, from the Department of Civil Engineering, for giving me access to his equipment when needed.

Finally, I would like to thank the Clean Growth program of Natural Resources Canada, Newmont Corporation and the Ministry of Economy and Innovation, Quebec, for their financial support.

Contributions of Authors

The author of this thesis is the primary author of all manuscripts. She was responsible for the conceptualization, methodology, analysis, and the production of the first draft.

Chapter 2:

Habib, K. M., Shnorhokian, S., Mitri, H. (2022). Evaluating the Application of Rock Breakage without Explosives in Underground Construction - A Critical Review of Chemical Demolition Agents. *Minerals*, 12(2), 220, 1-17.

Chapter 3:

Habib, K. M., Vennes, I., Mitri, H. (2022) Methodology for the estimation of expansive cement borehole pressure. *International Journal of Minin Science and Technology*. In press.

Chapter 4:

Habib, K. M., Vennes, I., Mitri, H. (2022) Laboratory investigation into the use of soundless chemical demolitions agents for the breakage of hard rock. *International Journal of Coal Science and Technology*, 9(1), 1-10.

List of Abbreviations

SCDA:	Soundless Chemical Demolition Agents
RASP:	Radial-Axial Splitter
DB:	Drill and Blast
XFEM:	Extended Finite Element Method
FE:	Finite Element
TFC:	Time of First Crack
MDT:	Minimum Demolition Time
TBM:	Tunnel Boring Machine
PBT:	Plasma Blasting Technology
CFI:	Controlled Foam Injection
OEM:	Original Equipment Manufacturer
NEEM:	Non-explosive expansive materials
ASTM:	American Society for Testing and Materials
PFC3D:	Particle Flow Code in 3 Dimensions
FLAC3D:	Fast Lagrangian Analysis of Continua in 3 Dimensions
UESM:	Upper End Surface Method
E:	Young's Modulus
LE33:	Tangential Strain
ANFO:	Ammonium Nitrate Fuel Oil
OPC:	Ordinary Portland Cement
S:	Spacing
G:	Shear Modulus
U:	Displacement
DAQ:	Data Acquisition System
Φ :	Hole Diameter
L _F :	Entire Length of Fracture
L _f :	Length of Fracture

SG:	Strain Gauge
I.D:	Inner Diameter
O.D:	Outer Diameter
r_i :	Inner radius
r_o :	Outer Radius

Chapter 1: Introduction

1.1 Background

The method of drilling and blasting with explosives is widely used in rock fragmentation applications in mining and civil industries for mine development, mining production, and underground construction such as tunnels and shafts. However, the use of explosives is associated with rigorous safety and environmental constraints as blasting creates toxic fumes, ground vibrations and dust. Due to these factors, there is a growing interest in transitioning from explosives-based rock fragmentation to methods without explosives, e.g., with Soundless, Explosive-Free Chemical Demolitions Agents (SCDA) – the focus of this study. SCDA are cementitious powdery substances with quicklime (CaO) as primary ingredient that expands during the moist curing process which results in high expansive pressure, if this CaO hydration reaction occurs in a confined condition. More specifically, this method of rock fragmentation works by means of injecting the SCDA into one or more boreholes drilled into the rock. The resulting crystallization pressure generated by the production of calcium hydroxide crystals creates an effective fracture network in the confined rock around the borehole. The use of SCDA as an explosive-free method has great potential considering the need for non-violent and pollution-free methods for breaking rocks. Presently, SCDA are used for rock fracturing in urban areas, rehabilitation projects, reinforced concrete cutting, granite and marble quarrying and surface excavation. However, SCDA have never been attempted in underground mines to break hard rock. Due to the negative impact of blasting in mining operations, there is a great importance in developing a safe method such as the use of SCDA, to fracture rock in underground mines when blasting is not the most desirable route for fracturing.

1.2 Study Problem

The technology of SCDA was developed more than 30 years ago but only came to commercial use 10-15 years later for the splitting of rock blocks in dimension stone quarries or breaking concrete foundations in demolition projects. Currently, SCDA are only being used to fracture rocks for surface applications and have never been attempted to break hard rock under high in-situ stress condition such as in an underground mine. An interest is drawn towards the use of SCDA in underground mines to mitigate the risks of explosives, predominantly the generation of toxic fumes. In current blasting practices, small amounts of noxious gases such as nitric oxide (NO), carbon monoxide (CO), NH₄ (ammonia), CH₄ (methane) and solid carbon resulting from non-ideal detonation, are generated (SME Handbook, 2011). With that, the use of explosives requires additional ventilation to exhaust the blast-induced fumes after each blast to dilute the toxic fumes released to the environment. Besides the negative impact on the environment, the use of explosives includes safety issues such as the risks of fly rock, ground vibration and air blast. The development of explosives-free rock excavation is of interest to eliminate the safety risks and environmental impacts associated with blasting.

The study problem in developing such technology lies in that SCDA have never been attempted before as a method of excavation in underground mines and tunnels. There are 3 reasons for this. Firstly, rock is much stronger than concrete. Secondly, if SCDA are to be attempted in an underground environment, the host rock around a borehole would exert confinement pressure on the borehole preventing it from fracturing. The third reason is that the curing time is too long for an active mining operation. A sound methodology is required to overcome the above challenges to implement SCDA in underground mines to break hard rock.

1.3 Scope of Work

The scope of this research is focused on the development of an explosives-free technology using Soundless Chemical Demolition Agents (SCDA) to break hard rock in underground mines. A comprehensive laboratory investigation is conducted to investigate the ability of SCDA to break hard rock and generate enough borehole pressure in a shorter time. Laboratory work on the SCDA mechanical performance is performed to assess its feasibility on a large scale.

1.4 Research Objectives

The long-term objective of this research program is to validate an explosives-free method for large-scale hard rock fragmentation in underground mines using sound chemical demolition agents and innovative drilling patterns. This study being the first phase of the research has the following objectives.

- a) Conduct a state-of-the art review of explosive-free rock breakage methods
- b) Investigate SCDA Performance in hard rock
- c) Investigate the influence of ambient conditions on SCDA
- d) Demonstrate SCDA applications in the field

The abovementioned objectives have led to the following questions to be addressed in this study

- 1) How much is the peak SCDA pressure in thick-walled cylinder test?
- 2) What is the influence of hole diameter and host medium rigidity?
- 3) What is the peak stiffness of SCDA material?
- 4) When does fracturing initiate and terminate?
- 5) What is the performance of SCDA under uniaxial loading conditions?
- 6) How long can the fracture be?

7) What is the optimal between SCDA holes?

1.5 Thesis Outline

The thesis is divided into eight chapters as follows. Chapter 1 provides an overview of the thesis research along with its background, scope of work and objectives. Chapter 2 presents a critical review of various methods that have been so far developed for rock fragmentation without explosives which include Thermal Fragmentation, Plasma Blasting, Controlled Foam Injection, Radial-Axial splitter, and liquid carbon dioxide. The method of Soundless Chemical Demolition Agents (SCDA) is evaluated in detail and its merits over other methods are highlighted as a potential alternative to blasting with explosives in underground excavation applications. Chapter 3 reports the results of laboratory tests conducted on thick-walled cylinders filled with expansive cement to estimate the expansive pressure and its variation with borehole diameter and radial rigidity of the host medium. Chapter 4 reports the results of a series of experimental tests to identify the effect of SCDA on hard rock breakage under no load and under uniaxial loading conditions. A borehole spacing to borehole diameter ratio is suggested for practical applications. Chapter 5 focuses on using Abaqus software to build and calibrate an Extended Finite Element Method (XFEM) model based on the experimental results obtained from investigating the effect of SCDA under uniaxial loading conditions. Based on the numerical results a borehole spacing is suggested for practical applications involving rock structures subjected to uniaxial loading such as pillars and excavation intersections. The application is known as “slashing”. Chapter 6 investigates the effect of different ambient conditions such as high humidity and low and high temperatures on SCDA. Small granite cubes with central SCDA holes are subjected to different environmental conditions using a controlled test chamber to simulate possible conditions encountered in underground mines. In Chapter 7, 4 field tests conducted at Hoyle Pond mine and Éléonore mine are presented. The

first set of tests included the fragmentation of large boulders while the second set involved excavation intersections (slashing). Chapter 8 concludes the research and recommends future studies to pursue for the implementation of SCDA into practice.

Bridging text between manuscripts

The following chapter reports an extensive literature review of various specialized explosive-free methods for the breakage of hard rock. These include thermal fragmentation, plasma blasting technology, controlled foam injection, radial-axial splitters, and supercritical carbon dioxide. A description of each method is given while highlighting its merits and limitations. More focus is then dedicated to the SCDA method to assess its potential use in underground excavations such as in underground mines while comparing it to typical drill blast cycle. To do so, a thorough review is conducted on the early and current research on SCDA to address the knowledge gaps for potential implementation for usage in mining applications. While numerous studies focus on characterizing and optimizing the performance of SCDA for subsurface applications, there is still a lack of research on its performance under confining stresses – the condition prevailing in underground mines. A systematic methodology is carried out throughout the thesis to validate SCDA an explosive-free method for large scale hard rock fragmentation while also using the classical methods used in previous research to characterize the performance of SCDA. Further research objectives are then set to further validate the use of SCDA for underground mining applications.

The following chapter is a published paper in the journal *Minerals* 2022, 12, 220 (17pp).

Chapter 2

Evaluating the application of rock breakage without explosives in underground construction- a critical review of chemical demolition agents

Abstract

The method of drilling and blasting with explosives is widely used in rock fragmentation applications in underground construction projects, such as tunnels and caverns. However, the use of explosives is associated with rigorous safety and environmental constraints, since blasting creates toxic fumes, ground vibrations, and dust. Because of these constraints, there has been a growing interest in transitioning away from explosives-based rock fragmentation. The use of explosives-free methods could lead to continuous operation by eliminating the need for idle time with additional ventilation required to exhaust the blast fumes. This paper first presents a critical review of various methods that have been developed so far for rock fragmentation without explosives. Such methods include thermal fragmentation, plasma blasting, controlled foam injection, radial-axial splitter, and supercritical carbon dioxide. Thermal fragmentation, as the name implies, uses high heat to spall high-grade ore. However, it requires high heat energy, which requires additional ventilation as compared to normal conditions to cool the work area. Plasma blasting uses a high temperature and pressure plasma to fracture rock in a safe manner. While this method may be environmentally friendly, its usage may significantly slow tunnel development due to the need to haul one or more large energy capacitor banks into and out of the work area repeatedly. Controlled foam injection is another chemical method, whereby foam is the medium for fracturing. Although claimed to be environmentally friendly, it may still pose safety risks such as air blast or fly rock due to its dynamic nature. A radial-axial splitter (RASP) is an instrument

specially designed to fracture a borehole in the rock face but only at the pace of one hole at a time. Supercritical carbon dioxide is used with the equipment designed to provide a high-pressure jet stream to fracture rock and replaces water in these instruments. The method of soundless chemical demolition agents (SCDA) is evaluated in more detail and its merits over others are highlighted, making it a potentially viable alternative to blasting with explosives in underground excavation applications. Future work involves the optimization of SCDA for implementation in underground mines. The discussion compares the key features and limitations, and future work needs are underlined

Keywords: Rock fragmentation; explosive-free rock breakage; tunneling; mining; plasma blasting; thermal fragmentation; controlled foam injection; radial axial splitter; supercritical carbon dioxide; soundless chemical demolition agents

2.1 Introduction

Rock excavation methods can be classified into three categories: drill and blast (DB), mechanical excavation, and specialized explosive-free approaches. The primary method for rock fragmentation in hard rock underground mines, tunnels, and caverns has typically included the use of explosives [1]. An explosive or a blasting agent is defined as a compound, or a mixture of compounds, that, when initiated by heat, can undergo rapid decomposition and release large amounts of heat and gas. The resulting end products are gases that are under compression, elevated temperatures, and very high pressures from ambient conditions, which results in a shockwave traveling through the surrounding rock mass. An ideal detonation is an oxygen-balanced mixture in which there is no excess or deficiency in oxygen so that the gaseous products produced are mainly H₂O (water vapor), CO₂ (carbon dioxide), and N₂ (nitrogen). In actual blasting practices,

small amounts of noxious gases, such as NO (nitric oxide), NH₄ (ammonia), CH₄ (methane), and solid carbon, are formed, resulting in non-ideal detonations resulting from either a deficiency or excess of oxygen [2]. Apart from the release of these fumes into the open air, the risk also lies in these fumes remaining in the ground after the blast. They have the potential to migrate hundreds of meters through the ground, to collect in confined spaces and be released later during subsequent blast loading operations, thus posing serious health risks [3]. Additionally, blasting can lead to poor fragmentation due to adverse joint orientation, resulting in oversized boulders or fine particles and low muck piles. Due to the concentrated energy of explosives, a blast can cause bedding plane separation or new fractures in the host rock; this is known as blast damage [4].

At the heart of the excavation process, there are several basic and fundamental tasks whose regular and repeated performance constitute the drill-and-blast (DB) cycle. Figure 2.1 presents such a cycle for the application of drift and tunnel advance, the primary method for development in underground mines and other engineering projects at depth. As can be seen, the cycle consists of six activities (1–3 during the first shift and 4–6 during the second one), with the third step being a period for blasting and ventilation of the area to vent out the toxic fumes produced. This period typically lasts for 2 h in Canadian mines and it usually occurs at the end of a work shift. Thus, for an operation that is running two 10-h shifts per day, it is possible to carry out blasting during four hours per day. Therefore, the inefficiencies associated with the drill-and-blast method comprise the need to vacate the work area (often the entire mine when several blasts are planned) before detonation. Ventilation then helps the gases generated to be evacuated and dilutes the toxic fumes released to the environment. The process for tunnel face advance in hard rock formations is similar to that of mine drift development.

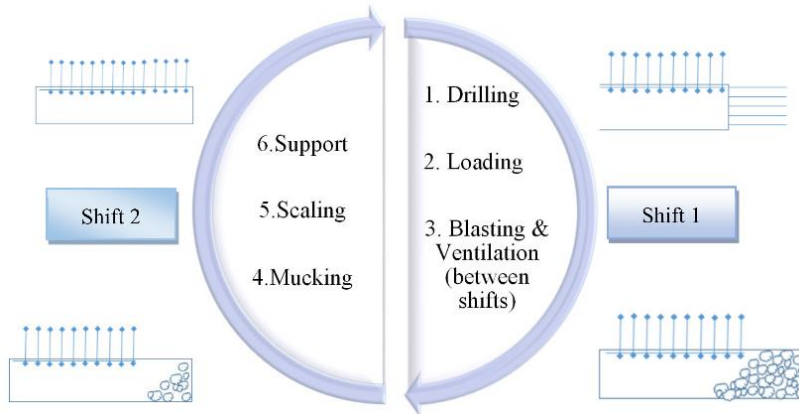


Figure 2.1 Typical Drill and Blast Cycle

While drill and-blast is the most conventional method for rock fragmentation in mine development and ore production, mechanical excavation is also commonly used, especially in soft rock formations. This category comprises the use of a tunnel boring machine (TBM), which can be adopted for tunnel driving in hard rock. Depending on the geology of the site to be excavated, the appropriate type of TBM is selected, such as Hard Rock TBM, Soft Ground, Slurry Shield TBM, Earth Pressure Balance TBM, and Open Face TBM [5]. TBMs have four basic systems to deem them operational: boring, thrust and clamp, muck removal, and support. Firstly, the boring system is responsible for cutting through the rock, which involves a cutterhead mounted with disc cutters. The force causes them to rotate and press against the rock face, exerting a higher pressure than the compressive strength of the rock. Secondly, the thrust and clamping system is responsible for moving the TBM via hydraulic cylinders. Thirdly, the muck removal system operates by removing the rock fragments or soil mixed with water or other substances. These are transported by a screw conveyor through the TBM. Lastly, ground support is installed to prevent loose material from falling as the TBM grinds along the tunnel [6].

As explained above, the use of TBMs offers continuous mining since loading and muck removal is done by a single machine as opposed to DB, which involves different equipment to advance a face. TBMs can achieve a daily advance over 20 m (39") per day, which is much higher than the DB method, being 4–6 m (157.5"-236") per day. When compared to DB, it is observed that TBMs do not generate blast gases; however, they do generate dust. Additionally, TBMs are high-cost machines and can sometimes be too large for a given site. Therefore, they may not always be suitable for general use in mine development applications [7]. Lastly, TBMs may be limited to applications where the compressive strength of the rock is relatively low. In this regard, various methods of rock preconditioning have been developed over the past few decades to assist with TBMs and other mechanical excavators to drill through hard rock formations and increase their penetration rate. Of these methods, microwave heating has been the most well-known approach.

Microwave heating has been used in the minerals industry to reduce energy requirements for comminution of ores and liberation of valuable particles [8,9]. In rock breakage and excavation applications, it is based on the principle of differential thermal expansion and induced stresses, similar to the fire setting technique used in the Bronze Age [10]. Lindroth et al. applied the technique of microwave heating to two igneous rock types and demonstrated an increase in penetration rate and a decrease in bit wear [11]. Hassani et al. discussed the use of microwave heating to precondition basalt, norite, and granite rock in lab and field demonstrations, as well as modeling the temperature effects [12]. Nekoovaght conducted an extensive investigation into the potential use of microwave assisted mechanical drilling in rocks for applications with tunnel boring machines (TBMs), especially in relation to reducing bit wear and replacement [13].

It should be underlined that microwave heating can only assist in rock breakage and excavation using mechanical methods and cannot be used on its own for these activities. Research is ongoing

to develop a methodology to assess whether a certain type of rock would benefit from microwave heating to render it more breakable. For example, Lu et al. developed a specialized apparatus that produced fractures in underground hard rock to help with their excavation and to reduce rock burst potential [14]. Xu et al. used microwaves to fracture diabase rock samples and modeled the thermal distribution in them [15]. Zheng et al. examined 15 rock types that were treated by microwaves in terms of their susceptibility to breakage, underlining the importance of effective dielectric loss factor and average grain size [16].

While drill-and-blast and mechanical methods are the two main categories for rock excavation techniques, an increasing amount of interest has been drawn in recent years towards the use of explosives-free specialized methods. The development of such methods offers the advantage of eliminating the disruption to tunneling activities—step 3 in Figure 2.1—and avoids blast fumes, dust, and noise, while potentially reducing damage to wall rock and achieving a better fragment size distribution. In the following sections, a review of recent methods for rock breakage without explosives is presented, briefly explaining the fundamental concepts behind each method, and highlighting its limitations and features.

2.2 Explosive-Free Specialized Methods

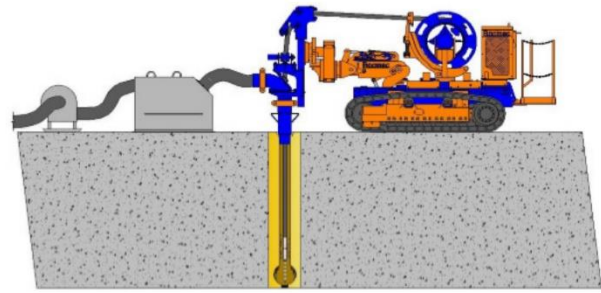
2.2.1 Thermal Fragmentation

Thermal fragmentation is a method patented in 2005 by Nippon Dragon Resources Inc., (Chicoutimi, QC, Canada) a Canadian junior mining company [4]. The “thermal fragmentation” process is developed for a specific mining application involving the extraction of high-grade, base metal, narrow-vein deposits, which impose a great challenge with respect to high levels of ore dilution. This occurs when a large and unaccounted quantity of waste rock must be processed to

retrieve a small quantity of desired material. As shown in Figure 2.2a, the thermal fragmentation method involves using a specialized machine named the Nippon Dragon that can move, drill, and mine ore from a sill drive.



(a)



(b)

Figure 2.2 Thermal fragmentation machinery, (a) Nippon Dragon Machine; (b) Mounted drill of the thermal fragmentation method (reprinted from [17])

Compared to the conventional blasting method, pilot holes are directly drilled into the desired vein below. The hole dimensions are typically 152.4 mm (6 inch) in diameter, and the stope height is 12–18 m. The pilot holes are subsequently enlarged by thermal fragmentation, which involves the insertion of a strong burner powered by diesel fuel and air and ignited. In underground mines, the burner can be a plasma torch where temperatures up to 1800 °C can be generated, thus creating thermal stresses that expand the pilot hole and cause the rock to spall. The hard rock breaks into a range of fragments ranging in size from fine grains to 40.64 mm (1.6 inch) pieces. Once the area of interest is fragmented, the burner is retracted, and the process is repeated until the top of the hole is reached. The fragmented pieces are then removed by a vacuum device. With that, the ore from the narrow vein deposit can be extracted while avoiding the undesired stripping of the surrounding waste rock that causes high dilution. The thermal fragmentation method is commonly

used in underground and open pit mines, mineral exploration, and tunneling in many countries, such as Canada, European countries, and Japan [4].

While thermal fragmentation may be beneficial in reducing ore dilution and, hence, the operational cost of narrow vein mining (ore deposits that are less than 2-m wide), there are other factors to consider. The thermal fragmentation method generates excessive amounts of heat, thus requiring far more ventilation energy to cool the working area than under normal conditions. The method also requires the use of specialized equipment that would necessitate increased capital expenditure and specialized training for the work force. Finally, thermal fragmentation relies heavily on the presence of ore minerals in the rock matrix—it would be inefficient in gangue or waste rock material. Therefore, it is not a suitable method for mine development activities, such as tunnels, drifts, and crosscuts, which are usually driven in waste rock.

2.2.2 Plasma Blasting Technology

The plasma blasting technology (PBT) developed by Noranda Minerals Inc. uses electrical energy as an excavation method to break hard rock in quarries and for fragmentation purposes in mines. The plasma method is based on the electrohydraulic principle and uses hydraulic energy to generate a shockwave through a liquid medium. These pulses propagate into the rock and lead to fracturing of the surrounding material. As shown in Figure 2.3, the method involves delivering electrical energy across a gap between two holes of coaxial electrode assembly in an electrolyte within a confined area of substance to be blasted. The electrolyte is subjected to a dielectric breakdown in the confined area, resulting in the formation of plasma, which is an ionized gaseous substance that is highly conductive electrically when subjected to high temperatures. The solution

subjected to dielectric breakdown for plasma formation can either be water or preferably copper sulphate [18].

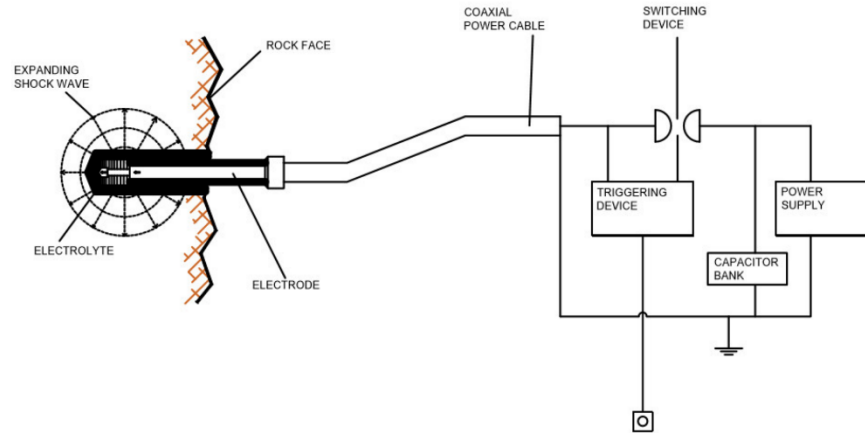


Figure 2.3 Components of the plasma blasting method (reprinted from [18])

A gelling agent such as bentonite or gelatin is often added to increase the viscosity of the solution, so that it does not run out of the confined area prior to blasting. The first step requires the drilling of a hole into the rock face by conventional methods, whereby a small amount of viscous electrolyte (20–50 g), such as copper sulphate, is injected into it. As shown in Figure 2.3, a coaxial blasting electrode is inserted into the hole to supply electrical energy to the electrolyte in the range of 300 to 1000 kJ. A typical size of the drill hole is 50 mm (1.96 inch) in diameter and 500 mm (19.69 inch) in depth. The peak pressure developed has been found to be in excess of 1 GPa, which is equivalent to blasting hard rock with a high explosive charge [18]. Other work conducted by Ikkurthi et al. on the simulation of crack propagation using two-dimensional numerical modeling showed that increasing the hole pressure beyond a certain threshold would have little incremental benefit to crack formation and propagation. The authors reported that this would be counterproductive, as it could damage the probe [19]. The electrical energy required for the blast is drawn from a capacitor bank which is charged by a DC power source. Once the switch is

triggered, the electrolyte in the hole undergoes a dielectric breakdown, producing plasma at extremely high temperature and pressure [18]. The energy created in the confined electrolyte around the electrode is released by way of pressure, which propagates in the rock mass and leads to fracturing. The plasma blasting technology has been tested on cubic concrete blocks (1200 kg) with successful fragmentation using electrical energies of 60–100 kJ. Another series of tests were conducted successfully on hard rock blocks, such as wollastonite, limey quartzite, and skarn (uniaxial compressive strengths of 140 to 350 MPa) with electrical energies of 30–180 kJ [20].

While the plasma blasting method is relatively safe and environmentally friendly, its use in underground applications may be limited. For a typical mine drift or tunnel face of 4.5 m × 4.5 m requiring many drill holes, the electrical energy supply for a single face advance would be very large considering that the plasma pulses would have to be triggered sequentially within a short time delay. Moreover, the need to haul one or more large-sized energy capacitor banks into and out of the work area repeatedly would significantly slow the drift or tunnel development cycle.

2.2.3 Controlled Foam Injection

The controlled foam injection (CFI) method was developed through extensive research funded by government, mining companies, and original equipment manufacturer (OEM) companies. The CFI method is a controlled process that works by means of pressurizing a fracture (or system of fractures) and maintaining it to propagate them further. The method is based on using high-pressure foam, which consists of a two-phase mixture of a liquid and a gas as the fracturing medium. The use of water alone is not enough because its incompressible behavior would cause a rapid loss of pressure as the fracture volume increases. The addition of a gaseous phase provides the necessary expansion to maintain the pressure for efficient fracturing. To compensate for the

separation of the water and air components due to the surface tension properties of water, commercially available surfactants are used to slow down the process. A slower penetration is preferable so that the pressures required to initiate and extend can develop the desired fractures. To obtain a desired viscosity, surfactants such as polyvinyl alcohol and a gel may be used. The process of CFI works by means of delivering the foam to the bottom of a predrilled hole and breaking the rock in tension. Typical operating pressures of the foam are less than 50 MPa and once the device reservoir is filled to the desired level, the foam is released into the predrilled hole by means of a rapid acting reverse firing poppet valve (RAP) (Figure 2.4) [21]. The typical diameter range is from less than one to several inches, and the hole depth varies from 4- to more than 10-hole diameters [22]. The equipment is mounted on a conventional wheel carrier that supports both the drill and the RAP [21]

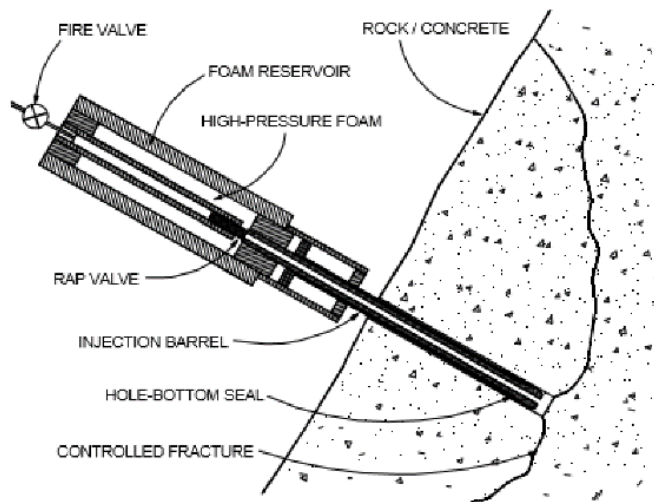


Figure 2.4 Controlled Foam Injection Components (reprinted from [21])

Records show that foam at 55 MPa (8000 psi) pressure prior to opening the valve rapidly drops to 48 MPa as the hole is loaded. Series of tests have demonstrated that foam pressures of 48 MPa were not able to immediately fracture granitic rock; however, it was fractured with a small delay

of 7.4 s. Once initiated, fracturing was completed in a fraction of a second with about 0.5 t of broken rock. The foam pressure then drops to zero, while the air cushion pressure drops to 45 MPa. Field tests were also conducted at the Colorado School of Mines test mine where CFI has been installed on several drilling machines to demonstrate its functionality. Presently, this method is used to enlarge tunnels but has not been attempted in underground mines [21].

The CFI is claimed to be a more environmentally friendly method due to a significant reduction in dust since exposed rock at the primary fracture is covered in a smear of foam. In addition, none of the surfactants is considered toxic. However, the CFI fracturing process seems to be of a dynamic nature and may still result in air blast or fly rock. There is also a limited depth of penetration, thus presumably preventing continuous excavation at the face.

2.2.4 Radial-Axial Splitter

A rock splitter is a mechanical tool designed to break or excavate rock or concrete by generating radial and/or radial-axial forces in a pre-drilled hole. The use of radial splitters dates to the beginning of the century and they are currently commercially available for construction and civil engineering applications but have not yet been implemented in hard rock mines. The radial splitter is based on the penetrating cone fracture concept, where a fracture is initiated and propagated by pressurizing a shallow hole through the generation of radial forces. It is initiated at the bottom of the pre-drilled shallow hole and then extends towards the free surface. The extension of the fracture results in the removal of a large volume of rock in the shape of a cone or a bowl, hence the name PCF, which refers to the residual shape left in the rock mass once the block has been broken and removed. This method involves the drilling of a borehole into the material where the radial splitter is inserted; during the penetration of the cone, the rock fails in tension [23]. A typical diameter is

63.5 mm (2.5 inch) with a hole depth of 381 mm (15 inch). For a rock splitter to be rendered effective, a free space must be available and in underground excavations from where a hole is drilled and the splitter inserted [24,45]. Radial-axial splitters (RASP) were introduced and designed by the Swedish Research Institute CERAC, and as the name implies, RASPs generate both radial and axial loads. Figure 2.5 shows the RASP consisting of the following in-hole components: wedge, thrust, rod, and feather, which are activated by a hydraulic cylinder [24,25]. The in-hole components shown in Figure 2.5 are the mechanical means in which the splitter generates rock breakage. The hydraulic cylinder containing two pistons individually activates the wedge and thrust-rod portion once inserted in a pre-drilled hole. The wedge is drawn back into the feathers, forcing these outwards against the borehole wall, which secures the radial anchorage of the splitter within. The thrust is then extended downwards until contact is made with the bottom and an axial load is applied to the rod. The resulting strain caused by both radial and axial loads, thus, fractures the rock.

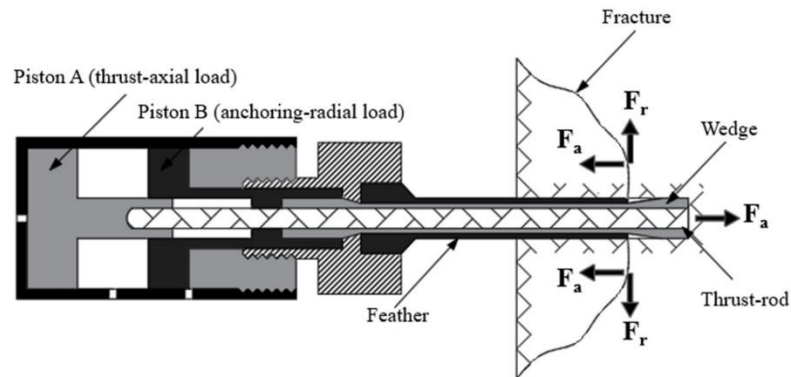


Figure 2.5 Radial-axial splitter (adapted from [25])

Large-scale testing was performed in an underground limestone mine near Davenport (IA), owned by Linwood Mining and Minerals Corp, where the operation used the room-and-pillar method.

During the field tests, the average depth of break was 254 mm (10 inch), with 1.25 tons of removed rock per break. The average size of broken rock fell into the range of 20 to 300 lbs (9 to 136 kg) [24]. Other studies by Paraszcak and Planeta have conducted feasibility evaluations on the potential use of radial-axial splitters in mining thin and narrow vein deposits for a more controlled fragmentation and to minimize dilution [25].

While this may be considered a safe method for the excavation or removal of hard rock, a significant number of splitters would have to be used for a large mining or tunnel face. They would also have a limited depth of penetration, thus rendering the method non-continuous one. One of the limitations of radial-axial splitters is that a considerable amount of thrust is needed for rock breakage, meaning that the need for the RASP to remain in place can present a challenge for the operator.

2.2.5 Supercritical Carbon Dioxide

The use of supercritical carbon dioxide (SC-CO₂) as a drilling fluid was developed at the turn of the 21st century for hydrocarbon reservoir applications [26]. The term “super- critical” indicates the temperature and pressure conditions above which the distinction of a liquid and gaseous phase for a given compound can no longer be made. Hence, the mixture is treated as a fluid since it is no longer in equilibrium. The limit above which CO₂ exists as a supercritical fluid is a temperature of 31.1 °C and a pressure of 7.38 MPa.

Caldwell reviewed three commercially available non-explosive technologies for excavation in rock [27]. One of these was Cardox, which was based on liquid carbon dioxide that would be converted to high pressure gas upon ignition, and that broke rocks in tension when it penetrated the pre-existing fractures. It had been developed in the mid 20th century in the UK and could

generate pressures of up to 300 MPa. In her study, Caldwell reviewed the use of Cardox for excavating a short shaft and tunnel for a sewerage system in Australia [27]. Gupta examined the feasibility of using the SC-CO₂ technology as a drilling fluid at a depleted gas well in Mississippi [28].

Kolle pioneered the use of SC-CO₂ with jet-assisted drilling to cut shale, marble, and granite at much lower pressures than with water [29]. A similar comparison of high-pressure jets of water and CO₂ was conducted by Du et al., who found that the latter was a much more efficient system than the former [30]. The use of SC-CO₂ in shale gas exploitation was examined by Wang et al. [31]. Liu et al. compared techniques relying on liquid CO₂ and SC-CO₂ for hydraulic fracturing applications and concluded that transitioning from the former to the latter would take place in the future [32]. Wang et al. experimented with breaking artificial and natural core samples with SC-CO₂ [33]. On the other hand, Li et al. (2020) developed a new cartridge system based on the Cardox concept and tested it at a construction site at the Hunan University Metro Station [34].

2.3 Soundless Chemical Demolition Agents (SCDAs)

The technology of SCDAs was developed more than 30 years ago but only came into commercial use some 10–15 years later for the fracturing of rock and concrete foundations. SCDAs, also known as expansive cements and non-explosive expansive materials (NEEM), are chemical powdery substances with lime (CaO or calcium oxide) as the primary ingredient, which expand during curing when under confinement. The crystallization process of lime during the hydration reactions results in a high expansive pressure. Notably, this method of fragmentation works by means of injecting the SCDA mixture into a borehole drilled into a concrete or rock foundation. The resulting crystallization pressure generated by the production of calcium hydroxide crystals

creates an effective fracture network around the borehole. Within a confined hole, the SCDA develops compressive normal stresses against its walls. This exerts pressure on the hole circumference in the radial direction and creates tensile stress in the tangential direction. As shown in Figure 2.6, a fracture is created in the radial direction at the weakest section in the circumference of the borehole. The initial production of the crack will only propagate when the generated stress exceeds the tensile strength of the rock. Therefore, the tensile stress generated by SCDA expansion produces the fracture mechanism responsible for concrete or rock breakage [35]. Based on linear elasticity theory, the stress generated by the SCDA at the hole edge is further reduced in proportion to the square of the distance from the edge of the hole boundary. Therefore, sufficiently high pressures are required to achieve longer fractures. Presently, SCDA's are commercially available; some of the products on the market include names such as Bristar and Dexpan. These are used in rehabilitation projects in urban areas where blasting with explosives is either prohibited or restricted. Applications include demolition of reinforced concrete and rock block splitting in dimension stone quarries.

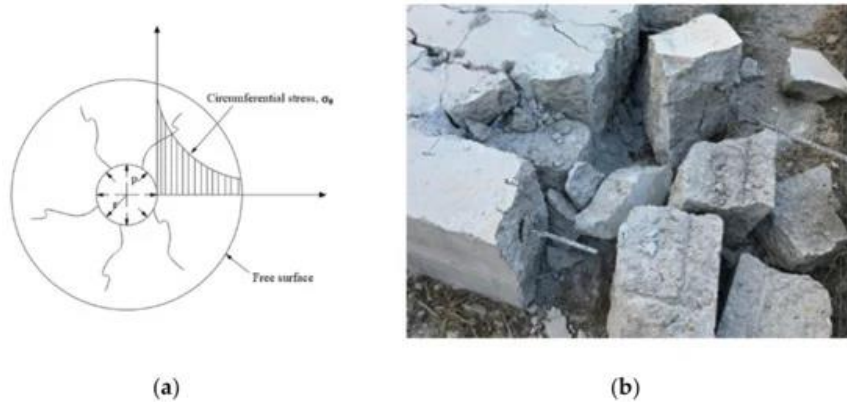


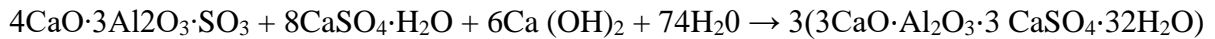
Figure 2.6 Soundless chemical demolition agents. (a) Fracture propagation around a pressurized borehole (adapted from [35]). (b) Broken rock with the use of SCDA (reprinted from [36]).

2.3.1 Types of SCDA

Based on the expansive additive in the product, there are three types of cements that are defined by ASTM C 845 “Standard Specification for Expansive Hydraulic Cement”: type K, type M, and type S. Although each one differs in the source of the aluminate component, they all commonly generate ettringite crystals, which is one of the driving forces of its expansive ability [37]. Class G is another type of expansive cement, and its expansive ability is driven by the generation of Portlandite [38].

Type K

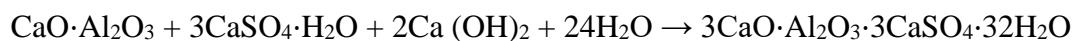
Type K expansive cement contains anhydrous calcium aluminosulfate ($4\text{CaO}\cdot 3\text{Al}_2\text{O}_3\cdot \text{SO}_3$), calcium sulphate (CaSO_4), and uncombined calcium oxide (CaO) [37].



Its performance can be enhanced even more by the addition of silica fume and plasticizer as reported by Sarkar [39].

Type M

Type M expansive cement contains calcium aluminate (CA) and calcium sulphate CaSO_4 [37].



Type S

Type S expansive cement is composed of tricalcium aluminate (C_3A) and calcium sulphate CaSO_4 [37].



Class G

Class G expansive cement is composed mainly of lime—usually at 80–90%—and SiO_2 , as well as a few additional substances, such as Al_2O_3 and Fe_2O_3 , for controlling the expansion rate. The hydration reaction of lime (CaO) is the source of its expansive force [38].



There are several SCDA products that are commercially available, and they all differ in performance, usage instructions, and borehole dimension specifications. The performances are dependent on the curing temperature, water content, borehole dimensions, and borehole design pattern. These affect the expansion rate of SCDA and have been extensively studied by many researchers to optimize their performance. According to studies conducted by Hinze and Brown, the water content is inversely proportional to the expansive pressure generated in the SCDA inside a confined volume [1]. Presumably, this occurs because a lower water-to-cement ratio results in a large agent particle density and smaller distances between neighboring particles. This means that a lower degree of hydration will bring them into contact with one another. Natanzi et al., Laefer et al., and Natanzi et al. have shown that curing and ambient temperatures are directly proportional to expansive pressure [40-42]. This conclusion is also supported by other studies, suggesting that expansive pressure is generated up to a certain threshold that, when exceeded, a blowout of SCDA could occur [1]. The expansive pressure development rate is also affected by the borehole size, and it increases with its diameter due to the hydration reaction and transformation of CaO into $\text{Ca}(\text{OH})_2$. A large diameter provides more space for free lime to be hydrated within the borehole. Since the hydration reaction is exothermic, the chemical reaction releases heat, thus increasing the temperature, which is itself related to the increase in the rate of hydration and one of the main sources of expansion development [1]. Further studies conducted by Soeda et al., Dessouki and

Mitri, de Silva and Ranjith, and Habib have shown that common concrete accelerators, such as calcium sulphate, calcium chloride, and calcium formate, can significantly increase the rate of expansive pressure [43-47]. De Silva et al. conducted an extensive study of mineralogical, morphological, and microstructural changes responsible for expansive pressure development in SCDA [48]. Similar studies have been conducted by other researchers as well, such as Fu et al. [49]. Investigations have also been conducted on borehole spacing patterns, sizes, and lengths to optimize fracture propagation. Etkin and Azarkovitch examined the impact of borehole diameter and length on the pressure developed within SCDA, while Xu et al. experimented with large-sized diameters in concrete [50,51]. Cho et al., Hutapea et al., and Kim et al. conducted laboratory and field testing specifically to determine borehole spacing and pattern configurations, while Leroy and Chebou studied borehole spacing through numerical modeling [52-55]. Wu et al. combined SCDA with notching for applications in coal mines where the weakening of the roof formation was required [56]. Arshadnejad (2019) conducted an extensive analytical and large-scale test study of the spacing between holes and compared it to those reported in the literature [57]. Studies conducted by Labuz et al. have shown that holes with gradual increased spacing in between—when compared to holes with uniform spacing—caused the fracture to be initiated much sooner and to propagate at a faster rate from the end where the spacing is smaller [58]. Other studies suggest that the fracturing of rock can be optimized by introducing non-injected SCDA holes of the same size as the injected ones. Boreholes with a diameter of 4.76 mm and a 6×6 , 4×4 , and 3×3 grid with non-injected holes were found to be beneficial. In the same study, a potential possibility was observed of reducing the amount of SCDA used and its incorporation into additional empty boreholes [59]. The effect of specimen loading was investigated by Musunuri and Mitri on norite samples by subjecting cubes with a single injected SCDA hole to a uniaxial

compression of 64 MPa. Results showed that the expansive agent used resulted in pressure generation for up to one week, causing the norite block to fracture and break into fragments [60].

2.4 Challenges Associated with SCDA Application to Underground Construction

SCDAs have traditionally been used in the demolition of concrete structures, debris, and parts of buildings in urban settings, and an extensive body of literature exists on the topic [35, 61-71]. Initial applications of expansive cements in general included replacement of the regular type in concrete where shrinkage compensation was required [72]. An extensive literature review of the use of SCDAs is given by Huynh and Laefer [73]. Their usage for rock breakage, mining, or tunneling applications have been fewer in number, with Dowding and Labuz and a related discussion by Ingraffea and Beech being some of the earliest references on the topic [74,75]. The former authors used expansive cements to break dolomite in a quarry. Hanif & Al-Maghrabi (2007) used them to break a block of rock from a granite quarry in Saudi Arabia [76]. Bhardwaj and Sharma reviewed the approach as one of the methods that could be used for granite extraction from quarries in India [77]. Arshadnadjad et al. conducted numerical modeling in RS2 to study hole spacing to enhance fracture enhancement and propagation [38,78]. Continuing these studies, Gholinajad and Arshadnadjad studied the developed pressure within metal cylinders filled with NEEMs extensively for the purpose of using the findings in numerical modeling and rock breakage purposes [79]. The experiment then moved to actual site tests at a granite quarry in Iran [57,80]. Cho et al. also used finite element modeling to examine crack propagation due to SCDA expansion [81]. Tiam et al. reported the use of CRACK.AG—an SCDA from China—at a gneiss quarry in central Cameroon at temperatures varying between 16 °C and 24 °C. They also used XFEM modeling in ABAQUS to study the influence of two adjacent holes on one another [82]. Expanding cements have also been used for well cementing, as well as stimulating and enhancing fracturing

for the oil and gas industry [83-86]. Recently, Xu et al. developed special self-swelling SCDA cartridges to be used in up- tilt boreholes [87].

In terms of direct mining and underground construction applications, Dunn reported on a number of non-explosives techniques to break rocks in South African gold mines, including the use of expansive cements that were successful when used in a burden of 200 mm in norite [88]. De Silva and Ranjith conducted extensive studies of SCDA use to enhance fracturing in host rocks to improve in situ leaching of low-grade ore deposits [46]. They performed laboratory tests and numerical modeling using PFC3D to examine various fracture patterns in cylindrical specimen of sandstone. Xu et al. and Tang et al. used SCDA to weaken the strong roof at the Pingdingshan coal mine to prevent rock bursts that usually accompanied extraction if blasting agents are used [89,90]. They also conducted an analysis of the borehole angle orientation using FLAC3D numerical modeling. Zhang et al. used SCDA for directional roof cutting at the Donglin coal mine [91]. Tang et al. and Cui et al. have also used it for fracturing and enhancing the permeability of coal seams to release methane and other gases [92,93]. The first trial in an underground hard rock mine has been reported at a manganese operation in Georgia [94]. The authors developed an SCDA capable of producing 130 MPa of expansive pressure and tested it in 42 mm boreholes in ore with tensile strengths of up to 8.1 MPa.

An increased interest has been drawn towards SCDA usage in recent years due to its safe and tremor-free breaking up of rock. For subsurface applications, there is the additional benefit of avoiding the generation of greenhouse gas emissions due to blasting with explosives, most notably nitric oxide (NO), carbon monoxide (CO), ammonia (NH₄), and methane (CH₄). However, SCDA applications have never been attempted in underground hard rock mines as part of the regular tunnel, drift, and crosscut excavation cycles. There are three main challenges associated with the

implementation of the technology in sub- surface engineering. Firstly, the time needed for SCDA to develop maximum expansive pressure—typically 12 h—is too long for practical underground applications. Secondly, for SCDA to be rendered feasible, it must overcome the high confining stresses while still achieving a reasonable time for rock breakage. The presence of in situ stresses would require a higher SCDA pressure to overcome not only the tensile strength of the rock, but also the induced compressive stress distribution around the SCDA borehole. The third challenge is that SCDA has only been tried on concrete and surface rocks formations, which are inherently weaker than the strong igneous lithologies that are commonly found at depth in metal mines and deep underground environments. A sound research methodology is required to overcome the above challenges to help introduce SCDA into underground construction as a viable alternative for hard rock fragmentation.

If the challenges previously discussed are properly addressed, it would permit the application of a new cycle for drift and tunnel development with SCDA. Figure 2.7 presents a proposed continuous, drill-and-fill with an SCDA cycle, with a comparison to the traditional one, shown previously in Figure 2.1. Firstly, the proposed SCDA cycle (Figure 2.7) aims at a continuous production schedule, e.g., 3×8 -h or 2×12 -h shifts with no interruption in between. The hole diameter of SCDA can range between 25.4 mm (1.0 inch) and 44.45 mm (1.75 inch) with a hole depth of at least five times the diameter and maximum 3 m long [36]. The fact that there is no blasting with explosives would allow for the operation to be continuous, as is the case in mechanical excavation such as road headers and TBMs. Productivity would then increase from the traditional 20 h (2×10 -h shifts) to 24 h. The change of schedule is also feasible for mines in the period of pre-production development, during which levels and sublevels in waste rock are driven before the beginning of ore extraction with drilling and blasting. The introduction of a mobile rock

breaker would be required to help dislodge the fragmented blocks, which is a readily available piece of equipment in most underground construction operations. The use of SCDA exhibits a quasi-static fracturing process and would presumably not cause damage to the drift sidewall. Thus, the use of SCDA would have the benefit of eliminating blast-induced vibration and damage, and the need for rock surface scaling would be minimal.

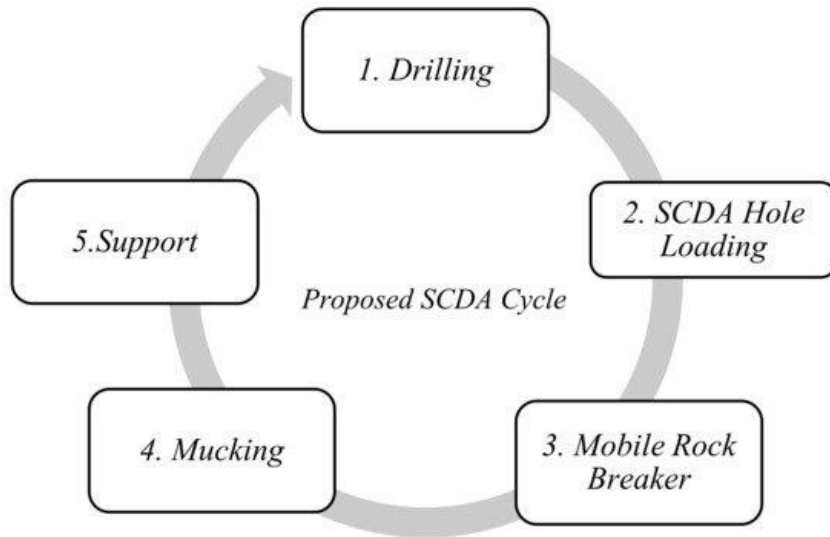


Figure 2.7 Proposed continuous, drill, and SCDA cycle for tunnel face advance

While other explosive-free rock breakage technologies demand the introduction of new and specialized equipment (e.g., radial axial splitter) that would further complicate the development schedule and inevitably increase capital and operating costs, SCDA-based technology uses existing standard excavation equipment. This includes the possible use of a mobile rock breaker for the separation of fractured blocks.

Finally, with the use of SCDA, there will be no blast-induced fumes and fugitive dust particles that get released to the atmosphere and cause air pollution. The SCDA cycle does not necessitate the additional ventilation normally needed to extract blast-induced fumes and dust particles from

underground openings. This is an environmentally friendly feature and constitutes a cost reduction factor as well.

Presently, research efforts are underway by the authors at McGill University to overcome challenges of implementing SCDA-based rock breakage in underground mines, tunnels, and caverns. The main challenges addressed to render this method feasible comprise a reduction in the time of rock breakage and overcoming the confining stress that could prevent fracturing. Of specific interest is the use of SCDA due to its procedural simplicity for operation as well as the minimal training required in handling the material.

SCDA is also found to be environmentally safe as it does not generate fumes, noise, and vibrations, thereby mitigating the risks of explosives blasting. Due to these features, SCDA has the potential to revolutionize rock fragmentation in underground mine, tunnel, and space developments and other hard rock excavation applications.

2.5 Conclusions

This paper describes six selected explosives-free methods for rock breakage, notably thermal fragmentation, plasma blasting technology, controlled foam injection, radial-axial splitter, supercritical carbon dioxide, and SCDA. Each method offers advantages that mitigate the risks of blasting with explosives while still having their own limitations. Thermal fragmentation is targeted for the extraction of narrow vein deposits to reduce ore dilution; however, its excessive heat requires additional ventilation energy to cool down the work area. While the thermal fragmentation method is presently used in the mining industry, the plasma blasting technology has yet to be implemented and its use may be limited in subsurface applications as a large supply of electrical energy is needed to advance a single face. The controlled foam injection technology is claimed to

be environmentally friendly; however, the fracturing method may be of dynamic nature resulting in air blast or fly rock, the safety risks of which explosive-free methods should avoid. The radial-axial splitter, a mechanical method of hard rock excavation, is also considered environmentally friendly; however, a significant number of splitters is needed for the excavation of a single face as well at its limited depth of penetration impeding continuous mining. Supercritical carbon dioxide is a more efficient replacement for water in high-pressure jets used for excavation, but their main function is to simply drill holes into the rock and not fragment a large enough face for mucking. From a practical perspective, it is shown that the proposed SCDA method has the most potential to become a viable alternative to blasting with explosives in underground mine drift advance applications. While SCDA technology is currently being used in demolition projects and dimension stone quarries, it is yet to be developed further for underground tunneling and mining applications. The merits of SCDA can be summarized as follows: (1) Reduced zone of influence around the tunnel excavation, thus having the potential to be implemented in shallow overburden projects near sensitive buildings and infrastructure; (2) Reduced potential for ground water leakage; (3) Noise reduction/elimination; (4) Reduced occurrence of overbreak and strata collapse; (5) Little or no nuisance to residents in the vicinity of the project.

References

1. Hinze, J.; Brown, J. Properties of soundless chemical demolition agents. *Constr. Eng. Manag.* 1994, 120, 816–827.
2. Dhekne, P.Y. Environmental impacts of rock blasting and their mitigation. *Int. J. Chem. Environ. Biol. Sci.* 2015, 3, 46–50.
3. Özmen, İ.; Aksoy, E. Respiratory Emergencies and Management of Mining Accidents. *Turk. Thorac. J.* 2015, 16 (Suppl. 1), S18.
4. Brisebois, D. Thermal Rock Fragmentation Application in Narrow Vein Extraction. U.S. Patent 7,195,320, 27 March 2007.
5. Encardio Rite. Available online: <https://www.encardio.com/blog/all-about-tunnel-boring-machine-components-typesadvantages/> (accessed on 22 January 2022).
6. Maidl, B.; Schmid, L.; Ritz, W.; Herrenknecht, M. *Hardrock Tunnel Boring Machines*; John Wiley & Sons: Berlin, Germany, 2008; pp. 15–19.
7. Stewart, P.; Ramezanzadeh, A.; Knights, P. Benchmark drill and blast and mechanical excavation advance rates for underground hard-rock mine development. In *Proceedings of the 2006 Australian Mining Technology Conference, Hunter Valley, NSW, Australia, 26–27 September 2006*.
8. Fitzgibbon, K.E.; Veasey, T.J. Thermally assisted liberation—A review. *Miner. Eng.* 1990, 3, 181–185.
9. Kingman, S.W.; Vorster, W.; Rowson, N.A. The influence of mineralogy on microwave-assisted grinding. *Miner. Eng.* 2000, 13, 313–327.

10. Satish, H. Exploring Microwave-Assisted Rock Breakage for Possible Space Mining Applications. Master's Thesis, McGill University, Montreal, QC, Canada, 2005.
11. Lindroth, D.P.; Berglund, W.R.; Morrell, R.J.; Blair, J.R. Microwave assisted drilling in hard rock. *Tunn. Tunn.* 1993, 25, 24–27.
12. Hassani, F.; Nekoovaght, P.M.; Gharib, N. The influence of microwave irradiation on rocks for microwave-assisted underground excavation. *J. Rock Mech. Geotech. Eng.* 2016, 8, 1–15.
13. Nekoovaght, P.M. Physical and Mechanical Properties of Rock Exposed to Microwave Irradiation: Potential Application Tunnel Boring. Ph.D. Thesis, McGill University, Montreal, QC, Canada, 2015.
14. Lu, G.M.; Feng, X.T.; Li, Y.H.; Zhang, X. The microwave-induced fracturing of hard rock. *Rock Mech. Rock Eng.* 2019, 52, 3017–3032.
15. Xu, T.; He, L.; Zheng, Y.; Zou, X.; Badrkhani, V.; Schillinger, D. Experimental and numerical investigations of microwave-induced damage and fracture formation in rock. *J. Therm. Stresses* 2020, 44, 513–528.
16. Zheng, Y.L.; Ma, Z.J.; Yang, S.Q.; Zhao, X.B.; He, L.; Li, J.C. A microwave fracturability index (MFI) of hard igneous rocks. *Int.J. Rock Mech. Min.* 2021, 138, 104566.
17. Poirier, S.; Fecteau, J.-M.; Laflamme, M.; Brisebois, D. Thermal rock fragmentation: Applications in narrow-vein extraction. *CIMBull.* 2003, 96, 66–71.
18. Kitzinger, F.; Nantel, J. Plasma Blasting Method. U.S. Patent 5,106,164, 21 April 1992; p. 6.
19. Ikkurthi, V.R.; Tahiliani, K.; Chaturvedi, S. Simulation of crack propagation in rock in plasma blasting technology. *Shock Waves* 2002, 12, 145–152.

20. Zhou, H.; Xie, X.; Feng, Y. Rock breaking methods to replace blasting. IOP Conf. Ser. Mater. Sci. Eng. 2018, 322, 022014.
21. Pickering, R.G.B.; Young, C. Controlled foam injection: A new and innovative non-explosive rockbreaking technology. J. S. Afr.Inst. Min. Metall. 2017, 117, 237–243.
22. Young, C., III. Controlled Foam Injection Method and Means for Fragmentation of Hard Compact and Rock and Concrete. U.S.Patent 6,375,271, 23 April 2002.
23. De Graaf, W.W.; Spiteri, W. A preliminary qualitative evaluation of a hydraulic splitting cylinder for breaking rock in deep level mining. J. S. Afr. Inst. Min. Metall. 2018, 118, 891–897.
24. Anderson, S.J.; Swanson, D.E. Capability Evaluation of the Radial-Axial Splitter; Report No. 9071; US Bureau of Mines: Minneapolis, MN, USA, 1987; 35p.
25. Paraszczak, J.; Planeta, S. Feasibility of Narrow Vein Mining Using a Mechanical Rock Splitter. Mine Plan. Equip. Sel. 2003, 1,415–422.
26. Ishida, T.; Aoyagi, K.; Niwa, T.; Chen, Y.; Murata, S.; Chen, Q.; Nakayama, Y. Acoustic emission monitoring of hydraulic fracturing laboratory experiment with supercritical and liquid CO₂. Geophys. Res. Lett. 2012, 39, <https://doi.org/10.1029/2012GL052788>.
27. Caldwell, T. A comparison of non-explosive rock breaking techniques. In Proceedings of the 12th Australian Tunnelling Conference, Sofitel, Australia, 17–20 April 2005.
28. Gupta, A.P. Feasibility of Supercritical Carbon Dioxide as a Drilling Fluid for Deep Underbalanced Drilling Operations. Master's Thesis, Louisiana State University, Baton Rouge, LA, USA, 2006.

29. Kollé, J.J. Coiled-tubing drilling with supercritical carbon dioxide. In Proceedings of the SPE/CIM International Conference on Horizontal Well Technology, OnePetro, Calgary, AB, Canada, 6–8 November 2000.
30. Du, Y.K.; Wang, R.H.; Ni, H.J.; Li, M.K.; Song, W.Q.; Song, H.F. Determination of rock-breaking performance of high-pressure supercritical carbon dioxide jet. *J. Hydrodyn. B* 2012, 24, 554–560.
31. Wang, H.; Li, G.; Shen, Z. A Feasibility Analysis on Shale Gas Exploitation with Supercritical Carbon Dioxide. *Energy Sources Part A Recovery Util. Environ. Eff.* 2012, 34, 1426–1435.
32. Liu, H.; Wang, F.; Zhang, J.; Meng, S.; Duan, Y. Fracturing with carbon dioxide: Application status and development trend. *Pet. Explor. Dev.* 2014, 41, 513–519.
33. Wang, H.; Li, G.; Shen, Z.; Tian, S.; Sun, B.; He, Z.; Lu, P. Experiment on rock breaking with supercritical carbon dioxide jet. *J. Pet. Sci. Eng.* 2015, 127, 305–310.
34. Li, Q.Y.; Chen, G.; Luo, D.Y.; Ma, H.P.; Liu, Y. An experimental study of a novel liquid carbon dioxide rock-breaking technology. *Int. J. Rock Mech. Min.* 2020, 128, 104244.
35. Harada, T.; Idemitsu, T.; Watanabe, A.; Takayama, S. The Design Method for the Demolition of Concrete with Expansive Demolition Agents. In *Fracture of Concrete and Rock*; Shah, S.P., Swartz, S.E., Eds.; Springer: New York, NY, USA, 1989; pp. 47–57.
36. Betonamit Technical Manual—Non-Explosive Cracking Agent. Available online: <http://www.betonamit.com/technical-manual/> (accessed on 9 April 2021).

37. ASTM International. Standard Specification for Expansive Hydraulic Cement. In Annual Book of ASTM Standards; 845 Standard;ASTM International: West Conshohocken, PA, USA, 2004, pp. 390–393.
38. Arshadnejad, S.; Goshtasbi, K.; Aghazadeh, J. A model to determine hole spacing in the rock fracture process by non-explosive expansion material. *Int. J. Miner. Metall.* 2011, 18, 509–514.
39. Sarkar, S.L. Strength Enhancement in Type K Expansive Cement Using Additives. *J. Mater. Civ. Eng.* 1990, 2, 1–14.
40. Natanzi, A.S.; Laefer, D.F.; Connolly, L. Cold and moderate ambient temperatures effects on expansive pressure development in soundless chemical demolition agents. *Constr. Build. Mater.* 2016, 110, 117–127.
41. Laefer, D.F.; Natanzi, A.S.; Zolanvari, S.M.I. Impact of thermal transfer on hydration heat of a Soundless Chemical Demolition Agent. *Constr. Build. Mater.* 2018, 187, 348–359.
42. Natanzi, A.S.; Laefer, D.F.; Connolly, L. Temperature-Induced Chemical Changes in Soundless Chemical Demolition Agents. *J.Mater. Civ. Eng.* 2019, 31, 04019098.
43. Soeda, K.; Hida, T.; Hayashi, H.; Kanbayashi, M. The Influence of Additives on the Expansive Stress of Quick Lime. *Gypsum & Lime. J. Korean Ceram. Soc.* 1992, 44, 79–84.
44. Soeda, K.; Matsuhisa, M.; Hayashi, H.; Tsuchiya, K. The Influence of. Chemical Composition on the Properties of Non-explosive Demolition Agent for Low Temperatures. *Gypsum Lime J-Stage* 1993, 247, 442–449.
45. Dessouki, A.E.; Mitri, H. Rock Breakage Using Expansive Cement. *Engineering* 2011, 3, 168–173.

46. De Silva, V.R.S.; Ranjith, P.G. Intermittent and multi-stage fracture stimulation to optimize fracture propagation around a single injection well for enhanced in-situ leaching applications. *Eng. Fract. Mech.* 2019, 220, 106662.
47. Habib, K. Laboratory Investigation into Soundless Chemical Demolition Agents for Rock Breakage in Underground Mines. Master's Thesis, McGill University, Montreal, QC, Canada, 2019.
48. De Silva, V.R.S.; Ranjith, P.G.; Perera, M.S.A.; Wu, B.; Rathnaweera, T.D. Investigation of the mechanical, microstructural and mineralogical morphology of soundless cracking demolition agents during the hydration process. *Mater. Charact.* 2017, 130, 9–24.
49. Fu, Y.; Sheikh, S.A.; Hooton, R.D. Microstructure of Highly Expansive Cement Pastes. *ACI Mater. J.* 1994, 91-M6, 46–53.
50. Etkin, M.B.; Azarkovich, A.E. Effect of Non-Explosive Splitting Compounds and Rational Work Parameters. *Power Technol. Eng.* 2006, 40, 23–29.
51. Xu, Q.; Jiang, N.; Long, Y.; Liao, Y.; Yang, T.; Ji, R. Investigation of the Large-Scale Borehole Soundless Cracking Experiment on the Concrete Members. *Appl. Mech. Mater.* 2015, 782, 219–226.
52. Cho, H.; Nam, Y.; Kim, K.; Lee, J.; Sohn, D. Effective Arrangement of Non-Explosive Demolition Agents and Empty Holes for Improving Fragmentation of Square Concrete Structures. *J. Comput. Struct. Eng. Inst. Korea* 2017, 30, 145–151.

53. Hutapea, E.H.; Simangunsong, G.M.; Widodo, N.P. Laboratory Investigation to Determine Hole Spacing into Rock Fracturing Using Non-Explosive Demolition Agent. In Proceedings of the ISRM Specialized Conference, Jeju, Korea, 10 May 2017.
54. Kim, K.; Cho, H.; Sohn, D.; Koo, J.; Lee, J. Prediction of the Minimum Required Pressure of Soundless Chemical Demolition Agents for Plain Concrete Demolition. *J. Comput. Struct. Eng. Inst. Korea* 2018, 31, 221–258.
55. Leroy, M.N.L.; Chebou, G.N. Numerical Study of Stresses around Holes Drilled and Filled by Expansive Cement: Case of Isotropic Linear Elastic Block of Rock. *Adv. Mater. Sci. Eng.* 2018, 2018, 8718452.
56. Wu, S.; Zhai, C.; Xu, J.; Qin, L.; Sun, Y.; Dong, R. The performance of soundless cracking agents for weakening rock roof under different notch angles. *Arab. J. Geosci.* 2019, 12, 365.
57. Arshadnejdad, S. Design of hole pattern in static rock fracture process due to expansion pressure. *Int. J. Rock Mech. Min.* 2019, 123, 104100.
58. Labuz, J.F.; Shah, S.P.; Dowding, C.H. Experimental analysis of crack propagation in granite. *Int. J. Rock Mech. Min.* 1985, 22, 85–98.
59. Gambatese, J.A. Controlled concrete demolition using expansive cracking agents. *J. Constr. Eng. Manag.* 2003, 129, 98–104.
60. Musunuri, A.; Mitri, H. Laboratory investigation into rock fracturing with expansive cement. *Int. J. Min. Miner.* 2009, 1, 327–345.

61. Gomez, C.; Mura, T. Stresses Caused by Expansive Cement in Borehole. *J. Eng. Mech.* 1984, 110, 1001–1005.
62. Tarricone, P. Less Bang for the Buck. *Civ. Eng.* 1990, 60, 64–66.
63. Abudayyeh, O.; Sawhney, A.; El-Bibany, H.; Buchanan, D. Concrete Bridge Demolition Methods and Equipment. *J. Bridge Eng.* 1998, 3, 117–125.
64. Laefer, D.F.; Ambrozevitch-Cooper, N.; Huynh, M.P.; Midgette, J.; Ceribasi, S.; Wortman, J. Expansive fracture agent behaviour for concrete fracking. *Mag. Concr. Res.* 2010, 62, 443–452.
65. Natanzi, A.S.; Laefer, D.F. Using Chemicals as Demolition Agents Near Historic Structures. In *Proceedings of the 9th International Conference on Structural Analysis of Historical Constructions*, Mexico City, Mexico, 14–17 October 2014.
66. Laefer, D.F. Emerging city-scale damage prediction options for urban tunnelling. In *Proceedings of the 10th International Conference on Structural Analysis of Historical Constructions*, Leuven, Belgium, 13–15 September 2016.
67. De Silva, V.R.S.; Ranjith, P.G.; Perera, M.S.A.; An Alternative to Conventional Rock Fragmentation Methods Using SCDA: A Review. *Energy J.* 2016, 9, 958.
68. Natanzi, A.S.; Laefer, D.F.; Mullane, S. Chemical Demolition of Unit Masonry: A Preparatory Study. In *Proceedings of the 10th International Conference on Structural Analysis of Historical Constructions: Anamnesis, Diagnosis Therapy, Controls*, Leuven, Belgium, 13–15 September 2016.
69. Natanzi, A.S. Soundless Chemical Demolition Agents Performance under Cold and Cool Temperatures in Concrete and Masonry Structures. Ph.D. Thesis, University College Dublin, Dublin, Ireland, 2017.

70. Wiggenhauser, H.; Kopp, C.; Timofeev, J.; Azari, H. Controlled Cracks in Concrete for Non-destructive Testing. *J. Nondestr.Eval.* 2018, 37, 67.
71. Saltas, V.; Peraki, D.; Vallianatos, F. The use of acoustic emissions technique in the monitoring of fracturing in concrete using soundless chemical demolition agent. *Frat. Integrita Strutt.* 2019, 13, 505–516.
72. Hoff, G.C. *Expansive Cements and Their Use*; U.S. Army Engineer Waterways Experiment Station Concrete Laboratory: Vicksburg,MS, USA, 1972.
73. Huynh, M.-P.; Laefer, D.F. Expansive cements and soundless chemical demolition agents: State of technology review. In *Proceedings of the 11th Conference on Science and Technology*, Tsukuba, Japan, 21–23 October 2009.
74. Dowding, C.H.; Labuz, J.F. Fracturing of Rock with Expansive Cement. *J. Geotech. Eng.* 1982, 108, 1288–1299.
75. Ingraffea, A.R.; Beech, J.F. Discussion to “Fracturing of Rock with Expansive Cement”. *J. Geotech. Eng.* 1983, 109, 1205–1208.
76. Hanif, M.; Al-Maghrabi, M.-N.N.H. Effective Use of Expansive Cement for the Deformation and Fracturing of Granite. *Gazi Univ. J. Sci.* 2007, 20, 1–5.
77. Bhardwaj, G.S.B.; Sharma, S. Granite Extraction and Treatment Techniques: A Study on Cost Effective Geo-Technical Aspects. *Min. Eng. J.* 2010, 11, 11–19.
78. Arshadnejad, S.; Goshtasbi, K.; Aghazadeh, J. Stress Concentration analysis between two neighboring circular holes under internal pressure of a non-explosive expansion material. *J. Earth Sci. Appl. Res. Cent. Hacet. Univ.* 2009, 30, 259–270.

79. Gholinejad, M.; Arshadnejad, S. An experimental approach to determine the hole-pressure under expansion load. *J. S. Afr. Inst. Min. Metall.* 2012, 112, 631–635.
80. Arshadnejad, S. Analysis of the First Cracks Generating between Two Holes under Incremental Static Loading with an Innovation Method by Numerical Modelling. *Math. Comput. Sci.* 2017, 2, 120–129.
81. Cho, H.; Nam, Y.; Kim, K.; Lee, J.; Sohn, D. Numerical Simulations of crack path control using soundless chemical demolition agents and estimation of required pressure for plain concrete demolition. *Mater. Struct.* 2018, 51, 169.
82. Tiam, F.F.K.; Danwe, R.; Konai, N.; Meva'a, L. Experimental Study and Numerical Simulation Using Extended Finite Element Method (XFEM) Combined with Cohesive Zone Model (CZM), of Crack Growth Induced by Non-Explosive Expansive Materials on Two Neighboring Circular Holes of A Gneiss Rock. *Open J. Appl. Sci.* 2020, 10, 592–612.
83. Parker, P.N.; Wahl, W.W. Expanding Cement—A New Development in Well Cementing. *J. Pet. Technol.* 1966, 18, 559–564.
84. De Silva, V.R.S.; Ranjith, P.G.; Perera, M.S.A.; Wu, B.; Rathnaweera, T.D. A modified, hydrophobic soundless cracking demolition agent for non-explosive demolition and fracturing applications. *Process Saf. Environ. Prot.* 2018, 119, 1–13.
85. De Silva, V.R.S.; Ranjith, P.G.; Perera, M.S.A.; Wu, B. Artificial Fracture Stimulation of Rock Subjected to Large Isotropic Confining Stresses in Saline Environments: Application in Deep-Sea Gas Hydrate Recovery. *Nat. Resour. Res.* 2019, 28, 563–583.

86. De Silva, V.R.S.; Ranjith, P.G.; Perera, M.S.A.; Wu, B. The effect of saturation conditions on fracture performance of different soundless cracking demolition agents (SCDAs) in geological reservoir rock formations. *J. Nat. Gas Sci. Eng.* 2019, 62, 157–170.
87. Xu, S.; Hou, P.; Li, R.; Cai, M. An Experimental Study on the Mechanical Properties and Expansion Characteristics of a Novel Self-Swelling Cartridge for Rock Breakage. *Rock Mech. Rock Eng.* 2020, 54, 819–832.
88. Dunn, P.G. The Non-Explosive Mechanization of the South African Gold Mine Stopping Operation. Master's Thesis, University of the Witwatersrand, Johannesburg, South Africa, 1989.
89. Xu, J.; Cheng, Z.; Ranjith, P.G.; Sun, Y.; Qin, L.; Ma, H.; Guo, J.; Ma, Z. Investigation of non-explosive expansion material in roof caving field application. *Int. J. Rock Mech. Min.* 2019, 120, 50–57.
90. Tang, W.; Zhai, C.; Xu, J.; Sun, Y.; Cong, Y.; Zheng, Y. The influence of borehole arrangements of soundless cracking demolition agents (SCDAs) on weakening the hard rock. *Int. J. Min. Sci. Technol.* 2021, 31, 197–207.
91. Zhang, Q.; He, M.; Wang, J.; Guo, S.; Guo, Z.; Liu, X.; Hu, J.; Ma, Z.; Fan, L.; Guo, P. Instantaneous expansion with a single fracture: A new directional rock-breaking technology for roof cutting. *Int. J. Rock Mech. Min.* 2020, 132, 104399.
92. Tang, S.B.; Huang, R.Q.; Wang, S.Y.; Bao, C.Y.; Tang, C.A. Study of the fracture process in heterogeneous materials around boreholes filled with expansion cement. *Int. J. Solids. Struct.* 2017, 112, 1–15.

93. Cui, X.; Zhang, J.; Guo, L.; Gong, X. Experimental Investigation of the Use of Expansive Materials to Increase Permeability in Coal Seams through Expansive Fracturing. *Shock Vib.* 2020, 2020, 7925724.

94. Akhvlediani, T.; Mataradze, E.; Chikhradze, N.; Gabadadze, T.; Suladze, I. Investigation of New Non-Explosive Demolition Agent for Use at Underground Mining of Hard Ores. *Min. Geol. Int. Sci. Conf.* 2008, 1, 281.

Bridging text between manuscripts

Following the literature review reported in Chapter 2, the first step in this research focuses on SCDA pressure estimation. The classical method in literature for pressure estimation uses a thick-walled cylinder that is filled with SCDA and monitored for tensile strain on the outer surface of the cylinder. Past research reported SCDA pressure for different commercial brands and for various inner diameter cylinders. The effect of host medium stiffness was never investigated before. As this could play a significant role on the SCDA pressure evolution, this research focused on examining the influence of host medium rigidity. Further, the determination of the SCDA pressure is based on an analytical solution for thick-walled cylinders subjected to uniform internal pressure. However, the calculated pressure in this way was never verified with direct measurements. In this research, direct measurement of SCDA pressure is done for the first time using a high-capacity pressure sensor. The results are used to validate the analytical model based on strain gauge readings. Based on the validation exercise, a new formula is derived to enable future use of the classical method – being more cost effective than the direct pressure measurement method – to estimate the actual SCDA pressure in the cylinder.

Previous studies did not attempt to estimate the modulus of elasticity of SCDA at peak pressure. This is an important input parameter for numerical modelling of the SCDA in a thick-walled cylinder. A new methodology based on numerical modelling and laboratory measurement is developed to help estimate the SCDA modulus of elasticity at peak pressure, a parameter that has not yet been determine in the literature.

The following chapter describes in detail the abovementioned research. It is a paper that is published in the International Journal of Mining Science and Technology.

Chapter 3

Methodology for the estimation of expansive cement borehole pressure

Note: This Chapter is a paper that is published in International Journal of Mining Science and Technology.

Abstract

This work is part of a multi-phase project which aims to develop a sound methodology for rock fragmentation in underground mines using expansive cement. More specifically, it is the first phase of the project which focuses on laboratory tests to investigate the mechanical performance of expansive cement, also known as Soundless Chemical Demolition Agents (SCDA). This paper reports the results of laboratory tests conducted on instrumented thick-walled cylinders filled with expansive cement. Expansive pressure evolution and temperature variation with time are first examined for different borehole diameters. The classical analytical method for expansive pressure estimation is validated with direct pressure measurement using high-capacity pressure sensor, and an empirical model is obtained. A new methodology based on iterative procedure is developed using axisymmetric finite element modelling and test results to derive the modulus of elasticity of the expansive cement at peak pressure. The results of this study show that the expansive pressure increases with borehole diameter when the rigidity of the steel cylinder is constant reaching 83 MPa for a 38.1 mm borehole. It is also shown that the expansive pressure decreases significantly with increased cylinder rigidity for the same borehole diameter. The newly developed methodology revealed that the modulus of elasticity of expansive cement at peak pressure is

estimated at 8.2 GPa. A discussion on the extension of the findings of this work to hard rock mining applications is presented.

3.1 Introduction

Class G cement, a common type of commercially available SCDA, is mainly composed of lime or calcium oxide which expands during curing when in confined conditions such as in a borehole. The source of expansion is owed to the hydration reaction of lime which results in the generation of portlandite crystals ($\text{Ca}(\text{OH})_2$ or calcium hydroxide) as shown in Eq. (3.1) [1].

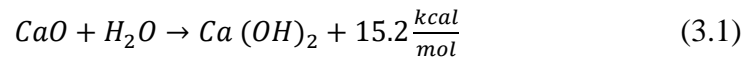


Figure 3.1 is a schematic presentation of the expansion mechanism for lime based expansive cement. As shown in Figure 3.1a) expansion starts off with the hydration of CaO resulting in the growth of solid calcium hydroxide crystals which come into contact with each other at a point, known as the critical degree of hydration (Figure 3.1b)). Beyond the critical degree of hydration (Figure 3.1c)), further growth of calcium hydroxide crystals results in the generation of expansive pressure under restrained condition.

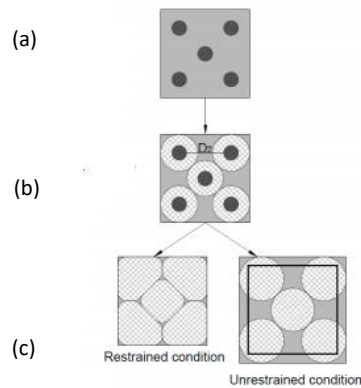


Figure 3.1 Sphere model for expansive pressure of calcium hydroxide. a) free lime b) critical degree of hydration, c) restrained and unrestrained conditions of calcium hydroxide crystals [2][3]

Expansive cement can be used as a method for rock or concrete fragmentation by means of injecting the mixture into drilled holes in the material of interest. Within a confined hole, pressure develops over time causing circumferential or tangential tensile stress. As shown in Figure 3.2, a fracture is created at the weakest section along the inside surface of hole. This occurs at a point where this surface intersects the free surface which is the hole boundary. The initial crack generation of the crack will only propagate when the tensile stress exceeds the tensile strength of the rock. Therefore, the tangential tensile stress generated by the SCDA or expansive cement, is responsible for fracturing of rock [4]. Currently, this method is used commonly in surface applications such as the demolition of concrete foundations in rehabilitation projects and fragmentation of rock in dimension stone quarries [5][6].

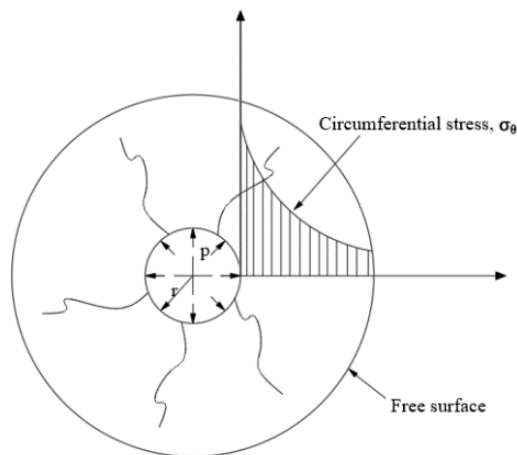


Figure 3.2 Fractural propagation in a borehole [modified after 4].

The early literature on expansive cement generally focuses on the investigation of the factors that affect the performance of expansive cement such as ambient temperature, borehole spacing and block pattern, water content etc. [1,7,8,9,10]. The research is now directed at the implementation of expansive cement in the field. To do so, finite element modeling has been used by Cho et.al

(2018) to predict the minimum pressure required of the SCDA for concrete demolition, hole spacing, and material properties [11]. Others used expansive cement to investigate discontinuity persistence along incipient discontinuities in the rock mass [12]. Expansive cements have also been used for well cementing as well as stimulating and enhancing fracturing for the oil and gas industry [13,14]. More recent work involved experimental work on dynamic propagation of fractures under various biaxial conditions where expansive cement is injected in two holes [15]. While much work has been dedicated to numerical simulation, researchers in Iran have suggested an algorithm to evaluate the first crack length with the use of expansive cement and verified it in a granite quarry in Iran [16]. More large-scale testing have been conducted by Tang et al (2021) whereby expansive cement was used to weaken the strong roof at the Pingdingshan coal mine to prevent rockbursts [17]. Zhang et al. (2020) used expansive cement or directional roof cutting at the Donglin coal mine [18]. Others focused on the handling of SCDA by developing special self-swelling SCDA cartridges to be used in up-tilt boreholes [19].

In this paper, the main research focus is proper quantification of expansive cement pressure and the role of host medium condition – an aspect that has often been overlooked by previous research. As shown in Table 3.1, manufacturers of different commercially available SCDA do report expansive pressures that range from 80 MPa to 137 MPa in temperatures between -8 °C to 40 °C [20-24]. However, how the expansive pressure is measured is unclear. The quantification of expansive cement pressure has been studied by many researchers in literature to explore potential applications that require a minimum pressure.

Table 3.1 Reported expansive pressure of different commercially available expansive cement [20-24]

Commercially Available SCDA	Recommended Temperature (°C)	Maximum Pressure (MPa)
Betonamit	-5° C to 35° C	80
Bristar	-5° C to 35° C	30
Dexpan	-5 °C to 40° C	124
Expando	0 °C to 35°C	124
Ecobust	-8 °C to 35°C	137

The thick-walled cylinder method is used by many researchers to quantify the expansive pressure of commercially available expansive cement, such as Bristar, Dexpan, and Betonamit. The expansive pressure can be calculated by pouring the expansive agent in a hollow thick-walled cylinder, whereby the cylinder is considered thick-walled when the thickness $t \geq 0.1$ the inner cylinder radius r_i (known as Hertzberg criterion). One or more strain gauges are installed on the outer surface of the cylinder in the tangential direction at about mid-height of the cylinder. The tangential strains of the specimen are then used to calculate the circumferential or radial pressure generated by the expansive agent as shown in Eq. (3.2) [25].

$$P_i = \frac{E\varepsilon_\theta(r_o^2 - r_i^2)}{2r_i^2} \quad (3.2)$$

where:

p_i : internal pressure, which in this case is the expansive pressure in MPa

E : modulus of elasticity of the steel cylinder (200,000 MPa)

r_o : outer radius of cylinder (mm)

r_i : inner radius of cylinder (mm)

ϵ_θ : circumferential or tangential strain on the external surface of the test cylinder

Natanzi et al., [7] investigated the effect of ambient temperature on the pressure development in two commercial expansive cement brands: Bristar and Dexpan. Using a 170 mm long, thick-walled cylinder ($r_o = 21 \text{ mm}, r_i = 18 \text{ mm}$) Dexpan exhibited a maximum expansive pressure of 28 MPa and 8 MPa at ambient temperature of 19 °C and 2 °C, respectively while Bristar exhibited an expansive pressure of 65 MPa and 18.5 MPa at the same ambient temperatures, respectively [7]. A recent study by Laefar et al. [26] has also conducted tests using thick-walled cylinders submerged in cold water baths to provide a heat sink to the surrounding rock or concrete. Their experimental results show that quadrupling the volume of SCDA and keeping the water bath temperature constant resulted in expansive pressure increase of 700%..Soeda [27] conducted studies on developing their own SCDA in granular form versus commercialized SCDA that is in its powder form to provide more space between grains for steam release and prevention of the gun phenomenon where the expansive cement spews out of the borehole. Using the thick-walled cylinder configuration, 19.6 MPa was achieved in 18 hours with the commercialized SCDA while their own developed SCDA, Type 1 and Type 2 generated 29.4 MPa in 2 hours and 29.4 MPa in 3 hours, respectively [27]. Studies conducted by Gholinejad & Arshadnejad [28] investigated the pressure in thick-walled cylinders made from different materials namely steel, aluminum, concrete, and high strength plastic were tested. Steel ($E=205 \text{ GPa}, r_i:10 \text{ mm}, r_o: 20 \text{ mm}$) generated 34 MPa in 30 hours, aluminum ($E=71 \text{ GPa}, r_i:20 \text{ mm}, r_o:30.25 \text{ mm}$) generated 30 MPa, concrete ($E= 12.1 \text{ GPa } r_i:18 \text{ mm}, r_o:41 \text{ mm}$) generated 16-17 MPa and high strength plastic ($r_i:7.5 \text{ mm}, r_o:12.5 \text{ mm}$) generated 0-1 MPa [28]. Other studies conducted by Hanif [6] studied the effect of

variable hole spacing in granite using Bristar-100S for optimal fracturing. Preliminary work involved the quantification of expansive pressure where 52 MPa was achieved in 144 hours using thick-walled cylinder where both ends were constrained by 18 mm thick steel plates [6]. Labuz & Dowding [29] have also used the thick-walled cylinder configuration to quantify the pressure of Bristar and selected the dimensions of the steel cylinder by equating the rigidity of the steel cylinder, R , to that of the rock as shown in Eq. (3.3).

$$R = \frac{E(r_o^2 - r_i^2)}{r_i^2} \quad (3.3)$$

It was shown that steel cylinders with approximately equal rigidities, but different geometries result in the same expansive pressure [29].

A modification of the thick-walled cylinder method termed the upper end surface method (UESM) was recently developed to estimate the pressure of SCDA. A notable difference between the thick-walled cylinder method and UESM is that the UESM container is composed of 7075 aluminum alloy rather than steel, which offers a longer path of heat transfer as well as a higher material heat conductivity, thereby avoiding lower temperature to the affixed strain gauge. Their studies confirm that both the thick-walled cylinder configuration and their newly developed UESM generate consistent results with each other [30].

The differences in expansive pressure estimates may be attributed to variations in the experimental configuration (in this case geometry) as well as the brand of expansive cement being used. Many researchers lack explanation behind the selection of the steel geometry which may differ in rigidities thereby may not reflect an accurate representation of SCDA pressure in hard rock. Since many factors must be taken into consideration when quantifying expansive cement pressure, no singular expansive pressure is reported for any expansive cement product. It is noteworthy that

due to the simplicity of Eq. (3.2), much of the previous studies rely on its use for borehole pressure estimation. A direct measurement of expansive pressure would be important not only to validate Eq. (3.2) but also to reveal the actual expansive cement pressure by deriving a correction factor to the analytical model Eq (3.2). A more robust approach in quantifying pressure is therefore required to properly estimate the obtained pressures in rock.

As shown in Eq. (3.1), the hydration reaction is an exothermic reaction which can sustain the expansive cement and host medium above ambient temperature. The relatively high temperature increases the rate of hydration of lime, one the main sources of expansion development [8]. Given the temperature of the expansive cement is also dependant on the thermal properties of the host medium, such as the heat capacity, heat conductivity, and density, the rate of reaction and therefore the rate of pressure generation is related to the thermal properties of the host medium. In addition, it is unclear if the rate of SCDA expansion affects the ultimate pressure given all other parameters are kept constant. It is therefore ideal to replicate the thermal properties of rock with the steel cylinder experiment, which is why past studies have tended to use thicker steel cylinders which provide a larger heat sink equivalent to an infinite rock medium [1,6,7,28,29]. However, given steel has a higher modulus of elasticity than rock, a balancing act between rigidity and heat sink size is required.

It is also postulated that larger SCDA borehole size increases the rate of reaction as the heat generating mass of SCDA increases proportional to the cube of the radius, while the borehole surface over which heat dissipates increases proportional to the square of the radius [8]. The effect of borehole size is therefore investigated while keeping the host medium rigidity, corrected for inner radius, constant. The effect of host medium radial rigidity is also investigated while keeping the borehole size constant. Overall, sufficient wall thickness is selected to fit the thick-walled

criterion while selecting sufficient wall thickness to dissipate heat. The goal of this study is to rationalize a systematic methodology to assess the pressure generation in varying host conditions to understand expansive cement performance in different host materials such as hard rock. Also, a simple iterative methodology is proposed for the estimation of the SCDA modulus of elasticity at peak pressure using direct pressure measurement and numerical modeling.

3.2 Materials and Method

3.2.1 Setup

Commercially available expansive cement selected for this investigation is Betonamit. The expansive cement was mixed with a water to cement ratio of 0.2 with a water temperature of 20°C. A water-to-cement ratio of 0.2 was adopted as per the manufacturer's instructions. Other ratios up to 0.3 were tried but did not produce optimal results. To ensure reliability and repeatability, all slurries were poured immediately upon mixing into a thick-walled steel cylinder. The expansive cement was poured by gravity into the borehole as per the instructions of the manufacturer. No sealing was deemed necessary. The expansive pressure was measured by using temperature compensating strain gauge glued to the outer surface of steel at mid-height. All test were conducted at room temperature of 21-22°C. The tangential strain was recorded over a period of 24 hours in ambient temperature of 21°C using the Micro-Measurements System 8000 Data Acquisition System. The expansive pressure is estimated using Eq. (3.2) with modulus of elasticity of the steel material $E = 200$ GPa. It is to be noted that while the rock mass is generally heterogeneous, the rock material surrounding an SCDA hole is considered intact. Clearly, the presence of joints in the rock mass would help accelerate the fracturing process. The assumption of using intact material as a host medium is reasonable considering the scale of the problem. Most research on borehole

mechanics considers intact rock material being stronger than the jointed rock mass, e.g., drilling and blasting [31-33]. Thus, the use of steel material as a host medium is deemed suitable. The rigidity of the steel for each test is also estimated using Eq. (3.3).

As Eq.3.2 [25] used to calculate the expansive cement radial pressure is based on the assumption of infinitely long pipe without a base, it deemed important to verify the minimum required length of the thick-walled cylinder to justify its use for pressure calculation. To validate the selected length of the cylinder and mid-height position of the strain gauge, several Finite Element (FE) axisymmetric Abaqus models were built: the first has an aspect ratio of 4 with a base plate as per the experiment while other FE models employed longer and shorter cylinders with a base plate, and aspect ratios larger and smaller than 4. Comparison of mid-height tangential strain of all FE models showed that the tangential strain readings are not influenced by the base plate when the aspect ratio is 4 or more. The tangential strain is nearly uniform along the length of the outer surface of the cylinder except near the base plate. Therefore, an aspect ratio of 4 (which is also the minimum recommendation by the manufacturer) is adopted for this study. FE modelling is discussed in section 3.6.

The experiment is designed to investigate the use of expansive cement for drift development in hard rock mines, with a hypothetical drift development cycle of 6 hours. Therefore, equal importance is given to the ultimate pressure as well as the pressure in 6 hours.

3.3 Test Identification

To identify different tests, the following nomenclature M-S-ID-OD-TB-XX was used. Refer to Table 3.2 for abbreviations.

Table 3.2 Abbreviations for Test Identification

M	Material e.g., S for steel
S	Shape of host medium, e.g., C for Cylinder
I.D	Internal Diameter in inches, e.g., 1.25 for 1.25"
O.D	Outer Diameter in inches, e.g., 1.75 for 1.75"
TB	Type of Base e.g., S for solid, W for welded
XX	Serial Number

The cylinder length was fixed at 4 times the inner diameter (4 x ID) as discussed above.

Refer to Figure 3.3 a-b) for steel configuration geometries.

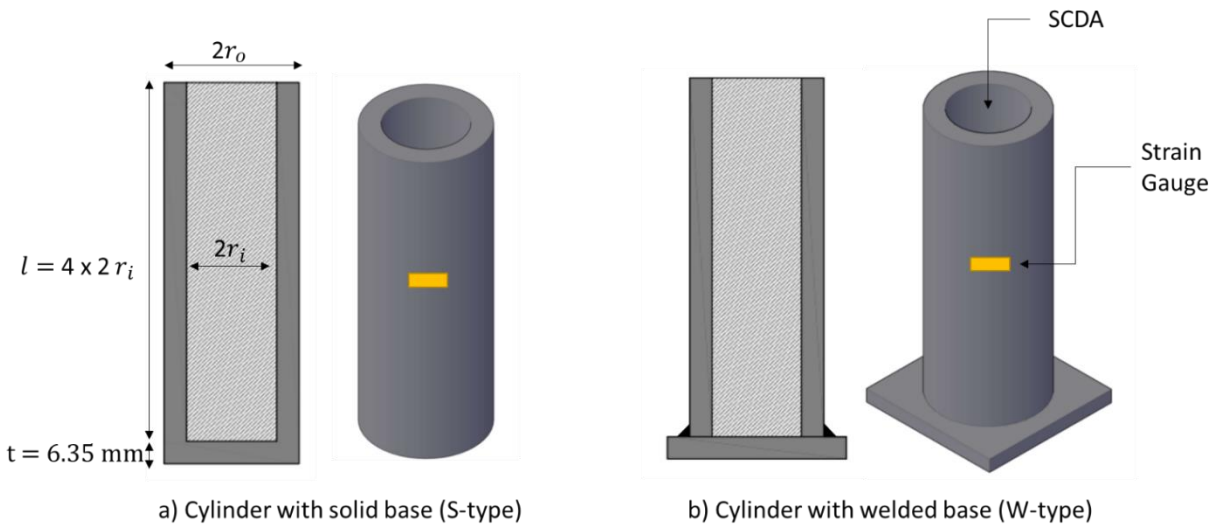


Figure 3.3 Steel cylinder configurations tested in this research

3.4 Tested configurations

Table 3.3 lists the three steel cylinder configurations that were tested in this study. As can be seen, the borehole sizes of 25.4 mm (1"), 31.75 mm (1.25") and 38.1 mm (1.5") are investigated in this

study. To ensure that the influence of the borehole size is adequately examined, the cylinders were fabricated to produce the same host medium rigidity as defined in Eq. (3.3).

Table 3.2 Summary of tested steel cylinder configurations.

Sample configuration	Inner diameter	Outer diameter	Rigidity (MPa) Eq. (3.3)
S-C-100-175-W	25.4 mm (1")	44.45 mm (1.75")	412500
S-C-125-227-S	31.75 mm (1.25")	57.60 mm (2.27")	460628
S-C-125-210-S		53.34 mm (2.1")	365384
S-C-150-275-S	38.1 mm (1.5")	69.85 mm (2.75")	472222
S-C-150-340-S		86.36 mm (3.40")	1008889
S-C-150-420-S		106.68 mm (4.20")	1368000

3.5 Experimental Results and Discussion

3.5.1 Effect of Borehole Size

As shown in Table 3.3, three borehole sizes of 25.4 mm (1"), 31.75 mm (1.25") and 38.1 mm (1.5") are investigated while keeping the steel cylinder rigidities nearly constant which were calculated from Eq. (3.3). Specimens S-C-100-175-W, S-C-125-227-S, and S-C-150-275 have rigidities of 412500 MPa, 460628 MPa and 472222 MPa respectively. Duplicates for each test were done to ensure repeatability and reliability. The 25.4 mm (1") borehole is used as reference to assess the effect of expansion pressure with increasing borehole size. A clear trend is observed with specimens of varying borehole size and similar rigidities as shown in Figure 3.4 whereby the development expansive pressure over time is proportional to the borehole size. The 38.1 mm (1.5") borehole exhibits a maximum pressure up of 60 MPa in only 6 h and the 31.75 mm (1.25") borehole shows a lower pressure 39.2 MPa in 6 h. However, a similar average maximum pressure is achieved for both 31.75 mm (1.25") and 38.1 mm (1.5") borehole size with pressures of 55.4 MPa

and 60 MPa respectively. Specimen S-C-100–175-W exhibits a lower pressure of 16.9 and 43 MPa in 6 and 24 h respectively.

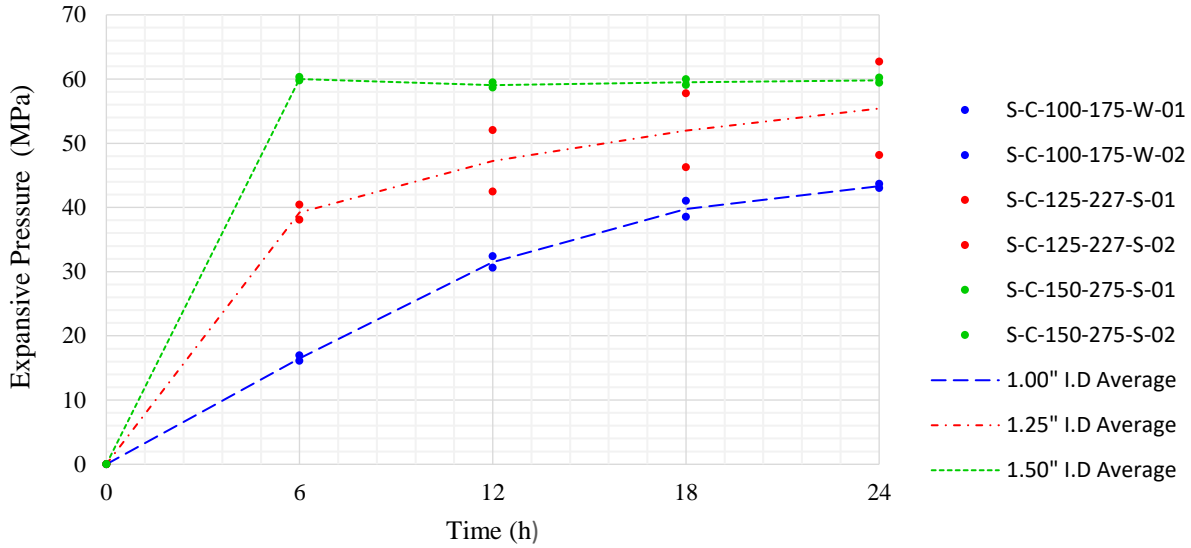


Figure 3.4 Expansive pressure of expansive cement with varying borehole size and constant rigidity (R)

3.5.2 Effect of host medium rigidity

The effect of host medium rigidity was tested while keeping the borehole size constant at 38.1 mm (1.5”). As shown in Table 3.2, three geometries were tested to investigate low to high rigidity host mediums calculated by Eq. (3.3) (low rigidity: S-C-150-275-S, medium rigidity: S-C-340-S, high rigidity: S-C-150-420). The experimental results are shown in Figure 3.5. As can be seen, a high host rigidity of 13680000 MPa (S-C-150-420-S) generates significantly less pressure than a low rigidity host of 472222 MPa (S-C-150-275-S) at 24 hours which generated expansive pressures of 29.7MPa and 60 MPa respectively while a medium host rigidity of 1008889 MPa (S-C-150-340-S) generated pressures of 43.6 MPa.

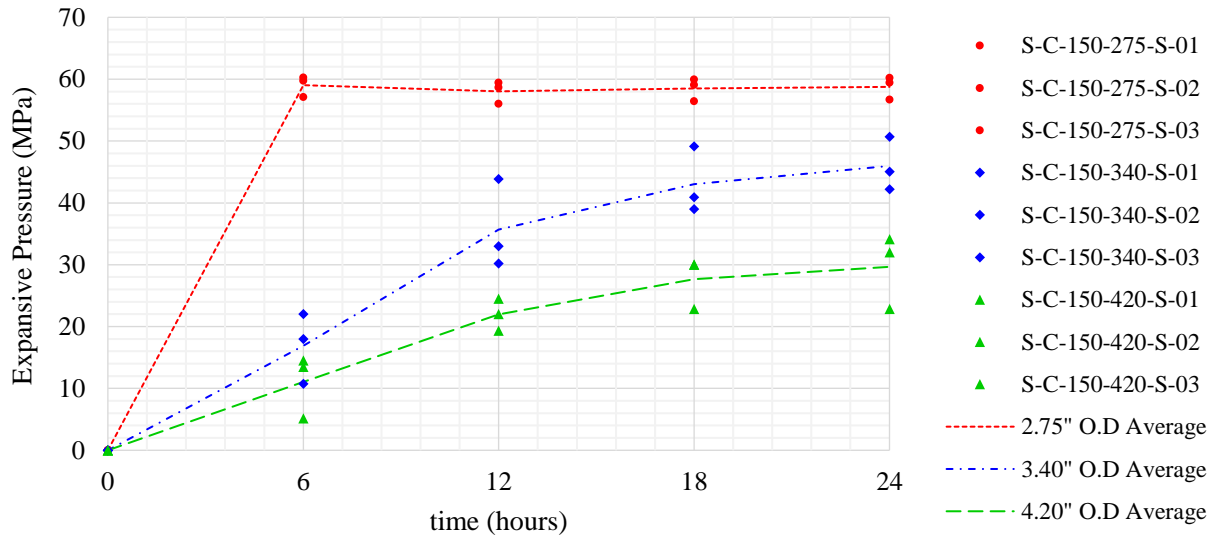


Figure 3.5 Expansive pressure evolution for varying host medium rigidity and a constant borehole size
38.1 mm (1.5")

The expansive pressure increases by 98.1% with a low rigidity compared to a high rigidity in 6 hours. It is also shown that the low rigidity host reaches its maximum expansive pressure early on in just 6 hours with 60 MPa. This increase in reaction rate can once again be attributed to an increase in expansive cement temperature. Since the specimens with a lower thickness provide a smaller heat sink for the expansive cement, the expansive cement temperature and therefore reaction rate is expected to be higher. However, it is also observed that the ultimate expansive cement pressure is also higher. It is once again unknown if the reaction rate and ultimate pressure are directly linked. Nonetheless, the experimental results show that the borehole size is not the only parameter affecting ultimate pressure, as tested in Section 3.5.1. It is observed that increasing the rigidity of the host medium to SCDA expansion may inhibit the reaction, reducing the ultimate pressure after 24 hours. In any case, it can be seen that ultimate pressures obtained in steel will differ from those obtained in rock, caused by either differing host rigidity, heat capacity, density, and heat transfer rate.

To conclude, the steel cylinder experiment is a well-established reference method that is commonly used to estimate the expansive cement peak pressure [8,25]. This test is adopted because the mechanical properties of the steel material are known, and the tensile strength is high enough to sustain the expansive pressure to its peak value. In practical rock fragmentation applications, it is reasonable to assume that $r_o \gg r_i$, hence the rigidity from Eq. (3.3) is reduced to:

$$R = E\left(\frac{r_o}{r_i}\right)^2 \quad (3.4)$$

However, these will be subject to further validation, which is beyond the scope of this work.

3.5.3 Direct Pressure Measurement

The thick-walled cylinder experiment for the expansive cement pressure calculation has the advantage of being simple and economical as it only requires the use of a strain gauge mounted on the outer surface of the cylinder. However, it has never been validated with direct measurement of the actual internal pressure in the cylinder. It is therefore important however to verify the accuracy of the method. To do so, a second experiment was designed and implemented with a pressure sensor inserted through the cylinder wall at its mid-height as shown in Figure 3.6a-c) along with a strain gauge on the outer surface. The sensor is model XPM6-1KBG and can measure a pressure range from 20 to 2000 bars. It would directly measure the actual pressure, P_a , which can then be compared to the calculated pressure P_c obtained from the strain gauge reading and Eq. (3.2).



Figure 3.6 Direct pressure measurement in specimen S-C-150-275-S with (a) Side view of XPM6-1KBG Miniature Pressure Sensor (b) Top view of XPM6-1KBG miniature pressure sensor threaded into wall cylinder (c) Expansive cement filled cylinder with embedded temperature sensor

The pressure sensor was directly connected to DAQ measuring the SCDA expansive pressure over a period of 24 hours. A series of six direct pressure measurement tests was conducted with 2 tests for each SCDA hole size namely 25.4 mm (1.00”), 31.75mm (1.25”), and 38.1 mm (1.5”). The pressure evolution and temperature readings with time is depicted in Figure 3.7 and Figure 3.8 respectively.

As shown in Figure 3.7, pressures of 8 MPa, 55 MPa and 65 MPa are achieved in 6 hours for specimen S-C-100-175-W, S-C-125-210-S and S-C-150-275-S respectively (Refer to Table 3.3 for specimen specifications). It is also shown that pressures of 56 MPa, 71 MPa and 83 MPa are achieved in 24 hours for specimen S-C-100-175-W, S-C-125-210-S and S-C-150-275-S respectively (Refer to Table 3.3 for specimen specifications). The measured pressure data is also in accordance with the results presented in Section 3.5.1, where a higher ultimate pressure is attained faster for larger borehole diameters.

As shown in Figure 3.6c), the heat of hydration produced during the SCDA reaction was also measured throughout the testing period using thermocouples embedded in the SCDA. As shown in Figure 3.8, a peak hydration heat of 50.8 °C was recorded at 5 hours for specimen ID S-C-150-

275-S while a peak hydration of 39.9°C and 40.1°C was recorded at 5 h for specimen ID S-C-100-175-W and S-C-150-275-S. Figure 3.8 shows that the borehole size is correlated to the degree of heat generation. Based on the experimental results, higher heat generation corresponds to higher SCDA expansive pressure which is owed to the increased mass of SCDA relative to the surface area on which pressure is applied and through which heat is exchanged with the host medium. This is in accordance with studies conducted with Hinze & Brown [8] which elucidate that a large diameter provides more space for free lime to be hydrated in the borehole. As shown in Eq. (3.1), the hydration reaction is an exothermic one where this heat indirectly speeds the rate of pressure evolution [8].

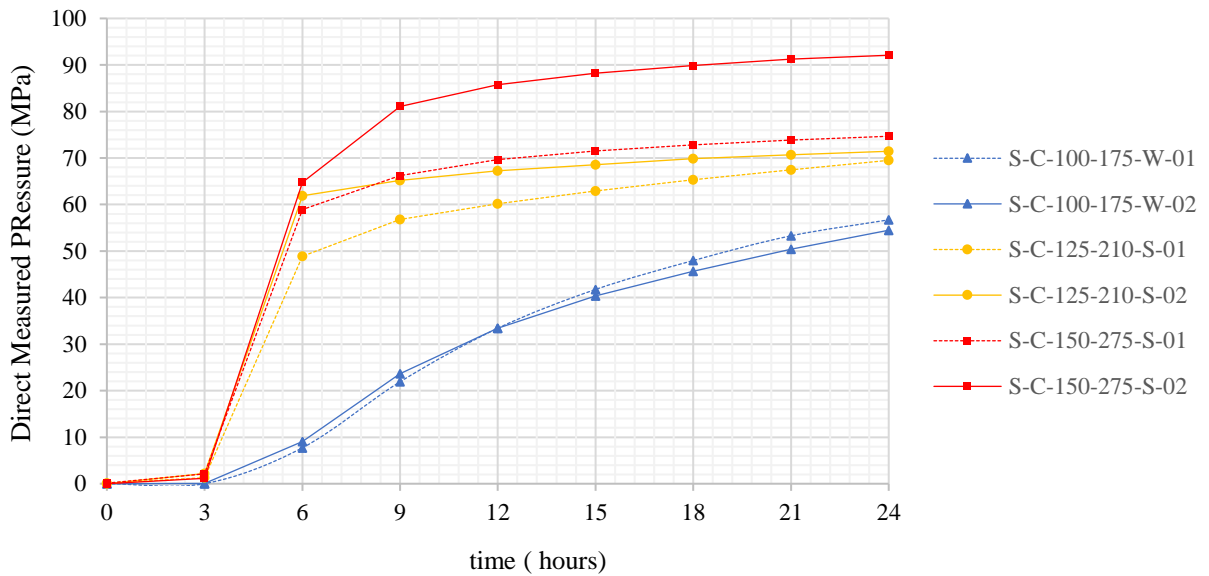


Figure 3.7 Measured Expansive Pressure of varying borehole size

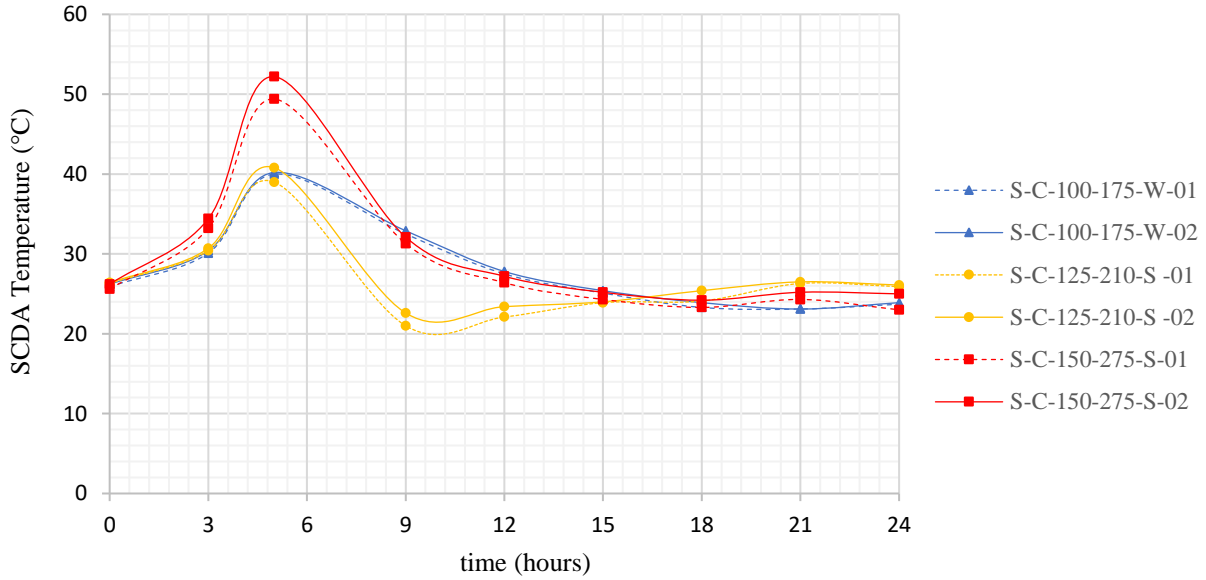


Figure 3.8 Expansive Cement heat of hydration with time of varying borehole size

Figure 3.9 plots the comparison between the actual and calculated peak pressure after 24 hours.

As can be seen, the actual peak pressure is consistently higher.

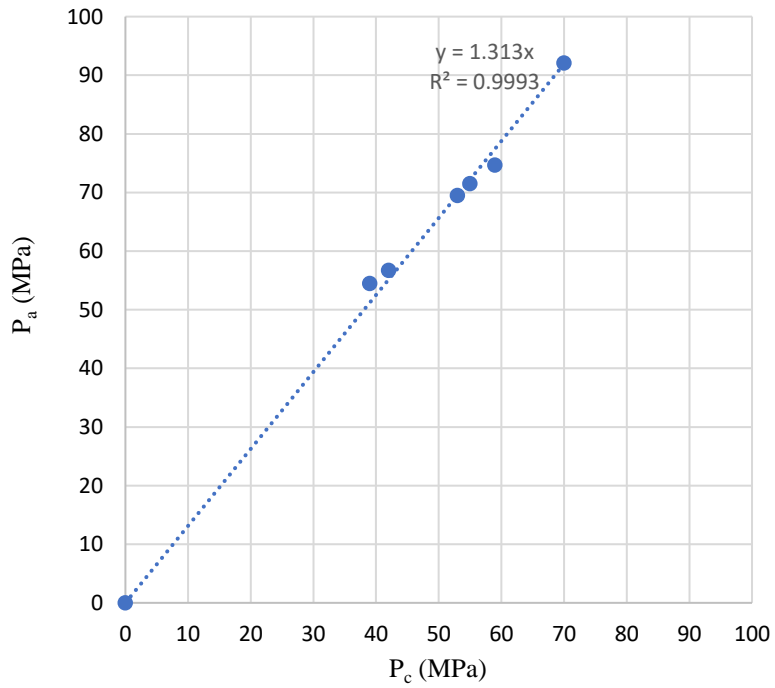


Figure 3.9 Measured peak pressure (Pa) vs. calculated peak pressure (Pc)

A best fit line with an R^2 factor of 0.999 is obtained as follows.

$$p_a = \alpha p_c \quad (3.5)$$

where $\alpha = 1.31$ is a correction factor to the calculated pressure. Although costly, the direct pressure measurement experiment confirms the validity of the less expensive method employing only a strain gauge on the outer surface, albeit with a correction factor.

3.6 Finite element model

Numerical modelling studies of expansive cement mechanical behaviour could benefit from the knowledge of the peak modulus of elasticity of the expansive cement at peak pressure, E_p . As the actual pressure value is known from the direct pressure measurement experiment, it is used as a model input parameter to obtain the modulus of elasticity of the expansive cement material using the axisymmetric model through simple iterative process.

First, an axisymmetric finite element (FE) model of the steel cylinder was constructed in Abaqus/CAE 2019. The purpose of the model is to derive the elasticity of the expansive cement material for a given expansive pressure as will be explained further. As shown in Figure 3.10, the FE model is axisymmetric and linear elastic; it consists of two zones: a steel cylinder part and an expansive cement part. The contact surface between the steel and SCDA is treated as hard contact in the normal direction and frictional in the tangential direction with a friction penalty of 0.3. Table 3.4 presents the material properties. The Poisson's ratio of the SCDA is assumed to be 0.2 and the modulus of elasticity is to be determined (TBD).

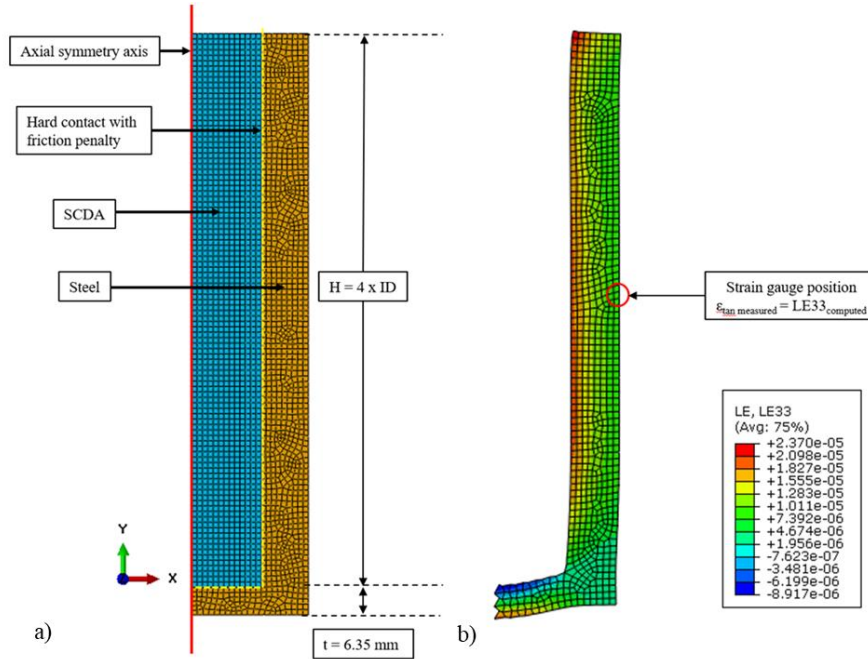


Figure 3.10 Model of axisymmetric steel cylinder (a) Geometry (b) Out-of-plane strain with scaled deformations

The SCDA pressure is modeled as initial stress or pre-defined field in the initial step. The pressure is subsequently released in a second static step. From the model output, the tangential strain component LE33 at the location of the strain gauge (see Figure. 3.10b) is extracted.

Table 3.4 Material Properties for the FE model

Material Properties		
Material	Young's modulus	Poisson's ratio
SCDA	TBD	0.2
Steel	200 GPa	0.3

As shown from the flowchart in Figure 3.11, the iteration begins with an initial value of $E=1$ GPa and subsequent increments $\Delta E =1$ GPa. For a given steel cylinder specimen ($r_0, r_i, L, E_{\text{steel}}$), the FE model is run for the tangential strain ϵ_θ from which the corrected pressure αp_c can be calculated from Eq. (3.5). Iteration continues with $\Delta E =1$ GPa and subsequently with $\Delta E =-0.1$ GPa until the

measured and calculated pressures match. The calculation process was done for all six specimens tested with the pressure sensor.

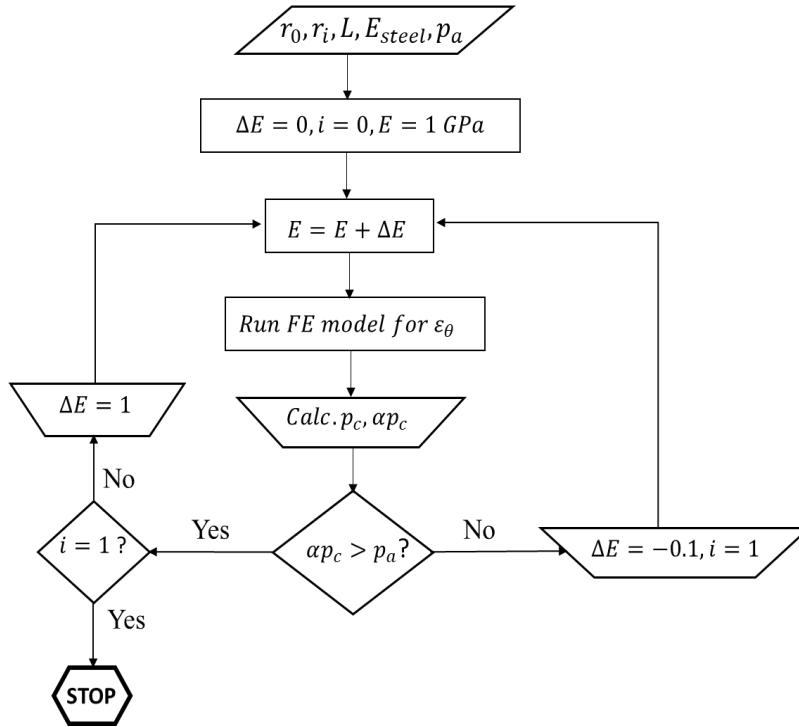


Figure 3.11 Iterative procedure to determine SCDA modulus of elasticity of expansive cement at peak pressure.

The results shown in Table 3.5 reveal that E_p varies between 8.1 and 8.35 GPa with an average of 8.2 and a coefficient of variation of only 0.01243. This SCDA peak modulus of elasticity can be used as an input parameter for future modelling studies on expansive cement.

Table 3.3 The modulus elasticity of expansive cement with varying borehole size

Specimen	100-175 -01	100-175-02	125-210-01	125-210-02	150-275-01	150-275-02
E_{Peak} (GPa)	8.1	8.1	8.2	8.2	8.3	8.35

3.7 Conclusions

This work is part of a multi-phase project which aims to develop a sound methodology for rock fragmentation in underground mines. More specifically, it is the first phase of the project which focuses on laboratory tests to investigate and optimize the mechanical performance of SCDA in various conditions. Based on the findings of this work, future work will extend to the investigation of SCDA performance in hard rocks commonly encountered in Canadian mines such as granite, gabbro, and norite. This chapter examines expansive cement pressure variation with host medium rigidity – an aspect that has often been overlooked by previous research. The effect of borehole size with time is first investigated while keeping the host medium rigidity constant for borehole sizes of 25.4 mm (1”), 31.75 mm (1.25”), and 31.8mm (1.5”). The results show that the estimated peak expansive pressure is proportional with the borehole diameter. This is in line with previous research findings [1,8]. However, when the host medium rigidity is increased, the estimated expansive pressure is reduced significantly. The practical implication of this finding is that the expansive SCDA peak pressure in hard rocks such as gabbro and norite commonly encountered in metal mines is likely to be less than that in sedimentary rocks such as limestone and mudstone commonly found in coal mines.

The classical analytical method for expansive pressure estimation in a thick-walled cylinder has been used extensively in previous research, however, it has never been validated with direct measurement of the actual internal pressure in the cylinder. A series of tests employing direct pressure measurement using high-capacity pressure sensor was carried out. The results show that the actual expansive peak pressure is consistently higher than the estimated peak pressure from the analytical model. A correction factor is derived with $R^2 = 0.999$. Finally, a new methodology based on iterative procedure is developed using axisymmetric finite element modelling and test results

to derive the SCDA modulus of elasticity. Recognizing the variation of pressure and elasticity with time, the focus is on the peak pressure and hence the peak modulus of elasticity. The methodology reveals that the modulus of elasticity of expansive cement at peak pressure is on average 8.2 GPa with a coefficient of variation of only 0.012. This result should prove useful in numerical modelling studies of SCDA hole pattern design in practical mining applications.

References

- [1] K. Soeda, T. Harada, The Mechanics of Expansive Pressure Generation with expansive demolition agent, *Trans. Jpn. Soc. Civ. Eng.* 19 (1993) 121–135.
- [2] A. Bentur, M. Ish-Shalom, Properties of type K expansive cement of pure components II. Proposed mechanism of ettringite formation and expansion in unrestrained paste of pure expansive component, *Cem. Concr. Res.* 4 (1974) 709–721. [https://doi.org/10.1016/0008-8846\(74\)90043-X](https://doi.org/10.1016/0008-8846(74)90043-X).
- [3] R.V. De Silva, R.P. Gamage, M.S. Anne Perera, An alternative to conventional rock fragmentation methods using SCDA: A review, *Energies.* 9 (2016) 1–31. <https://doi.org/10.3390/en9110958>.
- [4] T. Harada, T. Idemitsu, A. Watanabe, S. ichi Takayama, Design Method for the Demolition of Concrete With Expansive Demolition Agent., 1987. https://doi.org/10.1007/978-1-4612-3578-1_5.
- [5] D.F. Laefer, N. Ambrozevitch-Cooper, M.P. Huynh, J. Midgette, S. Ceribasi, J. Wortman, Expansive fracture agent behaviour for concrete cracking, *Mag. Concr. Res.* 62 (2010) 443–452. <https://doi.org/10.1680/macr.2010.62.6.443>.
- [6] M. Hanif, Effective Use of Expansive Cement for the Deformation and Fracturing of Granite, *Gazi Univ. J. Sci.* 20 (2010) 1–5.
- [7] A.S. Natanzi, D.F. Laefer, L. Connolly, Cold and moderate ambient temperatures effects on expansive pressure development in soundless chemical demolition agents, *Constr. Build. Mater.* 110 (2016) 117–127. <https://doi.org/10.1016/j.conbuildmat.2016.02.016>.
- [8] J. Hinze, J. Brown, Properties of Soundless Chemical Demolition Agents, *Constr. Eng. Manag.* 120 (1995)

816–827. [https://doi.org/10.1016/0148-9062\(95\)93364-U](https://doi.org/10.1016/0148-9062(95)93364-U)

- [9] M. Hanif, Deformation Behaviour of Rock around a Borehole Filled with an Expansive Cement, *J. King Abdulaziz Univ. Sci.* 9 (1997) 93–107. <https://doi.org/10.4197/eng.9-1.6>.
- [10] M.D. Cohen, Modeling of expansive cements, *Cem. Concr. Res.* 13 (1983) 519–528. [https://doi.org/10.1016/0008-8846\(83\)90011-X](https://doi.org/10.1016/0008-8846(83)90011-X).
- [11] K. Kim, H. Cho, D. Sohn, J. Koo, J. Lee, Prediction of the Minimum Required Pressure of Soundless Chemical Demolition Agents for Plain Concrete Demolition, *J. Comput. Struct. Eng. Inst. Korea.* 31 (2018) 251–258. <https://doi.org/10.7734/coseik.2018.31.5.251>
- [12] J. Shang, S.R. Hencher, L.J. West, K. Handley, Forensic Excavation of Rock Masses: A Technique to Investigate Discontinuity Persistence, *Rock Mech. Rock Eng.* 50 (2017) 2911–2928. <https://doi.org/10.1007/s00603-017-1290-3>.
- [13] P. Parker, W. Walh, Expanding Cement- A new development in Well Cementing, *J. Pet. Technol.* (1966) 559–564.
- [14] V.R.S. De Silva, P.G. Ranjith, M.S.A. Perera, B. Wu, T.D. Rathnaweera, A modified, hydrophobic soundless cracking demolition agent for non-explosive demolition and fracturing applications, *Process Saf. Environ. Prot.* 119 (2018) 1–13. <https://doi.org/10.1016/j.psep.2018.07.010>.
- [15] L. Wang, K. Duan, Q. Zhang, X. Li, R. Jiang, Study of the Dynamic Fracturing Process and Stress Shadowing Effect in Granite Sample with Two Holes Based on SCDA Fracturing Method, *Rock Mech. Rock Eng.* (2022). <https://doi.org/10.1007/s00603-021-02728-0>.
- [16] S. Arshadnejad, K. Goshtasbi, J. Aghazadeh, A model to determine hole spacing in the rock fracture process by non-explosive expansion material, *Int. J. Miner. Metall. Mater.* 18 (2011) 509–514. <https://doi.org/10.1007/s12613-011-0470-5>.
- [17] W. Tang, C. Zhai, J. Xu, Y. Sun, Y. Cong, Y. Zheng, The influence of borehole arrangement of soundless cracking demolition agents (SCDAs) on weakening the hard rock, *Int. J. Min. Sci. Technol.* 31 (2021) 197–207. <https://doi.org/10.1016/j.ijmst.2021.01.005>.

- [18] Q. Zhang, M. He, J. Wang, S. Guo, Z. Guo, X. Liu, J. Hu, Z. Ma, L. Fan, P. Guo, Instantaneous expansion with a single fracture: A new directional rock-breaking technology for roof cutting, *Int. J. Rock Mech. Min. Sci.* 132 (2020) 104399. <https://doi.org/10.1016/j.ijrmms.2020.104399>.
- [19] S. Xu, P. Hou, R. Li, M. Cai, An Experimental Study on the Mechanical Properties and Expansion Characteristics of a Novel Self-Swelling Cartridge for Rock Breakage, *Rock Mech. Rock Eng.* 54 (2021) 819–832. <https://doi.org/10.1007/s00603-020-02305-x>.
- [20] Betonamit (n.d).<https://www.betonamit.com/en/> 2021 (Accessed 17 September 2021).
- [21] Bristar cracking agent and expnasive mortar (n.d). <https://www.silentech.com.au/bristar.html> (Accessed 17 September 2021).
- [22] Dexpan, (n.d.). Dexpan.<https://www.dexpan.com/> (2021) (Accessed 17 September 2021).
- [23] Expando.<https://expando.com.au/> 2021 (Accessed 17 September 2021).
- [24] Ecobust.<http://www.ecobust.com/> 2011 (Accessed 17 September 2021).
- [25] J. S, Timoshenko, Goodier, Theory of elasticity, *Phys. Contin. Media.* (1951) 234–259. <https://doi.org/10.1201/b16095-7>.
- [26] D.F. Laefer, A.S. Natanzi, S.M.I. Zolanvari, Impact of thermal transfer on hydration heat of a Soundless Chemical Demolition Agent, *Constr. Build. Mater.* 187 (2018) 348–359. <https://doi.org/10.1016/j.conbuildmat.2018.07.168>.
- [27] H. K, Soeda, H, Fast-Acting Non-Explosive Demolition Agent, *Conf. Demolition Reuse Concr.* (1994) 231–241.
- [28] M. Gholinejad, S. Arshadnejad, An experimental approach to determine the hole-pressure under expansion load, *J. South. African Inst. Min. Metall.* 112 (2012) 631–635.
- [29] L. Charles H, Dowding, Joseph F, Fracturing of Rock with Expansive Cement, *J. Geotech. Eng. Div.* (2017).
- [30] S. Xu, P. Hou, R. Li, F.T. Suorineni, An improved outer pipe method for expansive pressure measurement of static cracking agents, *Int. J. Min. Sci. Technol.* (2021). <https://doi.org/10.1016/j.ijmst.2021.11.011>.

- [31] E. Hoek, C.D. Martin, Fracture initiation and propagation in intact rock - A review, *J. Rock Mech. Geotech. Eng.* 6 (2014) 287–300. <https://doi.org/10.1016/j.jrmge.2014.06.001>.
- [32] J. Peng, G. Rong, M. Cai, X. Wang, C. Zhou, An empirical failure criterion for intact rocks, *Rock Mech. Rock Eng.* 47 (2014) 347–356. <https://doi.org/10.1007/s00603-012-0355-6>.
- [33] J. Park, K. Kim, Use of drilling performance to improve rock-breakage efficiencies: A part of mine-to-mill optimization studies in a hard-rock mine, *Int. J. Min. Sci. Technol.* 30 (2020) 179–188. <https://doi.org/10.1016/j.ijmst.2019.12.021>.

Bridging text between manuscripts

The next step in this research is to focus on the breakage of hard rock using SCDA injected in a single hole in a block of hard rock. The goal is to gain better understanding of 1) the time at which cracking initiates, to be called time to critical strain or TCS, 2) time to first crack that can be visualized or TFC, and 3) minimum time needed for demolition or MDT. To do so, two sets of experimental tests are carried out to identify the effect of SCDA on hard rock breakage with the first set conducted on unloaded blocks, and the second under uniaxial loading condition.

Stanstead granite prismatic specimens of 152.4 mm (6'') x 152.4 mm - 203.2 mm (6-8'') x 406.4 mm (16'') are instrumented with strain gauges and used to test the influence of borehole size on the time to fracturing (TCS, TFC, and MDT) with SCDA borehole size of 25.4 mm (1''), 31.75 mm (1.25'') and 38.1 mm (1.5''). Strains are recorded over time until MDT is reached. It is shown that the fracturing time decreases with increasing borehole size. It is also shown that specimens subjected to uniaxial compression of 5 MPa fracture as early as 7 hours after SCDA mixing. A borehole spacing to borehole diameter ratio of 12.8 to 14.6 is suggested for practical applications. This work, reported in Chapter 4, is now a paper published in the International Journal of Coal Science and Technology.

Chapter 4

Laboratory investigation into the use of soundless chemical demolitions agents for the breakage of hard rock

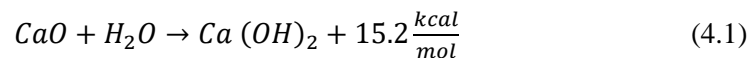
Note: This Chapter is a paper that is published in International Journal of Coal Science and Technology.

Abstract

The method of drilling and blasting with explosives is widely used in rock fragmentation applications in the mining industry for mine development and ore production. However, the use of explosives is associated with rigorous safety and environmental constraints as blasting creates toxic fumes, ground vibrations, and dust. This study is focused on the use of Soundless Chemical Demolition Agents (SCDA) as a more environmentally friendly method for rock breakage and a potential replacement of explosives. In this paper, the results of a series of experimental tests are reported to identify the effect of SCDA on hard rock breakage under no load and under uniaxial loading conditions. Stanstead granite prismatic specimens of 152.4 mm (6'') x 152.4 mm - 203.2 mm (6-8'') x 406.4 mm (16'') are used to test the influence of borehole size on the time to fracturing with SCDA borehole size of 25.4 mm (1''), 31.75 mm (1.25'') and 38.1 mm (1.5''). It is shown that the fracturing time decreases with increasing borehole size. It is also shown that specimens subjected to uniaxial compression of 5 MPa fracture as early as 7 hours after SCDA mixing. A borehole spacing to borehole diameter ratio of 12.8 to 14.6 is suggested for practical applications.

4.1 Introduction

The most conventional method of hard rock fragmentation in the mining industry is the drill and blast method. Commonly used explosives in the mining industry are ammonium nitrate fuel oil (ANFO), black powder, and to a lesser extent dynamite. Ammonium nitrate is an oxidizing agent that not only supplies oxygen to initiate and support combustion of the fuel, but it is also an explosive where on occasion ammonium nitrate can self-detonate posing a higher risk to workers (Farnfield & Wetherelt, 2004). Given the risks posed by using explosives underground, along with the negative impacts such as the generation of toxic fumes and dust, there is a demand for alternative methods to fracture rocks. During the past three decades, several methods have been proposed for rock fragmentation without explosives. Such methods include Thermal Fragmentation, Plasma Blasting, Controlled Foam Injection, Radial-Axial Splitter, and Supercritical Carbon Dioxide. More details on the pros and cons of such methods are in Habib et al., (2022). Soundless Chemical Demolition Agents (SCDA) is a promising method for rock fragmentation without explosives. SCDA, otherwise known as expansive cement, is a self-stressing cement containing Ordinary Portland Cement (OPC) and an expansive agent which is the source of the expansion pressure. The high expansion and hardening of the SCDA causes the breakage of the surrounding material such as rock (Taylor, 1997). A common expanding agent is calcium oxide (CaO) which upon hydration, the generated calcium hydroxide crystals exert significant pressure in a confined space (Refer to Eq. (4.1)).



This explosive-free method has been explored by many researchers to optimize crack propagation in rock. Studies conducted by Hanif (2010) have investigated the effect of borehole spacing in

granite rock to optimize crack propagation. It was shown that holes with gradually increasing spacing between consecutive holes cause the fracture to be initiated much sooner compared to the holes with uniform spacing (Hanif, 2010). Gambatese (2003) studied controlled fracturing on concrete by introducing non-injected holes, and observed that cracks migrated to the non-injected holes of the block (Gambatese, 2003). Large scale studies done by Laefar et al. (2010) have tested breakage of concrete with the use of Bristar, a commercially available SCDA, testing several concrete blocks (0.76 m^3) of varying target strengths between 3-42.9 MPa with a central hole with 38 mm in diameter and 640 mm in depth. Key findings are that higher material strength took longer to initiate cracking and to obtain a 25.4 mm crack width. However, in a material having a tensile strength of less than 12 MPa, a cracking width of 25.4 mm was consistently observed within 24 hours (Laefar et al., 2010). Small-scale laboratory experiments were conducted to test the efficacy of a commercially available SCDA, Betonamit, on norite rock subjected to uniaxial compression. Under uniaxial loading conditions, rock breakage occurs in the direction of the major principal stress. Under no load, rock breakage occurs in a randomized pattern (Musunuri & Mitri, 2009). Other works conducted by Habib (2019) have also investigated the effect of the addition of calcium chloride in SCDA to accelerate the breakage of crack initiation in concrete. It was shown that with the addition of 3% of calcium chloride BWOW (by weight of water), a higher degree of crack growth is noticed compared to the control sample without additive (Habib, 2019). Gomez & Mura (1984) proposed a minimum spacing between SCDA holes to be less than 8 times the hole diameter for hard rocks, 8 to 12 times for medium hard rock, and 12 to 18 times the SCDA hole diameter for soft rocks (Gomez & Mura, 1984). Arshadnejad et al. (2011) developed a more comprehensive empirical formula to estimate the optimal spacing in rock between holes in terms of hole diameter, expansive pressure as well as the material's tensile strength and fracture

toughness (Arshadnejad et al., 2011). Apart from the extensive work done on breaking concrete and hard rock with the use of SCDA, much research has been dedicated to quantifying the pressure of SCDA using steel pipes. The most common experiment uses the thick-walled cylinder configuration where SCDA is poured into the cylinder or borehole and a strain gauge is affixed to the outer surface to record the tangential strain due to expansive pressure. This serves as the main output to estimate the pressure of SCDA (Soeda & Harada, 1993; Hinze & Brown, 1994; Hanif, 2010; Laefer et al., 2010; Arshadnejad et al., 2011; Gholinejad & Arshadnejad, 2012).

The expansive pressure is estimated from the analytical equation of thick-walled cylinder subjected to internal pressure (Timoshenko & Goodier, 1951). However, numerous studies neglect to consider the influence of the stiffness of the steel cylinder and its relation to that of rock. Since the effect of host stiffness is not well studied, the reported pressures may not be valid for rock. Moreover, given that the high heat of hydration associated with the chemical reaction of lime-based expansive cement (refer to Eq. (4.1)), can also affect the SCDA pressure, and since steel is highly conductive compared to rock, it is of critical importance to estimate the pressure in real conditions such as in rock where a much higher heat sink is present.

So far it is known that the breakage of rock occurs when the tensile strength of the rock to be demolished is exceeded (Harada et al., 1989). However, it is not clear what the pressure evolution is over time up until crack initiation occurs in rock. This study performs a series of experiments on granite slabs with a single SCDA hole under load and no load to retrieve raw strain measurements up until fracture for future work and to be used as a basis of calibration.

4.2 Experimental Program

To begin, the influence of borehole diameter on SCDA in Stanstead granite slabs is investigated. The slab dimensions are 152.4 mm (6'') x 152.4 mm - 203.2 mm (6-8'') x 406.4 mm (16'') and no load is applied. The tested borehole size diameters are 25.4 mm (1''), 31.75 mm (1.25'') and 38.1 mm (1.5''). The second part of the experimental program studies the effect of SCDA-filled borehole subjected to uniaxial compressive stress with two borehole diameter sizes namely 38.1 mm (1.5'') and 44.45 mm (1.75''). The commercially available SCDA selected for this study is Betonamit. All SCDA grouts are mixed consistently for 10 minutes and poured directly into the borehole. SCDA performance was assessed in three ways:

1. Measured strains around the borehole; 2 strain gauges, one above (SG1) and one below (SG3) the borehole, placed horizontally, and 2 strain gauges, one to the right (SG2) and one to the left (SG4) of the borehole, placed vertically (refer to Figure 4.1 for the location of strain gauges).
2. Visual cracking with a time-lapse camera.
3. Time of first crack (TFC) and at time at which the slab is fully fractured.

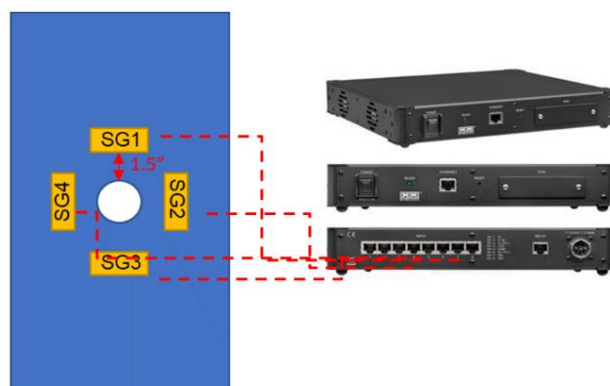


Figure 4.1 Location of strain gauges

A total of 10 rock slabs were tested in this study. To identify each sample, the following nomenclature M-SL#-ID-HD-HL-L-XX was adopted.

- M: Material, e.g., G for Granite
- SL#: Slab #, e.g., SL1 (152.4 mm (6'') x 152.4 mm (6'') x 406.4 mm (16'')) or SL2 (152.4 mm (6'') x 203.3 mm (8'') x 406.4 mm (16''))
- ID: Internal Diameter in inches, e.g., 125 for 158.75 mm (1.25'') borehole.
- HD: Hole Depth in inches, e.g., 625 for 158.75 mm (6.25'')
- HL: Hole location, e.g., M for middle, LT for lower third, UT for upper third
- L: Loaded Slab at 5MPa
- XX- Serial Number

The hole depth was fixed at 4-5 times the SCDA hole diameter. The strain gauges were placed 38.1 mm (1.5'') away from the edge of the borehole; 2 below and 2 on the sides (refer to Figure 4.1). As shown in Figure 4.2a), a 200-tonne uniaxial compression frame was used for the loaded specimens. For the loaded specimens, the top surface of the granite slab was greased with MoS₂ to reduce friction between the metal loading plate and the rock. Table 4.1 reports the configuration of the slabs tested in this study.

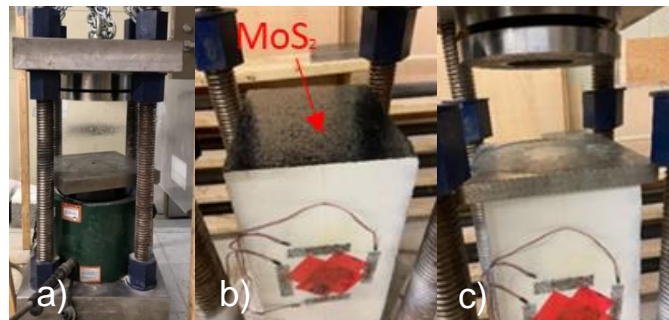


Figure 4.2 Test set-up for loaded specimens a) 200-tonne uniaxial compressive rig b) greased top surface of rock specimen c) metal loading plate placed on rock specimen

Table 4.1 Description of tested specimens

Sample Configuration	SCDA Borehole Diameter	Borehole Depth
G-SL1-100-500-M-01	25.4 mm (1.00'')	127 mm (5.00'')
G-SL1-100-500-M-02	25.4 mm (1.00'')	127 mm (5.00'')
G-SL1-100-500-M-03	25.4 mm (1.00'')	127 mm (5.00'')
G-SL2-125-625-M-01	31.75 mm (1.25'')	158.75mm (6.25'')
G-SL2-125-625-M-02	31.75 mm (1.25'')	158.75mm (6.25'')
G-SL2-150-600-M-01	38.1 mm (1.50'')	152.4 mm (6.00'')
G-SL2-150-600-M-02	38.1 mm (1.50'')	152.4 mm (6.00'')
G-SL2-150-600-UT-L	38.1 mm (1.50'')	152.4 mm (6.00'')
G-SL2-175-700-LT-L	44.45mm (1.75'')	177.8 mm (7.00'')
G-SL2-175-700-M-L	44.45mm (1.75'')	177.8 mm (7.00'')

4.3 Results and Discussion

4.3.1 Rock Characterization

A series of Brazilian tests were conducted to determine the tensile strength on the slabs (refer to Figure 4.3 for test set-up). The Stanstead granite samples were cored from the granite slab and prepared in compliance with the ASTM D3967 Standard. The results give a mean value of 7.5 MPa with a standard deviation of 0.33.

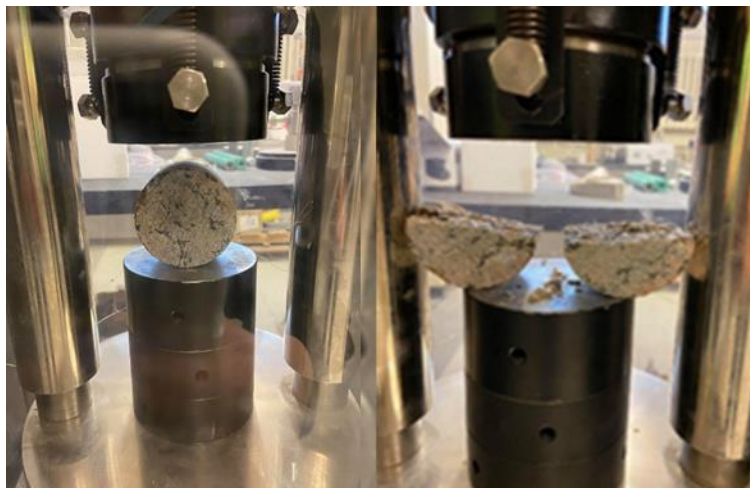


Figure 4.3 Brazilian test set-up on Stanstead granite core

4.3.2 The influence of borehole size on granite

The effect of three borehole sizes (25.4 mm (1''), 31.75 mm (1.25'') and 38.1 mm (1.5'')) was investigated in a Stanstead granite slab with dimensions 152.4 mm (6'') x 152.4 mm- 203.2 mm (6-8'') x 406.4 mm (16'') (width x length x height). Each configuration was tested in duplicates to ensure repeatability and reliability. As shown in Figure 4.1, the strain gauges were placed 38.1 mm (1.5'') away from the borehole on each side, above and below borehole, and on the sides. The strains were measured until the first fracture appears, after which the strain gauges are potentially damaged due to localised splitting of the rock. The goal of the experiment is to identify the time of cracking using the measured strains in conjunction with timelapse photos of the slab. Within a confined hole, radial pressure develops over time causing radial and tangential tensile stresses in the surrounding rock. A fracture is created at the weakest section along the inside surface of hole (Harada et al.,1989). The time of cracking was identified by plotting the measured strains over time. When the rock is undamaged, its reaction to the SCDA pressure is linear. Therefore, if the expansive pressure exerted by the SCDA is also linear, the measured strains will also increase linearly. Consequently, the strain at which this linear increase terminates, or the onset of nonlinear behaviour, is interpreted as an indication that cracking has initiated. This point is referred to in this work as the "critical strain". On the other hand, both the time of visual fracture initiation and visual fracture completion were recorded, where the time of crack completion represents the point in time at which the fracture reaches the free surface of the slab. The 25.4 mm (1'') borehole is used as a base case to assess the time of fracturing with increasing borehole sizes (31.75 mm (1.25'') and 38.1 mm (1.5'')). As shown in Figure 4.4-4.6, for a 1'' hole, the first fracture occurs at 18 hours, 15 hours, and 23 hours for slabs M01, M02, and M03, respectively. Figures 4.7-4.8 show the recorded strains for specimens G-SL1-100-500-M-02 and G-SL1-100-500-M-03. The strains for

test G-SL1-100-500-M-01 were discarded. As summarized in Table 4.2, crack completion occurs after 21 to 27 hours. As can be seen in Figures 4.4-4.6, it takes on average 5 hours after crack initiation for a crack to propagate to the-free surface of the granite-slab. As shown in Figure 4.7-4.8, the critical strain at which the linear behaviour ends for specimen G-SL1-100-500-M-02 and G-SL1-100-500-M-03 is 6 hours and 19 hours respectively. It is also apparent that the non-linear behaviour is exponential, suggesting that there has been significant brittle damage to the rock at those points. This is in accordance with the visual cracking at which the time of initial cracking for G-SL1-100-500-M-02 and G-SL1-100-500-03 occur at 15 hours and 23 hours respectively, both times at which the strains increase exponentially as shown in Figure 4.7-4.8 (SG2 was damaged at the beginning of the test and is therefore omitted from the results in Figure 4.7). It is also shown that non-linear strain increase starts before cracking is visible on the slab surface, suggesting that visual identification of superficial cracking alone is not sufficient to determine the time at which fracturing initiates. This could be due to fracture initiating deeper in the block, or that the crack width is too small to capture with the camera.

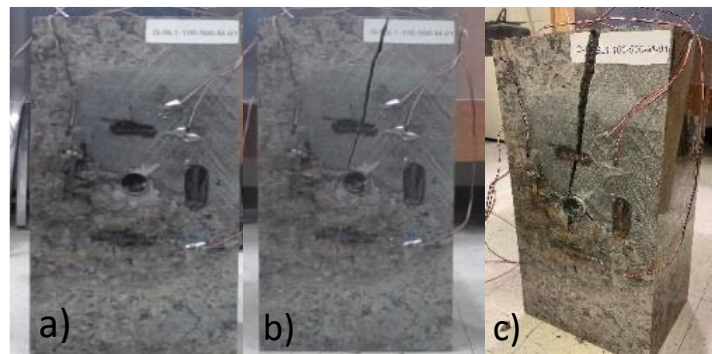


Figure 4.4 Slab G-SL1-100-500-M-01 a) At time t_0 b) Initial breakage at time t_{18} c) Complete breakage at time t_{24}

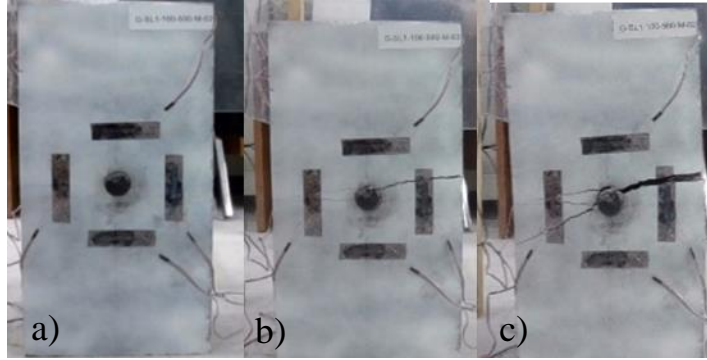


Figure 4.5 G-SL1-100-500-M-02 a) At time t_0 b) Initial breakage at t_{15} c) Complete breakage at t_{21}

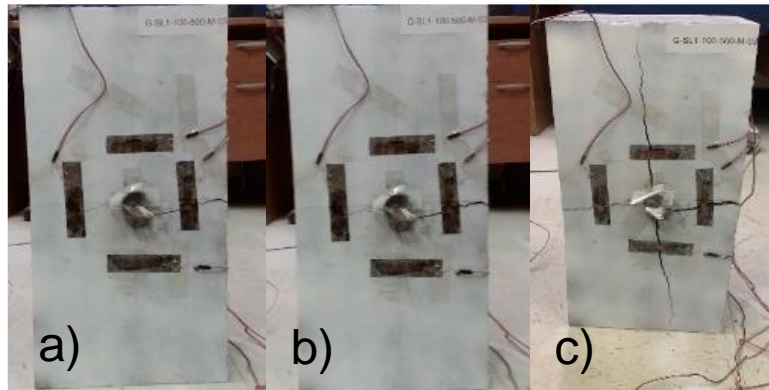


Figure 4.6 G-SL1-100-500-M-03 a) At time t_0 b) Initial breakage at t_{23} c) Complete breakage at t_{27}

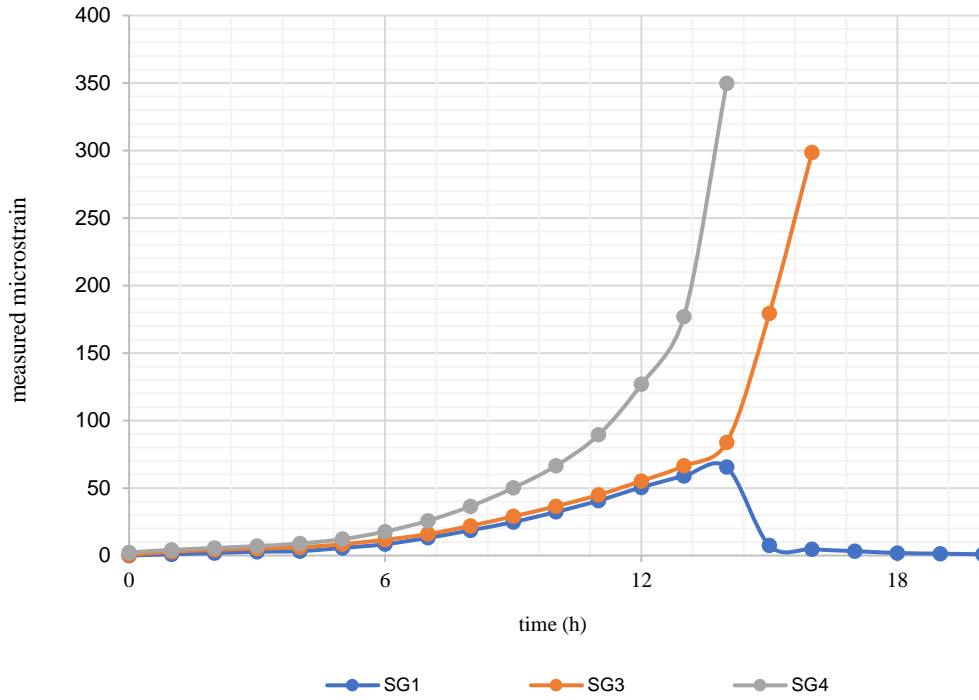


Figure 4.7 Measured strains in specimen G-SL1-100-500-M-02

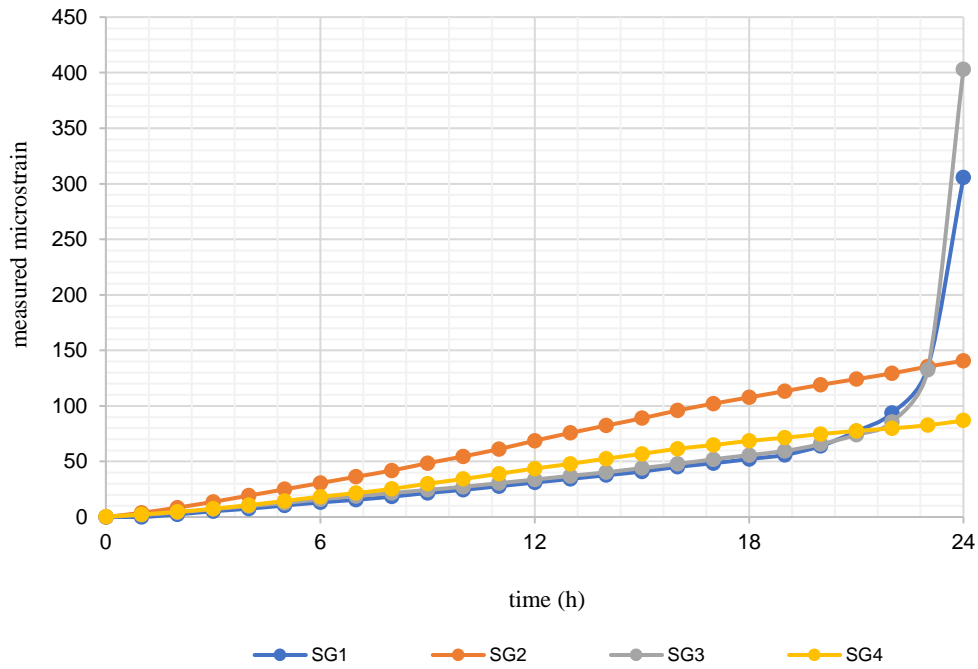


Figure 4.8 Measured strains in specimen G-SL1-100-500-M-03

The delay between visible crack initiation and non-linear strain increase is also observed in all specimens with an increased borehole size of 31.75 mm (1.25”). Specimens G-SL2-125-625-M-01 and G-SL2-125-625-M-02 show a TFC of 11.5 hours and 16 hours, respectively after SCDA is injected into the hole (Refer to Figs 9-10 for visual cracking). The onset of non-linear behaviour for specimens G-SL2-125-625-M-01 and G-SL2-125-625-M-02 begins after 5 hours and 8 hours, respectively (Refer to Figure 4.11-12 for strain values). The 31.75 mm specimens exhibited a faster reaction than the 25.4 mm where the time of initial cracking is decreased by an average of 5 hours.

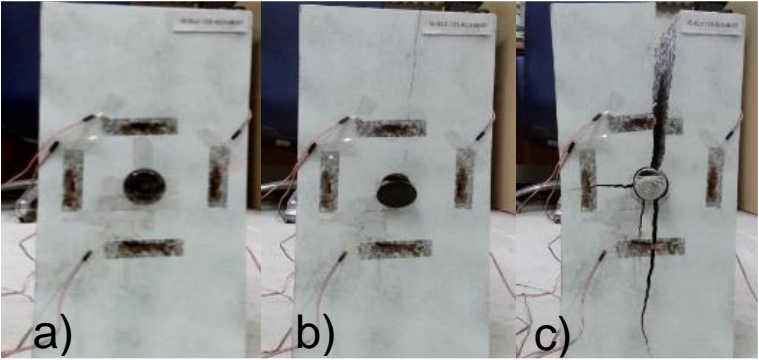


Figure 4.9 G-SL2-125-625-M-01 a) At time t_0 b) Initial breakage at $t_{11.5}$ c) Complete breakage at t_{17}

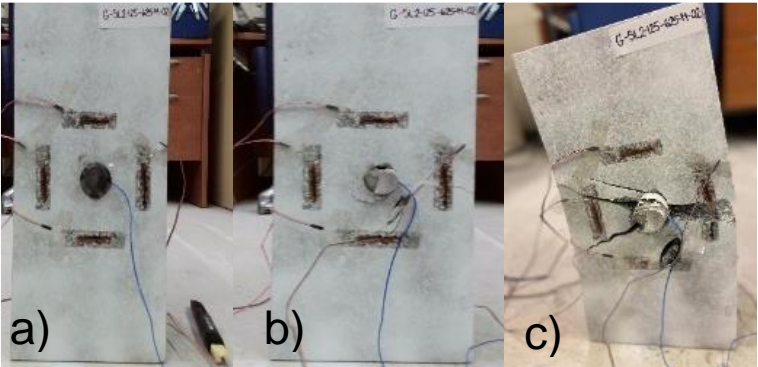


Figure 4.10 G-SL2-125-625-M-02 a) At time t_0 b) Initial breakage at t_{16} c) Complete breakage at t_{20}

Compared to specimens, G-SL1-100-500-M-01, G-SL1-100-500-M-02, G-SL1-100-500-M-03, crack completion occurs slightly earlier between 17 and 20 hours.

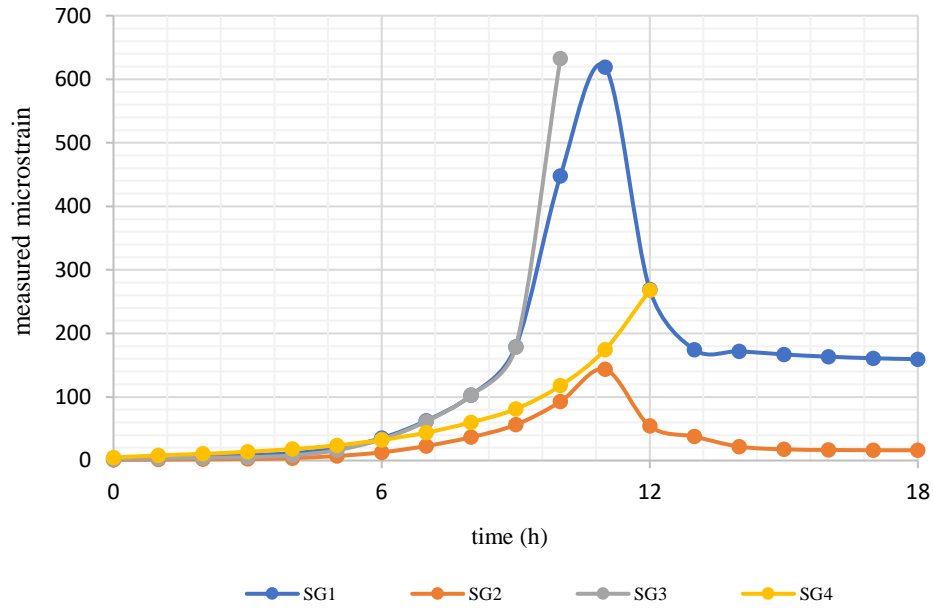


Figure 4.11 Measured strains in specimen G-SL2-125-625-M-01

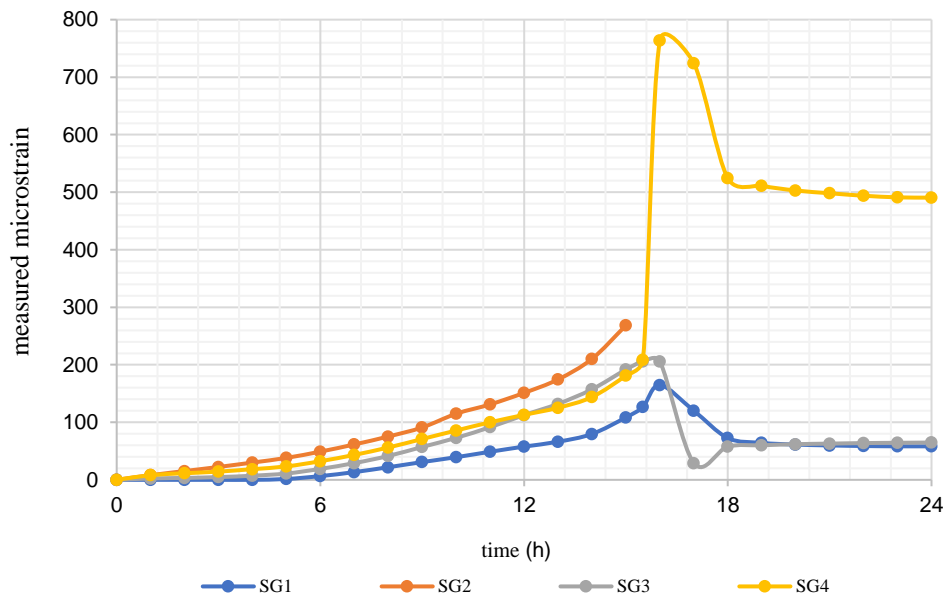


Figure 4.12 Measured strains in G-SL2-125-625-M-02

The sharp decrease in strains shown in Figure 4.11-4.12 is attributed to local stress relief due to cracking. When the strain gauges were not damaged, the observed relaxation corroborates with visual cracking. With a 38.1 mm (1.5'') SCDA injected hole, the time of breakage is reduced by

half when compared to a 25.4 mm (1") hole. The TFC is also significantly decreased, at 7.5 hours and 10 hours for specimens G-SL2-150-600-M-01 and G-SL2-150-600-M-02 respectively. For both specimens, complete slab fracturing occurred relatively quickly after cracking initiated, in 2.5-4 hours as shown in Figure 4.13-15. Figure 4.15 shows the rapidly increasing strains after 7.5 hours and quickly decreasing strains once the slab splits, indicating that the slab is fully relaxed, and all stresses have dissipated. Given that the strain gauges were not bisected by any cracks, the observed relaxation corroborates with the visual cracking. Figure 4.16 shows that at the time of visual breakage (11 hours), a small decay in strains is also observed shortly after indicating a relaxation of strains.

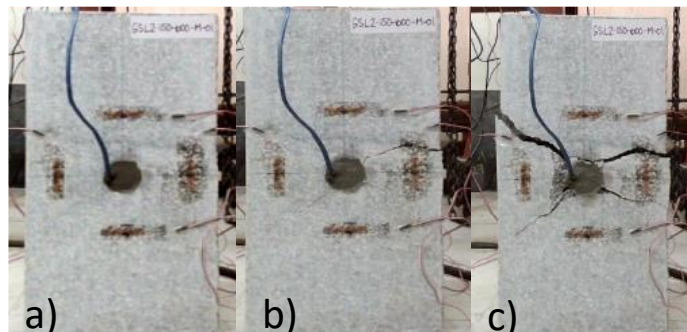


Figure 4.13 G-SL2-150-600-M-01 a) At time t_0 b) Initial breakage $t_{7.5}$ c) Complete breakage t_{10}

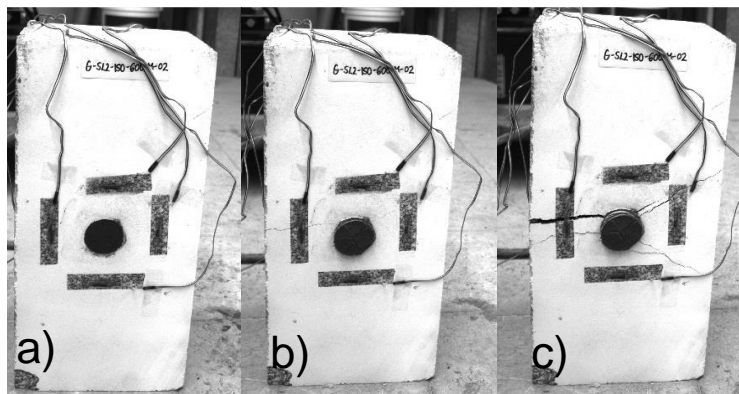


Figure 4.14 G-SL2-150-600-M-02 a) At time t_0 b) Initial breakage t_{11} c) Complete breakage at t_{13}

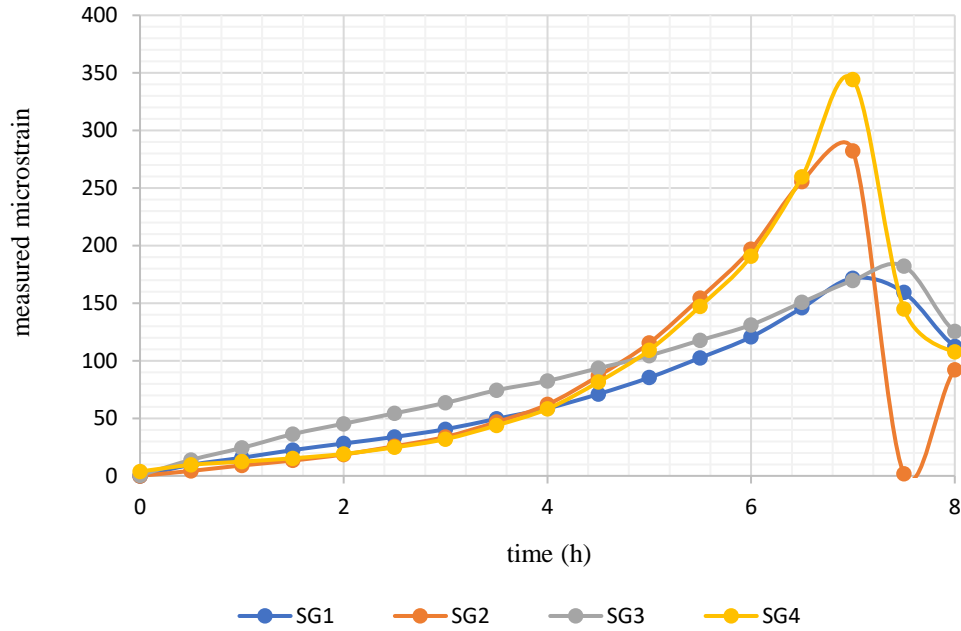


Figure 4.15 Measured strains of specimen G-SL2-150-600-M-01

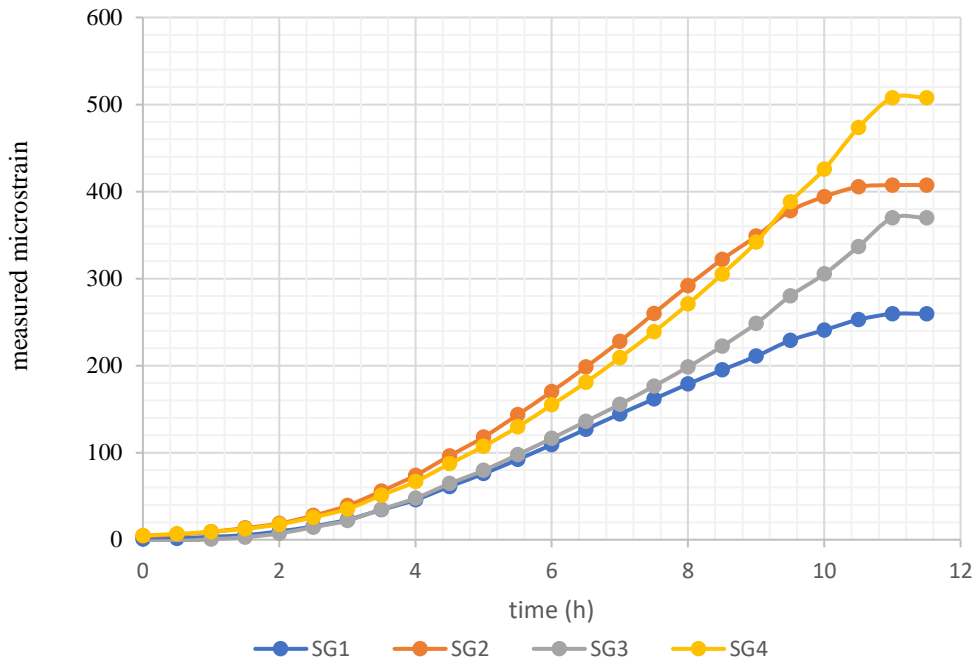


Figure 4.16 Measured strains in specimen G-SL2-150-600-M-02

Overall, the specimens under no loading showed that visual cracking is delayed according to the measured strains. The measured strains indicate tensile damage in the slab before any superficial

crack is apparent. This suggests that crack initiation may have occurred deeper in the slab before superficial cracking, or that the crack width is too small to observe. Therefore, the strain measurements are deemed a reliable tool to detect cracking without physical monitoring such as using a timelapse camera.

Table 4.2 Summary of test results under no load

Sample Configuration	TFC (hours)	Time of Crack Completion (hours)
G-SL1-100-500-M-01	18	24
G-SL1-100-500-M-02	15	21
G-SL1-100-500-M-03	23	27
G-SL2-125-625-M-01	11.5	17
G-SL2-125-625-M-02	16	20
G-SL2-150-600-M-01	7.5	10
G-SL2-150-600-M-02	11	14

4.3.3 Effect of SCDA on rock breakage under load

The effect of uniaxial loading on rock breakage with SCDA was tested by subjecting a slab with a single SCDA-filled hole to uniaxial compressive stress using a 200-tonne uniaxial loading frame. This part of the study aims to quantify the fracture propagation rate of granite subjected to uniaxial far-field pressure and radial pressure from the expansive cement. As shown in Table 4.1, a total of 3 specimens were tested under a uniaxial stress of 5 MPa. Such loading level was selected so that the tensile stresses around the hole do not exceed the tensile strength of the granite. All Stanstead granite slabs were 6'' x 8'' x 16'', and three different hole locations were tested. All specimens were greased with a thin coat of MoS₂ to reduce friction between the rock and the loading plate as shown in Figure 4.2b. As the first part of the investigation shows a decrease in TFC with the

increase of borehole diameter, it was decided to adopt only the largest diameter of 38.1 mm (1.5") for the second part as uniaxial loading condition was thought to delay fracturing. To confirm the trend, another size of 44.45 mm (1.75") hole was also tested. Three specimens were tested; specimen G-SL2-150-600-UT-L with a 38.1 mm (1.5") SCDA hole located in the upper third of the slab, specimen G-SL2-175-700-M-L with a 44.45 mm (1.75") SCDA hole located in the middle of the slab and specimen G-SL2-175-700-LT-L with 44.45 mm (1.75") SCDA hole located in the lower third of the slab. Regarding the positioning of the holes, the goal is to observe the influence of hole diameter and its position on the TFC and time of complete breakage, all while monitoring the longest fracture path. Due to the limited number of samples available, it was not possible to return to the smaller SCDA hole sizes. The adopted holistic approach deemed adequate. As shown in Figure 4.1, strain gauges were fixed 38.1 mm (1.5") away above (SG1) and below (SG3), and to the right (SG2) and left (SG4) side of the borehole. Both timelapse photos and strains were recorded to detect the time of initial cracking and crack completion. Crack completion was assessed based on the time that cracking below and above the borehole reached the metal loading plates. As shown in Figures 4.18, 4.20, 4.22, the strains for SG2 (right gauge) and SG4 (left gauge) remain in constant compression indicating that all slabs remained fully loaded over the entire duration of the test. As shown in Figure 4.17b, a 38.1 mm (1.5") SCDA-filled hole located in the upper third of the slab (Specimen G-SL2-150-600-UT-L) shows initial cracking after 7 hours and crack completion shortly after in 10 hours. Figure 4.17b-d) shows that initial cracking propagates towards the greased upper metal loading plate end first and then to the lower plate 3 hours later when complete breakage of the specimen has occurred.

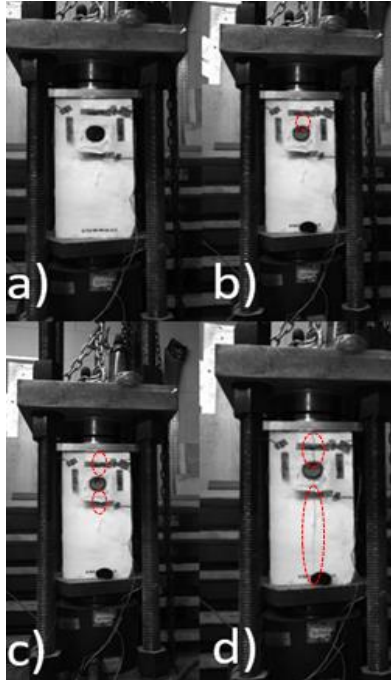


Figure 4.117 G-SL2-150-600-UT-L a) At time t_0 b) TFC at t_7 c) Breakage at $t_{7.5}$ d) Complete breakage at t_{10}

As shown in Figure 4.18, the measured strains for SG1 (strain gauge above the borehole) and SG3 (below the borehole) experience a sudden change in strain rate at 6 hours leading to a TFC of 7 hours.

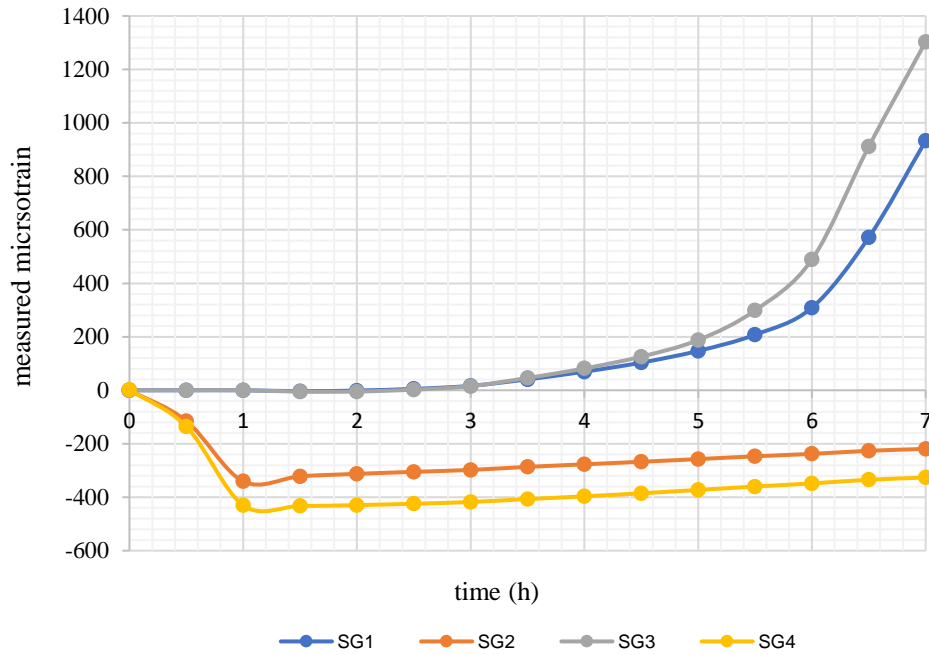


Figure 4.18 Measured strains in specimen G-SL2-175-700-M-L

This will help estimate an L_f/ϕ (length of fracture/ diameter of SCDA borehole) ratio to design the hole spacing in practical applications where uniaxial loading conditions are present. Figure 4.19 b shows a 1.75'' SCDA-filled hole located in the middle of the slab (G-SL2-175-700-M-L). Superficial cracking initiation is shown after 6.8 hours and crack completion after 9.8 hours. Compared to G-SL2-150-600-UT-L, the time of initial fracture is very close and does not significantly differ from the time of complete fracturing. Similarly, the fractures above the borehole propagated to the greased upper plate before the crack below the borehole has reached the metal plate. As shown in Figure 4.20, there is a sharp increase in the strain rate at 6 hours before visual cracking is detected.

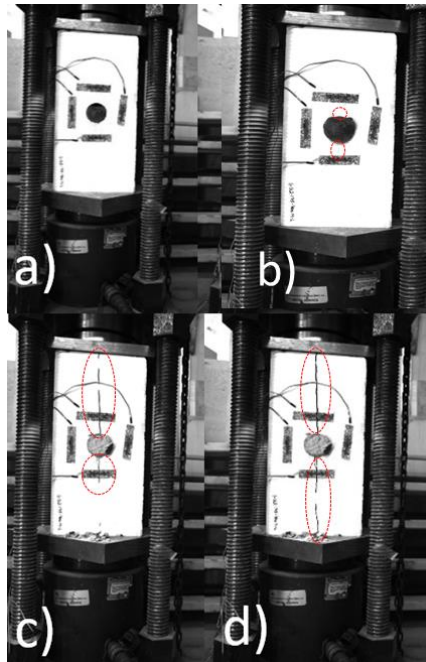


Figure 4.19 G-SL2-175-700-M-L a) At time t_0 b) Initial breakage $t_{6.8}$ c) Breakage at t_9 d) Complete breakage $t_{9.73}$

This shows that the visual behavior of cracking is once again delayed relative to the measured strains by 1 hour. However, a different fracture pattern is observed with the 1.75" SCDA filled hole located in the lower third of the granite slab (G-SL2-175-700-M-L).

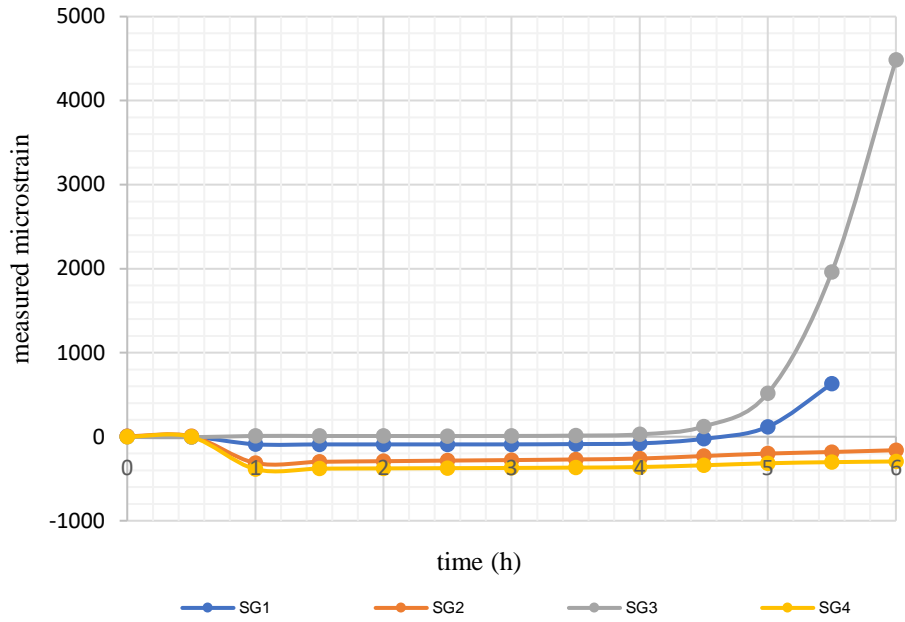


Figure 4.20 Measured strains in specimen G-SL2-175-700-M-L

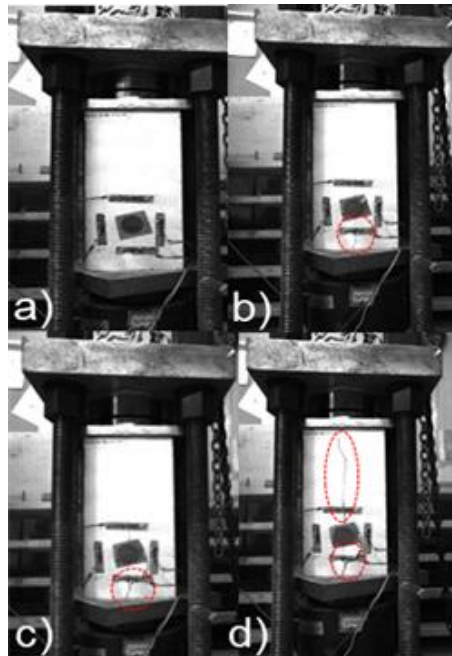


Figure 4.21 G-SL2-175-700-LT-L a) At time t_0 b) Initial breakage c) Breakage at t_7 at d) Complete breakage at t_{12}

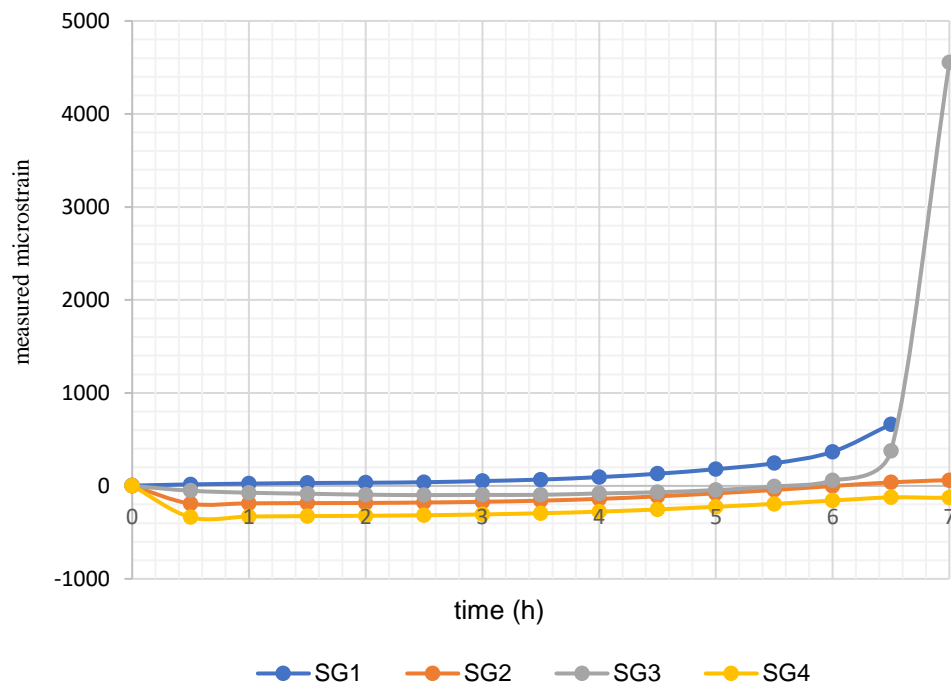
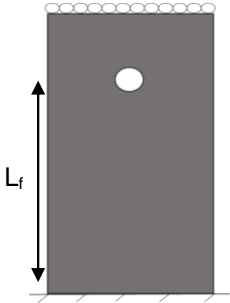
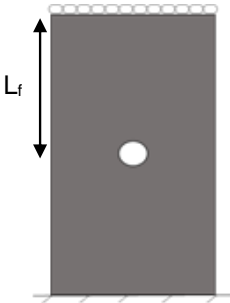
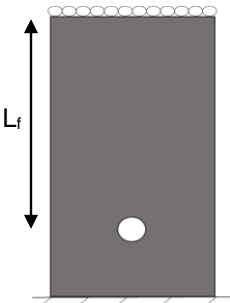


Figure 4.22 Measured strains in specimen G-SL2-175-700-LT-L

As shown in Figure 4.21c, cracking first propagates towards the lower bearing plate and then propagates slowly towards the greased upper loading plate. The delay in fracture completion can therefore be related to the non-greased bottom plate offering increased frictional resistance, resisting the extension strain that causes slab separation. Overall, Figures 4.17,4.19,4.21 show that all fractures propagate in the direction of the major principal stress, unlike the unloaded slabs where fracturing generally propagated towards some or all the nearest faces. Since the loaded specimens had directional cracking as opposed to the unloaded specimens, optimal borehole spacing can be estimated. The ratio of the length of fracture over the SCDA hole diameter (Φ) is an indicator for maximum hole spacing. As each SCDA can generate a fracture length L_f , the spacing, S , between two SCDA holes is calculated as $S=2L_f/ \Phi$. As shown in Table 4.3, the illustration for each specimen depicts which end of the granite slab is used to measure the length

of fracture. The length L_f was selected based on the longest crack path measured from the borehole center. As the specimens have different hole configurations, it should be noted the L_f/Φ ratio reported in Table 4.3 is not a direct comparison between the specimens to judge their performance. Rather, it is used to help delineate the required SCDA borehole spacing in practice. As can be seen in Table 4.3, the L_f/Φ ratio for the loaded granite can be up to 6.4 to 7.3. As the top surface is greased, it acts as a line of symmetry. Thus, for practical applications, it can be claimed that the maximum allowable spacing between two SCDA boreholes is $2L_f/\Phi$, or 12.8 to 14.6 Φ to achieve complete fracturing. According to work done by Gomez & Mura (1984), a proposed spacing between SCDA holes of 8Φ is suggested (Gomez & Mura ,1984), however, for unloaded specimens.

Table 4.3 Summary of L_f/Φ

Specimen ID	G-SL2-150-600-UT-L	G-SL2-175-700-M-L	G-SL2-175-700-LT-L
Specimen Configuration			
SCDA Hole Size	31.8 mm (1.5")	44.45 mm (1.75")	44.45 mm (1.75")
TFC (hours)	7	6.8	7
Complete Breakage (hours)	10	9.7	12
L_f/Φ	7.3	4.6	6.4

4.4 Conclusions

In this chapter, the results of a series of experimental tests are reported to identify the effect of SCDA on hard rock breakage under no load and under uniaxial loading conditions. Stanstead granite specimens of 152.4 mm (6'') x 152.4 mm- 203.2 mm (6-8'') x 406.4 mm (16'') are used to test the influence of borehole size on the fracturing time with 25.4mm (1''), 31.75 mm (1.25'') and 38.1 mm (1.5'') SCDA holes under no load. It is shown that fracturing time decreases with increasing borehole size. The time of initial fracturing for a 38.1 mm (1.5'') borehole size is half of that of a 1'' filled SCDA hole. Moreover, the measured strains for all specimens increase exponentially at some point in time, and this exponential behavior is interpreted as tensile damage progression in the slab. The results demonstrate that strain measurement is a reliable indicator for fracture initiation, and that this fracture initiation could not be detected visually. Another series of tests were performed to verify the influence of a uniaxial pressure of 5 MPa on the slab fracturing with SCDA. Three tests with a single SCDA hole at 3 different locations were tested: 38.1 mm (1.5'') borehole size in the upper third of the slab (G-SL2-150-600-UT-L), 1.75'' in the middle of the slab (G-SL2-175-700-M-L) and 1.75'' in the lower third of the slab (G-SL2-175-700-LT-L). SCDA expansion-initiated fracturing as early as 7 hours for all tests. Specimens SL2-150-600-UT-L and G-SL2-175-700-M-L split after 10 hours, whereas specimen G-SL2-175-LT-L split after 12 hours. The delay in fracturing completion could be due to the non-greased bottom plate resisting fracture propagation due to the increased friction. Based on the experimental results, the fracture length to borehole diameter ratio L/Φ , was calculated to estimate the maximum allowable spacing between SCDA holes subjected to uniaxial stress. It is suggested that the spacing between SCDA boreholes be $12.8-14.6\Phi$ for practical applications involving uniaxial compression. Such

higher borehole spacing suggestion for loaded samples than the 8Φ for unloaded sample suggested by Gomez & Mura (1984) implies that uniaxial loading is beneficial for hard breakage with SCDA.

References

Arshadnejad S, Goshtasbi K, Aghazadeh J (2011) A model to determine hole spacing in the rock fracture process by non-explosive expansion material. *Int J Miner Metall Mater* 18:509–514. <https://doi.org/10.1007/s12613-011-0470-5>

Farnfield R, Wetherelt A. (2004), After-Blast Fumes from ANFO Mixtures, *Quarry Management*, 31, (2), 11-19.

Gambatese J.A. (2003) Controlled concrete demolition using expansive cracking agents. *J. Constr. Eng. Manag* 129,98-104

Gholinejad M, Arshadnejad S (2012) An experimental approach to determine the hole-pressure under expansion load. *J South African Inst Min Metall* 112:631–635

Gómez C., Mura T (1984). Stresses caused by expansive cement in borehole. *J. Eng. Mech.* 110(6), 1001-1005.

Habib, K. (2019) Laboratory Investigation into Soundless Chemical Demolition Agents for Rock Breakage in Underground Mines. M.Sc. thesis. McGill University, Montreal, QC,

Habib, K. M, Shnorhokian S., Mitri H. (2022). Evaluating the Application of Rock Breakage without Explosives in Underground Construction—A Critical Review of Chemical Demolition Agents. *Minerals*, 12(2), 220.

Hanif M (2010) Effective Use of Expansive Cement for the Deformation and Fracturing of Granite. *Gazi Univ J Sci* 20:1–5

Harada T, Idemitsu T, Watanabe A, Takayama S. (1989) The Design Method for the Demolition of Concrete with Expansive Demolition Agents. In: Shah S.P., Swartz S.E. (eds) Fracture of Concrete and Rock. Springer, New York, NY, 1989, 47-57

Hinze J, Brown J (1994) Properties of Soundless Chemical Demolition Agents, *Constr. Eng. Manag.* 120 816–827. [https://doi.org/10.1016/0148-9062\(95\)93364-U](https://doi.org/10.1016/0148-9062(95)93364-U)

Laefer DF, Ambrozevitch-Cooper N, Huynh MP (2010) Expansive fracture agent behaviour for concrete cracking. *Mag Concr Res* 62:443–452. <https://doi.org/10.1680/macr.2010.62.6.443>

Musunuri A, Mitri H (2009) Laboratory investigation into rock fracturing with expansive cement. *Int J Min Miner Eng* 1:327–345. <https://doi.org/10.1504/IJMME.2009.029318>

Soeda, K., and T. Harada. (1993) The mechanics of expansive pressure generation with expansive demolition agent *Trans. Jpn. Soc. Civ. Eng* 19 :121-135.

Taylor HF (1997) *Cement Chemistry*. London: Thomas Telford

Timoshenko S, Goodier J (1951) - Theory of elasticity. *Phys. Contin. Media* 234–259

Chapter 5: Effectiveness of Soundless Chemical Demolition Agents for rock breakage under uniaxial loading condition

5.1 Introduction

Recent research has been dedicated to modelling crack patterns under different loading conditions with numerical modelling (Tang et al., 2017; Zhai et al., (2018); De Silva et al., 2018a; De Silva et al., 2018b; Wang et al., 2022; Tang et al., 2021; Wang et al., 2018). Initially, the simulation of cracking solely from the expansion force generated by the expansive cement is modeled. Such studies include Tang et al. (2017) where the finite element method in conjunction with damage mechanics were employed to simulate crack initiation and propagation in heterogeneous materials to reproduce crack patterns in samples tested in laboratory experiments. It was shown that failure patterns are influenced by the degree of heterogeneity of the rock sample (Tang et al., 2017). Other work done by De Silva et al. (2018b) examined the charging of a single SCDA hole under various confining pressures using Particle Flow Code (PFC3D 5.0) (De Silva et al. 2018a). Their findings corroborate with those by Zhai et al. (2018), who showed that the number of radial fractures and the total fracture damage in the rock increases with the confinement pressure (V. R. S. De Silva et al., 2018) . Wang et al. (2022) conducted an experimental study on fracture propagation in 150 mm granite cubes with 2 adjacent boreholes of 12 mm diameter under biaxial loading conditions σ_h, σ_H where $\sigma_H > \sigma_h$. Their research shows that the smaller σ_h/σ_H the more fractures are observed. It was also shown that initial cracking connected the two boreholes, subsequently propagating along the maximum principal stress. The same trend is also observed by Tang et al. (2021) who simulated a three-hole specimen with confinement pressures using the numerical modeling with finite difference code FLAC3D. They analyzed the weakening of hard roof in a

coal mine using SCDA under biaxial stress conditions. Other works also studied the characteristics of SCDA induced crack propagation in rock under different stress conditions and the influence of hole notching. A cohesive element method was developed in Abaqus to demonstrate that the borehole notch orientation controls the direction of crack propagation from the SCDA hole (Wang et al., 2018). Chapter 4 presents the behavior of SCDA-injected hole in granite blocks subjected to uniaxial loading conditions. It was found that uniaxial loading accelerates the initiation and propagation of SCDA-induced fractures. It was also found that fractures propagate in the direction of loading to complete splitting of the rock block. However, due to the limited size of the tested blocks, it was not possible to delineate the full fracture length that would be generated under uniaxial loading condition in the field.

In this chapter, the experimental results from Chapter 4 are used to develop and calibrate a numerical model in Abaqus using Extended Finite Element Method (XFEM). The effect of uniaxial loading conditions is investigated for its implementation in underground mining practical applications. Such applications may include intersection slashing and breakage of hard rock in and around areas where mine services have already been put in place where the use of blasting is not feasible. The XFEM model is used to simulate crack propagation to its full natural limit and based on the calibrated model results, a new spacing between SCDA holes under uniaxial conditions is proposed. A separate section of this chapter reports the results of an experimental program aimed at exploring the influence of the so-called shield holes. Stress relief holes are commonly used in blasting applications. In this chapter, the notion of stress shield holes – analogous to stress relief in blasting – is examined with SCDA application for the first time with a view of testing the merits of adding unloaded holes in the direction of the field stress. To do so, two shield holes are placed

along the loading axis of the specimen above and below the SCDA hole. The experimental results are compared with those without hole shielding and suggestions for practical applications are made.

5.2 Single SCDA hole under uniaxial condition

5.2.1 Data

The data analyzed in this study is extracted from the investigation reported in Chapter 4. It consists of three prismatic specimens from Stanstead granite with a central borehole for the injection of SCDA. Figure 5.1 shows a typical specimen configuration. Table 5.1 lists the geometric properties of the specimens and borehole diameters. Specimens are identified as M-SL-D-HD-HL-L whereby

- M: Material, e.g., G for Granite
- SL2: Slab dimensions (152.4 mm (6'')) wide x 203.3 mm (8'')) thick x 406.4 mm (16'')) high
- D: SCDA hole diameter in inches, e.g., 150 for 38.1 mm or 1.5''.
- HD: Hole depth in the thickness direction, e.g., 600 for 152.4 mm or 6''
- HL: Hole location, e.g., M for middle, LT for lower third, UT for upper third

All specimens were loaded uniaxially at 5 MPa. To reduce end friction, MoS₂ grease is applied between the top loading plate and the specimen. The SCDA selected for their study is Betonamit (Betonamit, n.d). Each specimen was instrumented with four strain gauges as shown in Figure 5.1. Measured strains will be used to calibrate the numerical model.

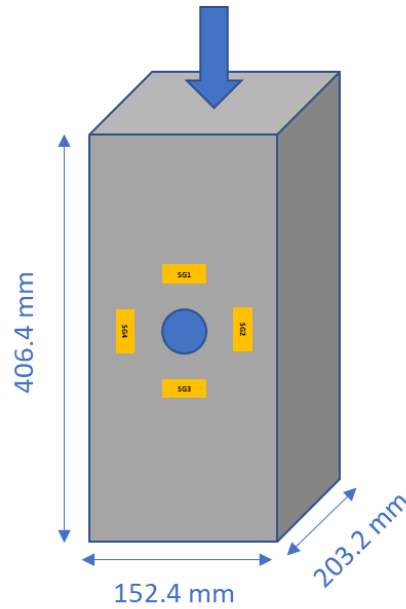


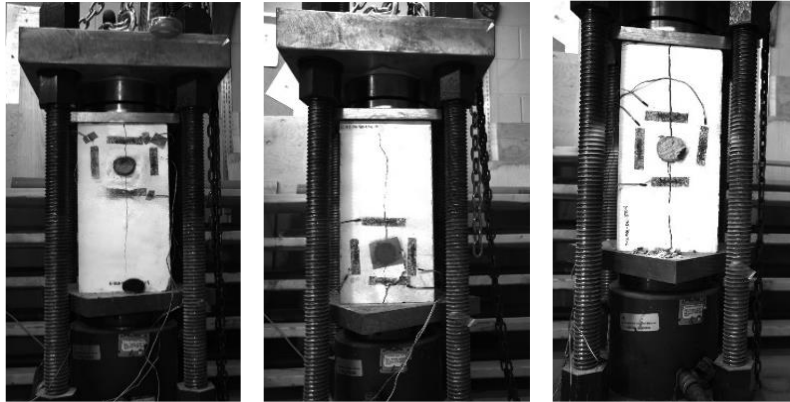
Figure 5.1 Specimen configuration with strain gauge locations for a single SCDA-injected hole subjected to uniaxial loading

Table 5.1 Description of tested specimens (extracted from Chapter 4)

No.	ID	Width (mm)	Height (mm)	Thickness (mm)	ϕ (mm)	Hole length (mm)	Hole location	Brazilian Test ¹ (N=5)
1	G-SL2-150-600-UT	152.4	406.4	203.3	38.1	152.4	Upper third	BTS=7.5 MPa
2	G-SL2-175-700-LT	152.4	406.4	203.3	44.5	177.8	Lower third	
3	G-SL2-175-700-M	152.4	406.4	203.3	44.5	177.8	Middle	

¹ The Stanstead granite samples were cored from the granite slabs and prepared in compliance to the ASTM D3967 Standard

All 3 specimens showed an initial time of cracking of about 7 hours under the same uniaxial stress of 5 MPa. Complete fracturing took place after 10 hours, 12 hours, and 9.7 hours for specimens G-SL2-150-600-UT, G-SL2-175-700-LT, and G-SL2-175-700-M, respectively. Figure 5.2 shows the fracture patterns. As expected, fractures align with the applied stress direction. As can be seen, fractures intersect strain gauges 1 and 3 located above and below the SCDA hole.



a) G-SL2-150-600-UT b) G-SL2-175-700-LT c) G-SL2-175-700-M-L

Figure 5.2 Fracturing of tested specimen under 5 MPa load.

Figure 5.3 displays the SCDA-induced strain evolution with time for each specimen. The strain readings shown for each specimen in Figure 5.3 are for the strain gauge where cracking first occurs. Chapter 4 reports that cracking initiates towards the greased end of the specimen except for specimen G-SL2-175-700-LT where it initiates towards the bottom as the distance between the SCDA hole the bottom end is only 1/3 of the specimen height. As the strain gauges record the total strain, the initial strain due to uniaxial stress is subtracted from the total strain to obtain the net strain due to SCDA pressure – shown in Figure 5.3.

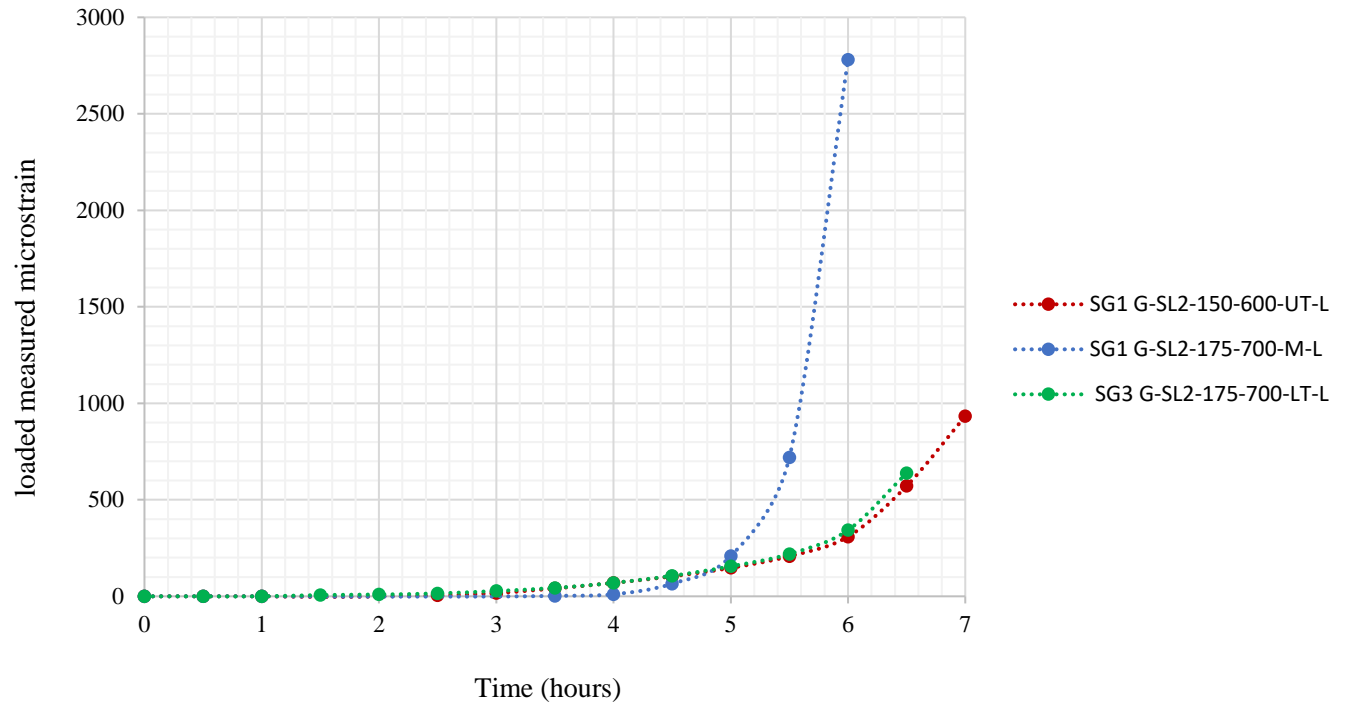


Figure 5.3 Measured SCDA-induced strains (Refer to Figure 5.1 for strain gauge location)

5.2.2 XFEM Model

The purpose of the numerical modelling study is to determine the true extent of fracturing under uniaxial loading condition in an infinitely long medium, hence an appropriate spacing between SCDA holes can be proposed for practical applications. To achieve this, a damage model is needed to simulate crack propagation in the model domain. The extended finite element method (XFEM) was developed in by Belytschko (1999) and since then, it has been successfully used to model the propagation of a wide range of discontinuities. XFEM can model two types of discontinuities: strong (displacement-based) such as cracks, and weak (strain-based) discontinuities such as bi-material interfaces. Since the SCDA crack orientation is known a priori, it is easy to define the XFEM domain when generation of the finite element mesh. Thus, XFEM was deemed suitable for modelling SCDA crack initiation and propagation. Abaqus finite element software is used to build

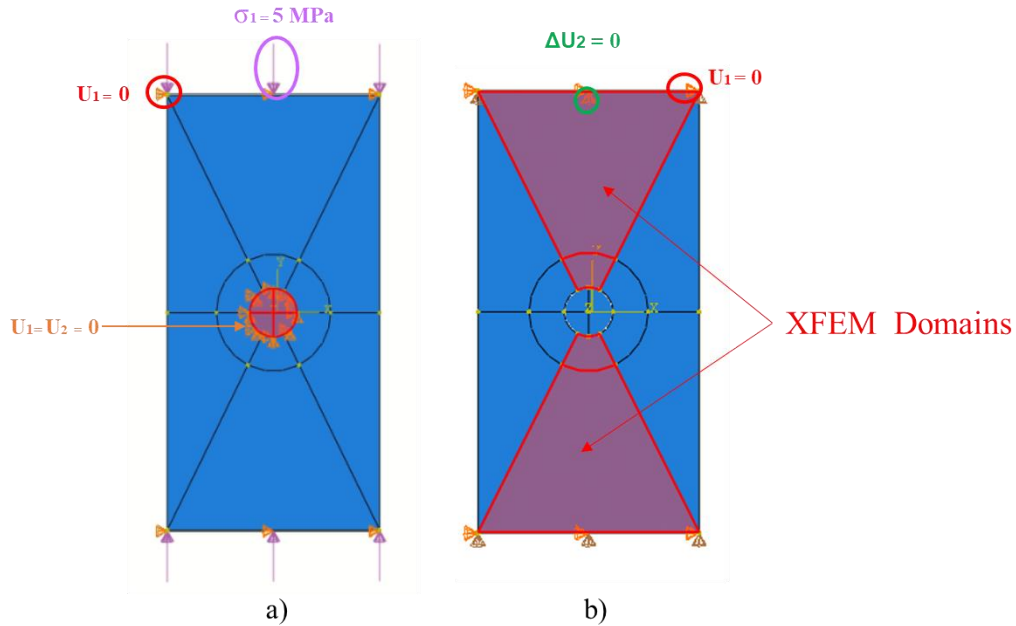
a 2D numerical model of the rock specimen with a single SCDA hole. Three models were built to simulate the tested specimens; see Table 5.1 for geometric properties. Table 5.2 lists the mechanical properties of granite and SCDA. The mechanical properties of granite are obtained from laboratory testing. The properties for SCDA are assumed. The expansive cement or SCDA is introduced as a solid material to allow for the interaction between the expansive cement and host rock. A hard contact between the SCDA and granite is applied with a frictional coefficient of 0.3. A compressive isotropic stress regime is initialized in the SCDA to represent the expansive cement pressure. As the initial stress is released, it causes the SCDA material to expand and press against the surface of the borehole. Figure 5.4 depicts the modelling steps. First, a uniaxial stress of 5 MPa is applied in the vertical direction while both the top and bottom boundaries are restrained in the x-direction (Figure 5.4a). In step 2, the initial compressive stress of the SCDA is released. A crack tip is positioned at the crown and invert of the SCDA hole to help guide crack initiation and propagation. The XFEM domains are built in the shape of a cone radiating from the hole as shown in Figure 5.4. A simple traction-separation law is applied to XFEM domains, such that a crack will initiate when the maximum principal stress at a point exceeds the tensile strength of 7 MPa determined from Brazilian test in laboratory. Crack damage is expressed in a range from 0 to 1, where 1 represents complete damage when the fracture energy reach 50 J. The 4-node bilinear plane-stress quadrilateral (CPS4R) element is selected. A mesh sensitivity analysis was conducted for the linear elastic model to reach an optimal mesh. A mesh seeding of 0.1 mm around the SCDA hole and at least 30 elements along the direction of the crack was selected. The meshing scheme yields 7784 elements.

Table 5.2 Material, interface, and crack properties

Material	Mechanical Behaviour		Young's Modulus (E) (GPa)	Poisson's Ratio (ν)	Additional Properties
Granite	Linear Elastic		30	0.2	
SCDA	Linear Elastic		8	0.2	NA
Crack	Traction-separation		N/A	N/A	Tensile strength = 7 MPa Fracture Energy = 50J
Interface	Greased	Cohesive element	1000	N/A	G = 12.5 GPa Shear Strength = 0.25 MPa
	Granite Steel				G = 12.5 GPa Shear Strength = 1 MPa

To simulate the interaction between the greased end of the specimen and the top steel loading plate, a strip of cohesive elements is used with a tie constraint to its top and bottom faces. The loaded face of the strip is then constrained in the x-direction. Both top and bottom cohesive element interfaces have a granite shear modulus, G , of 12.5 GPa. The shear strength of the cohesive strip is calculated based on the coefficient of friction of the contact surface and normal pressure applied. For the greased end, the cohesive element has a shear strength of 0.25 MPa under a normal pressure of 5 MPa and a coefficient of friction of 0.05. For the steel-granite end without grease, a cohesive element with a shear strength of 1 MPa is introduced, representing a friction coefficient of 0.2 between the granite and the steel. The analysis is conducted in two static standard steps. Step 1 is the loading step where the vertical stress is applied to the top and bottom boundaries of the model and where the SCDA material is locked in place, i.e., prevented from expansion. Step 2 is the application of the SCDA pressure. First, the applied stress of 5 MPa is replaced by a zero change in vertical displacement constraint ($\Delta U_2=0$). This locks in the applied vertical stress. The boundary

around the SCDA is then removed allowing the SCDA to expand, releasing the initial stress into the rock and initializing crack propagation in the XFEM domain.



a) Step 1: Vertical stress is applied

b) Step 2: SCDA pressure is released

Figure 5.4 Model loading steps and boundary conditions

5.2.3 Modeling Results: Single SCDA Hole

Crack Initiation and Complete Breakage Pressure

To estimate the crack initiation pressure in the SCDA, the strain at which the onset of nonlinear behavior begins is determined for all specimens. This will be termed the critical strain; see Table 5.3. The critical strains are selected based on where crack initiation was observed to occur, e.g., strain gauge SG1 for specimen G-SL2-150-600-UT-L is selected because crack initiated towards it first. To calibrate the numerical model, it is run iteratively by varying the input SCDA initialized pressure until the computed strain matches the measured critical strain at the selected strain gauge location. This procedure allows for the estimation of the initial stress in SCDA when cracking

occurs as shown in Figure 5a. As shown in Table 5.4, the initialized SCDA stress for fracture initiation varies between 14 to 17.8 MPa with an average of 16 MPa.

Table 5.3 Critical Strain of specimens (extracted from Figure 5.3)

Specimen #	Specimen I. D.	Strain Gauge #	Critical Strain
1	G-SL2-150-600-UT-L	SG1	207
2	G-SL2-175-700-M-L	SG1	106
3	G-SL2-175-700-LT-L	SG3	219

The next step is to run the model by initializing the input SCDA pressure that will result in complete breakage of the specimen as shown in Figure 5.5b. The results are shown in Table 5.4 where the peak initialized SCDA stress needed for complete breakage of the specimen varies between 57-95 MPa with an average of 71 MPa. As expected, higher SCDA pressure (90 MPa) is needed to break the specimen with the smaller diameter of 38.1mm (G-SL2-150-600-UT-L).

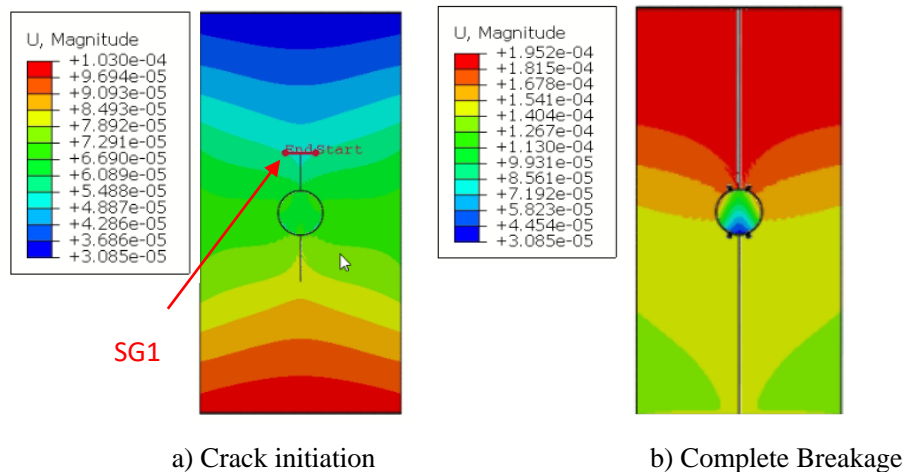


Figure 5.5 Model of specimen G-SL2-175-700-M

Table 5.4 SCDA pressure at Crack Initiation and Complete Breakage

Specimen #	Specimen I. D	SCDA Pressure (MPa)	
		Crack Initiation	Complete Breakage
1	G-SL2-150-600-UT-L	17.8	95
2	G-SL2-175-700-M-L	14	57
3	G-SL2-175-700-LT-L	16.2	60

5.3 Hole Shielding

5.3.1 Experimental Program

As previously discussed, stress relief holes are commonly used in blasting applications. In this section, the effect of hole shielding on SCDA under loading conditions is explored with a view of testing the merits of adding the load in the direction of the field stress. The SCDA hole is shielded by 2 relief holes along the loading axis (see Figure 5.6). Specimen dimensions are 52.4 mm (6”) x 203.2 mm (8”) x 406.4 mm (16”). As mentioned in previous section, the chemical reaction of SCDA is exothermic and it was demonstrated in Chapter 3 that increasing borehole size increases the rate of heat generation, which can increase the speed of reaction and therefore pressure generation. With a 25.4 mm (1”) SCDA hole, a constant temperature of 21°C is maintained throughout the entire breakage period of the rock. Figure 5.6 shows a schematic of the experimental setup for hole shielding. As can be seen, strain gauges are fixed around the borehole and connected to a data acquisition system (DAQ) to record the strains up until fracture initiation.

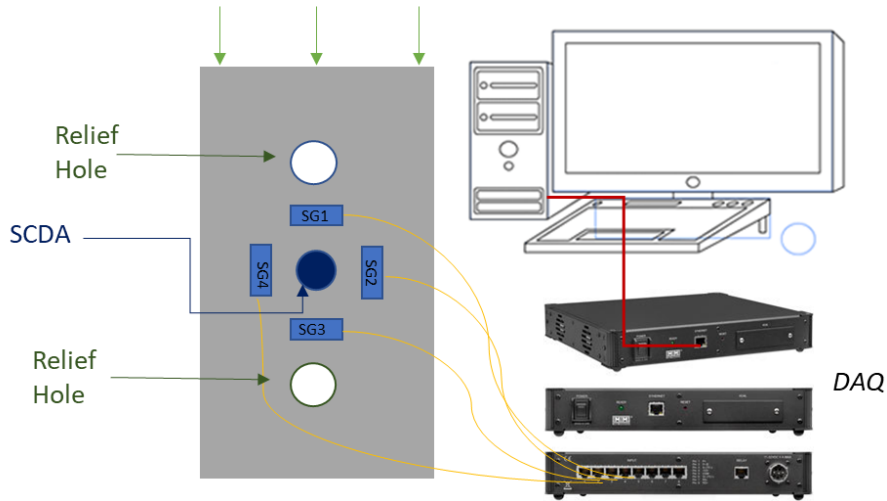


Figure 5.6 Experimental setup for hole shielding experiment

The nomenclature M-SL#- SH-RH-DRH-XX is adopted for the hole shielding specimens, where:

- M: Material, e.g., G for Granite
- SL : Specimen dimensions, 152.4 mm (6") x 203.3 mm (8") x 406.4 mm (16")
- SH : Shielded Hole
- RH: Relief hole size in inches.
- DRH: Distance between relief hole and SCDA hole, e.g., 1D for one time the diameter of the SCDA hole
- XX: Serial number

Table 5.5 presents the geometric properties of the tested specimens. The first specimen has no relief holes (G-SL2-100-400-M-L), the second test introduces two 38.1 mm (1.5") relief holes (G-SL2-SH-1.5-1D) and the third introduces two 50.8 mm (2") relief holes (G-SL2-SH-2.0-1D).

Table 5.5 Description of tested specimens for hole shielding

Test Type	Specimens	SCDA Hole Size	Relief Hole Size	Spacing to SCDA Hole	Brazilian Test ¹
Single Hole	G-SL2-100-400-M-L-01	25.4 mm (1.00")	-	-	N=3 BTS= 6.1 MPa
	G-SL2-100-400-M-L-02	25.4 mm (1.00")	-	-	
Hole Shielding Test	G-SL2-SH-1.5-1D-01	25.4 mm (1.00")	38.1 mm (1.5")	1.5	N=3 BTS= 7.7MPa
	G-SL2-SH-1.5-1D-02	25.4 mm (1.00")	38.1 mm (1.5")	1.5	
	G-SL2-SH-2.0-1D-01	25.4 mm (1.00")	50.8 mm (2.0")	2.0	N=3 BTS = 6.8 MPa
	G-SL2-SH-2.0-1D-02	25.4 mm (1.00")	50.8 mm (2.0")	2.0	

¹ The Stanstead granite samples were cored from the granite slabs and prepared in compliance to the ASTM D3967 Standard

5.3.2 Experimental Results and Discussion

As shown in Figure 5.7 a-c, three specimen configurations were tested in duplicates to study the effect of hole shielding on a single SCDA injected hole of 25.4 mm (1"). The base configuration for comparison is a specimen with a single (25.4 mm) 1" SCDA hole. All specimens are subjected to a uniaxial load of 5 MPa (Refer to Figure 5.7a). Figure 5.7b, shows the second configuration where two 38.1 mm (1.5") are introduced above and below the SCDA hole. Figure 5.7c) shows the third and final configuration, where two 50.8 mm (2") are introduced above and below the SCDA hole.

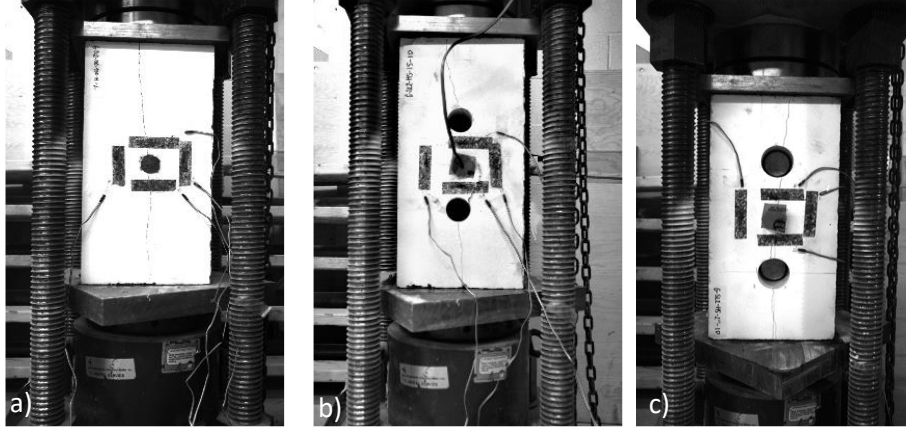


Figure 5.7 Complete Breakage of specimens a) G-SL2-100-400-M-L b) G-SL2-SH-1.5-1D c) G-SL2-SH-2.0-1D

Table 5.6 presents the time of first crack and the time of complete breakage. A single 25.4 mm (1”) SCDA hole generated an initial fracture between 10-10.5 hours and the specimen was fully split after 17 hours. For specimens G-SL2-SH-1.5-1D and G-SL2-SH-2.0-1D, where relief holes are present, fracture initiation similarly occurred between 9.5- 11.5 hours. However, more time was needed for the slab to fully split at 18-23 hours for the two configurations where 38.1 mm (1.5”) and 50.8 mm (2”) relief holes are present.

Table 5.6 Summary of test results for Hole Shielding

Test Type	Specimen	Time of initial fracture (TFC) (hours)	Time of complete breakage (hours)
No shield hole	G-SL2-100-400-M-L-01	10	17
	G-SL2-100-400-M-L-02	10.5	17
Hole shielding	G-SL2-SH-1.5-1D-01	9.5	21
	G-SL2-SH-1.5-1D-02	10	23
	G-SL2-SH-2.0-1D-01	9.8	18
	G-SL2-SH-2.0-1D-02	11.5	23

The measured strains are presented in Figure 5.8-5.10. It appears that the measured strains for all specimens increase exponentially over time. This exponential strain increase can be attributed to fracturing which is corroborated by images from the high-resolution camera. The measured strains will serve as basis for calibration for the XFEM model.

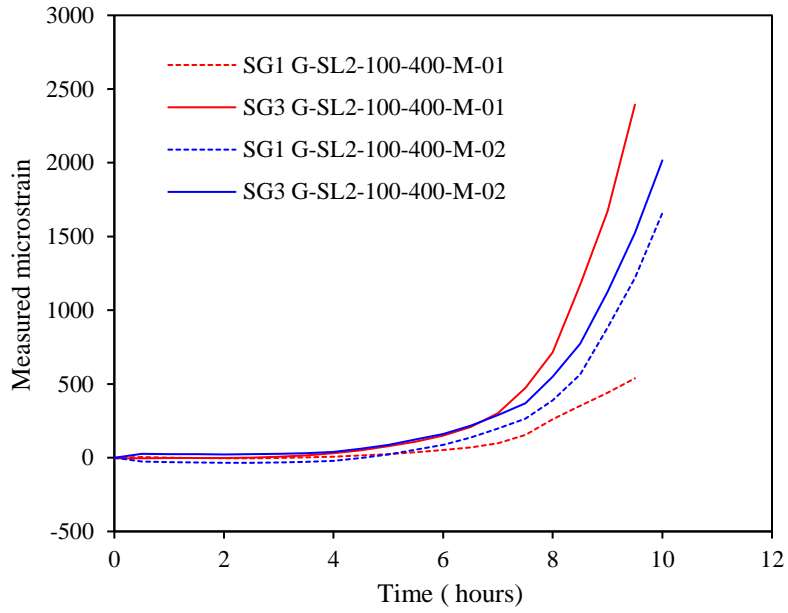


Figure 5.8 Specimen G-SL1-100-400-M-01,02 measured strain

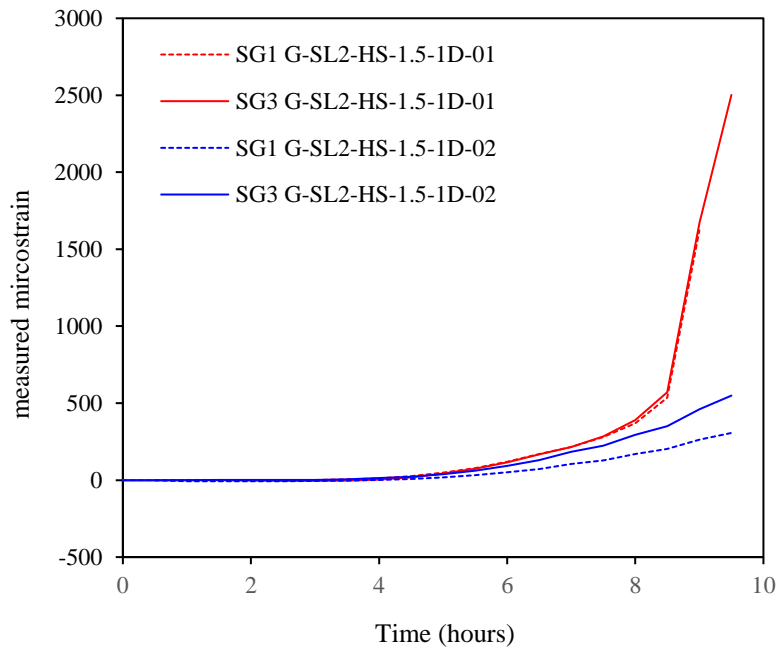


Figure 5.9 Specimen G-SL2-HS-1.5-1D-01,02 measured strain

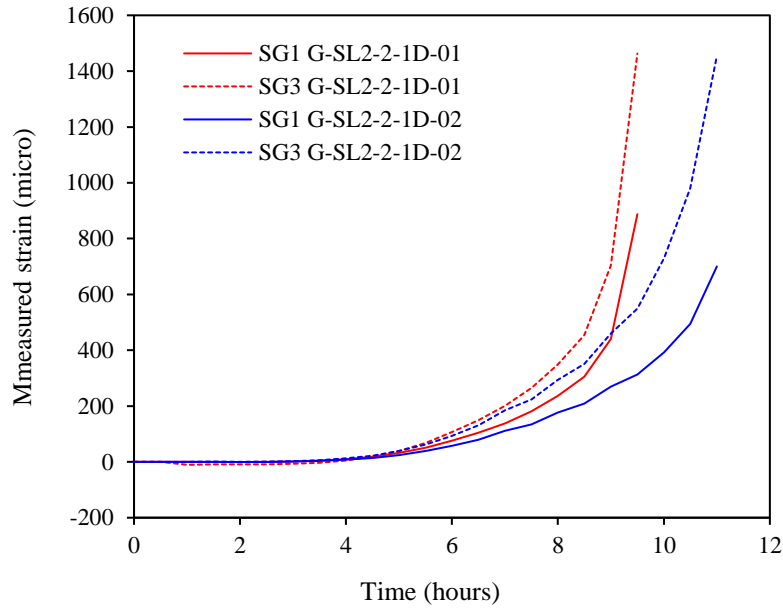


Figure 5.10 Specimen G-SL2-HS-2-1D-01,02 measured strain

5.3.3 XFEM Model

A numerical model was constructed in Abaqus to determine the required initialized SCDA stress to split the slab. The model parameters are similar to those presented in Section 5.2.1 with a few modifications. First, both ends of the slabs are greased with MoS₂; and a cohesive element with a shear strength of 0.25 MPa is therefore attached to both ends of the slabs. Second, the relief holes were introduced, and XFEM crack initiation points were added to the relief holes. The XFEM domain is highlighted in Figure 5.11.

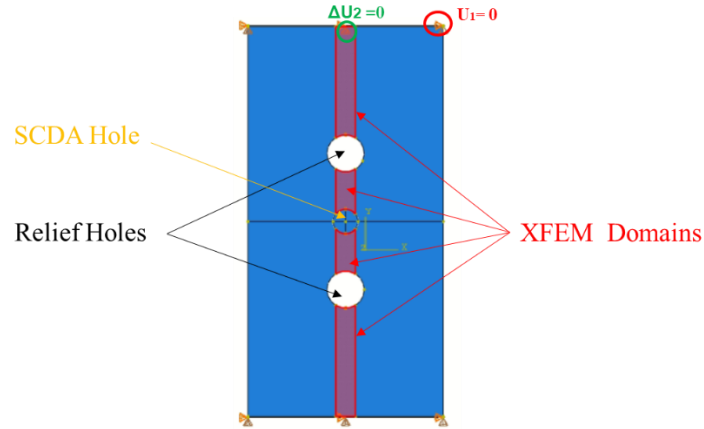


Figure 5.11 XFEM model for hole shielding test

5.3.4 Numerical Modeling Results

With the numerical model, the initialized stress required to split the slab can be determined. As discussed in Section 5.3.1, it is postulated that the addition of relief holes above and below the borehole will prolong the time needed for complete breakage to occur. In terms of model inputs, the initial SCDA stress required to split the slab will be higher, meaning more time is needed to attain this pressure. The same procedure is followed from Section 5.3.3 to estimate the initialized SCDA stress needed for crack initiation and complete breakage. As shown in Table 5.7, the critical strain is taken at SG1 for all specimens due to their symmetry

Table 5.7 Critical Strain of specimens (extracted from Figure 5.8-10)

Specimen #	Specimen I. D	Strain Gauge #	Critical Strain
1	G-SL1-100-400-M-01,01	SG1	86
2	G-SL2-SH-1.5-1D-01,2	SG1	115
3	G-SL2-HS-2-1D-01,02	SG1	69

As shown in Table 5.8, the initialized SCDA stress for fracture initiation in the hole shielding

specimens varies between 36 to 39.5 MPa with an average of 37.8 MPa. The initialized stress in a single SCDA hole for fracture initiation is lower at 27 MPa. Overall, the initialized SCDA stress required for fracture initiation increases in the specimen with shielding holes. The applied uniaxial stress is deviated around the SCDA hole by the relief holes, reducing the magnitude of the tensile stresses at crown and floor of the SCDA hole which contribute to Mode I fracture initiation. The potential SCDA pressure for complete fracturing is also assessed for all 3 sets of tests. As shown in Table 5.8, an initialized SCDA stress of 85MPa is required to completely fracture the specimen with single SCDA hole, G-SL1-100-400-M-01. Specimen G-SL2-SH-1.5-1D requires an initialized stress of 128MPa while specimen G-SL2-SH-2.0-1D with a 2” relief hole requires even higher potential SCDA stress at 131 MPa. These results indicate that the presence of relief holes in the direction of the major principal do not benefit crack propagation and in fact impedes faster crack growth. Based on both experimental and simulation results, the relief holes create a stress shadow which encompasses the SCDA hole. This decreases the loading-induced tensile stress at the crown and floor of the SCDA hole, thus hindering crack initiation.

Table 5.8 SCDA Pressure at Crack Initiation and Complete Breackage

Specimen #	Specimen I. D	SCDA Pressure (MPa)	
		Crack Initiation	Complete Breackage
1	G-SL1-100-400-M-01	27	85
2	G-SL2-SH-1.5-1D-01	36	128
3	G-SL2-SH-2-1D-01	39.5	131

5.4 Estimation of SCDA Hole Spacing

This section aims to estimate the spacing of SCDA in uniaxial conditions in an infinite medium,

representing in-situ rock with no boundary effects influencing crack propagation. As concluded in the previous section, the introduction of relief holes does not cause faster crack propagation compared to a single SCDA hole. Therefore, the numerical results obtained for a single SCDA hole from Section 5.3.4 are employed to estimate the spacing between SCDA holes in an infinite medium. The initialized stresses for complete breaking of specimens 1, 2, and 3 in Section 5.3.4 are applied to a larger slab simulating an infinite medium, and the maximum crack extension is measured from the model. The XFEM model is 1 m x 0.15 m with a 1.75” SCDA hole (infinite medium). Crack length above and below the SCDA hole is measured from the numerical model to estimate SCDA hole spacing under uniaxial loading condition. Both 1.5” and 1.75” SCDA are modelled. Table 5.4 presents the initialized SCDA stress required to fully break a slab 0.4 m x 0.15 m in the 150UT, 175M and 175LT. Note that these input stress represent a minimum of SCDA pressure potential, as the SCDA continues to expand after the slab is fully split. The hole spacing estimation provided in the study is therefore conservative. This limitation causes the hole spacing estimation to be conservative.

Table 5.9 Summary of initialized stress in SCDA and length of fracture

Numerical Model	Initialized SCDA Stress (MPa)	Φ (mm)	Longest XFEM Fracture, L_F (mm)	L_F/Φ
150-M-L (1 m x 0.15m)	95	38.1	845.8	22.2
175-M-L (1 m x 0.15m)	60	44.45	787.4	17.1

Given that the input stresses calibrated to split a much smaller slab, the stress is not sufficient to fully split the larger slab representing an infinite medium. The crack is measured in the model for the entire length of fracture (L_F) (Refer to Figure 5.12).

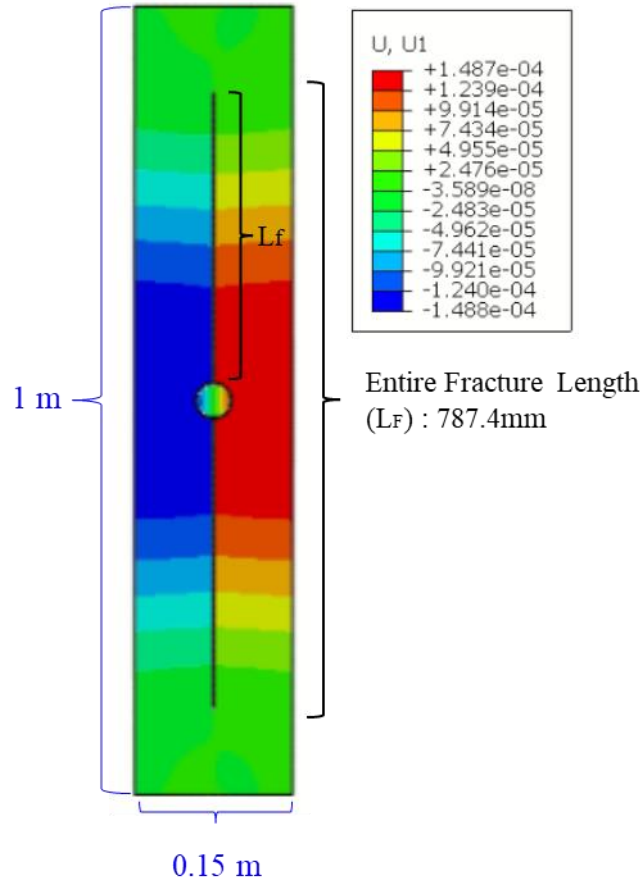


Figure 5.12 Typical XFEM model results

As shown in Figure 5.12, the length of fracturing caused by the initialization and release of an isotropic stress of 60 MPa in the SCDA in a 152.4 mm x 1000 mm granite slab is 14.5” from the edge of the hole. As shown in Table 5.9, the ratio of the length of fracture over the SCDA hole diameter (Φ), an indicator for maximum hole spacing, is presented for both a 1.5” and 1.75” SCDA hole in an ‘infinite medium’. As each SCDA can generate a fracture length L_f , the spacing, S , between two SCDA holes is calculated as $S=L_f/\Phi$. Thus, for practical applications, it postulated that the maximum allowable spacing between two SCDA boreholes is L_f/Φ , or 17.1 to 22.4. Given the conservative nature of the analysis, these values represent a minimum hole spacing at which crack coalescence will occur between 2 holes.

5.5 Conclusions

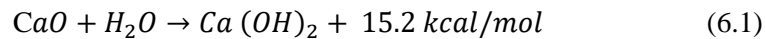
In this chapter the results of a series of experiments are used to calibrate a numerical model based on XFEM to estimate the true fracture length induced by a single SCDA hole, hence the spacing between them when used in an application involving uniaxial loading condition. The effect of hole shielding on crack initiation propagation is also investigated both experimentally and using XFEM. A set of 3 Stanstead granite specimens of 152.4 mm (6") x 203.2 mm (8") x 406.4 mm (16") with a single SCDA injected hole where the strains around the SCDA are measured. It was found that initialized stress required to initiate cracking is validated with a numerical model and ranges between 14 MPa and 17.8 MPa. The initialized SCDA stress required to split the slab is also determined with the numerical models and ranges between 57 MPa and 95 MPa. The optimal hole spacing is then determined based on the validated initialized stress required to split the slab by applying the initialized stress in an infinite medium. It is suggested that the spacing between SCDA boreholes should be between 17.1Φ and 22.2Φ for practical applications involving uniaxial compression. Such higher borehole spacing is suggested from the numerical modeling compared to the loaded specimen in Chapter 4 with a L_t/Φ of 12.8-14.6 Φ ; however, the lower ratio is attributable to the size limitation of the specimen which could not account for further crack propagation. A separate experiment is then conducted to determine the effect of hole shielding using the same instrumentation and modelling scheme. It was found that the initialized SCDA stress ranges between 36 MPa and 39.5 MPa. It was also found that the specimens are harder to split overall with the introduction of relief holes of 38.1 mm (1.5") and 50.8 mm (2") above and below a 25.4 mm (1") SCDA filled hole. Higher initialized SCDA stresses of 128-131 MPa are needed to split the slab with relief holes compared to an initialized SCDA stress of 85 MPa required to split a slab without the introduction of relief holes. These results corroborate with the

experimental results which showed that the introduction of relief holes did not speed up crack propagation.

Chapter 6: The influence of different environmental conditions on SCDA

6.1 Introduction

As discussed in Chapter 5, the breakage of rock due to expansive cement pressure occurs when the tensile strength of the rock is exceeded (Harada et al., 1989). The source of this expansion comes from the hydration of CaO or lime – the main ingredient in Betonamit – which generates calcium hydroxide crystals. As shown in Eq. (6.1), the generation of calcium hydroxide crystals is exothermic and can generate up to 150° C of heat (Hinze & Brown, 1994).



In Chapter 3, the pressure was quantified using miniature pressure sensors while also monitoring the heat of hydration of SCDA. It was demonstrated that the generation of heat during hydration of SCDA is dependent on the hole size. The peak heat of hydration of SCDA generates up to 40°C for a 25.4 mm (1”) hole and 51°C for a 38.1 mm (1.5”). Based on experimental results, a higher heat generation corresponds to high SCDA expansive pressure in thick-walled steel cylinders. However, the heat of hydration of Betonamit has not been investigated in different environmental conditions where more or less hydration heat might be released to the environment. Monitoring the heat of SCDA in different temperature and humidity conditions could serve as an indicator of the TFC (time of first crack) of rock in the field.

In this chapter, the effect of different ambient conditions such as high humidity and low to high temperatures on SCDA is investigated. Granite cubes with a 38.1 mm (1.5”) central SCDA holes are subjected to various humidity levels (35°C at 30%, 70% and 90% humidity), hot conditions (30°C and 40°C) and cold conditions (-5°C, 5°C, 10°C) to simulate a range of possible conditions encountered in underground mines using a controlled test chamber (Microclimate benchtop

chamber, Model #: MCB (H)-1.2, Figure 6.1). Two samples were subjected to 20°C and 25°C to serve as a frame of reference. The recording of strain measurements along with the monitoring of the heat of hydration of SCDA hydration evolution are tools used to detect the TFC and MDT (minimum demolition time). Thus, the goal of this study is to be able to use strain measurements and peak hydration temperature of SCDA to the TFC.



Figure 6.1 Microclimate benchtop chamber (Model #: MCB (H)-1.2).

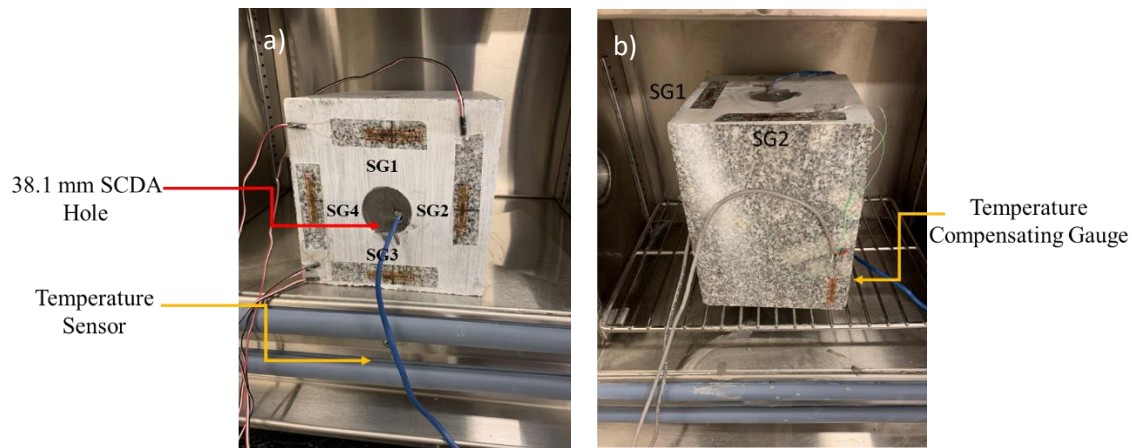
6.2 Experimental Program

A series of tests is conducted on Stanstead granite specimens of dimensions 152.4 mm x 152.4 mm x 203.2mm (6'' x 6'' x 8'') with a single central 38.1 mm (1.5'') SCDA hole. Commercially available Betonamit is selected for this study. SCDA is mixed with 20% water by weight for 10 minutes and poured directly into the borehole. SCDA performance under different environmental conditions are assessed in three ways as follows.

- 1) Measured strains around the borehole; 2 strain gauges, one above (SG1) and one below (SG3) the borehole, placed horizontally, and 2 strain gauges, one to the right (SG2) and one to the left (SG4) of the borehole, placed vertically (refer to Figure 6.2a for the locations

of strain gauges). For extreme temperature conditions such as -5°C to 10°C and 35°C to 40°C , a dummy gauge is introduced to compensate for temperature change. In these cases, only two strain gauges are used; SG1 (Left side of borehole) and SG2 (below borehole) with a dummy gauge each (Refer to Figure 6.2b for strain gauge configuration for temperature compensating wiring of gauges).

- 2) Visual cracking with a thermal image camera to detect the TFC and MDT (minimum demolition time) which is defined as point in time at which fracture reaches all free surfaces of the sample.
- 3) Temperature Sensor to monitor the hydration of SCDA up until fracture



a) For $20-0^{\circ}\text{C}$ ambient temperature

b) For -5°C to -10°C and $35-40^{\circ}\text{C}$

Figure 6.2 Strain gauge configurations

A total of 10 rock samples were tested in this study. To identify each sample, the nomenclature M-C-ID-HD-T-H-XX is adopted whereby

- M: Material, e.g., G for Granite
- C: Specimen Dimension e.g. (152.4 mm (6'') x 152.4 mm (6'') x 203.3 mm (8''))

- ID: Internal Diameter in inches, e.g., 381 for 38.1 mm (1.5”) borehole.
- HD: Hole Depth in inches, e.g., 600 for 152.4 mm (6”)
- T: Temperature (Degree Celsius)
- H: Humidity (%)

The hole depth is fixed at 4 times the hole diameter. Table 6.1 summarizes the samples tests.

Table 6.1 Description of tested specimen

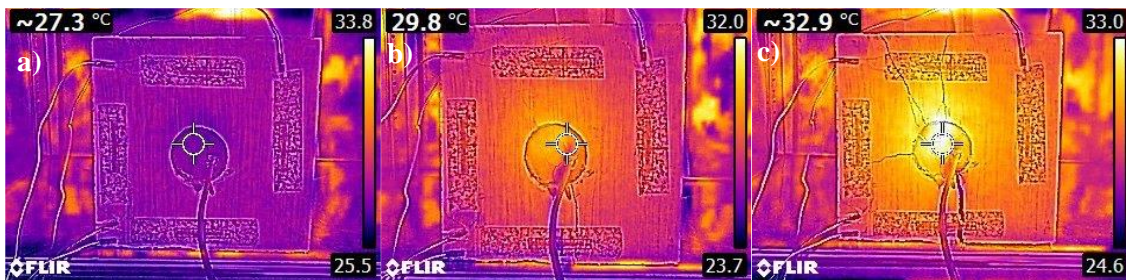
Effect	Sample ID	Temperature (°C)	Humidity (%)
Cold Conditions	G-C-150-600- (-5)-30	-5	30
	G-C-150-600-5-30	5	30
	G-C-150-600-10-30	10	30
Hot Conditions	G-C-150-600-20-30	20	30
	G-C-150-600-25-30	25	30
	G-C-150-600-30-30	30	30
	G-C-150-600-40-30	40	30
Humid Conditions	G-C-150-600-35-30	35	30
	G-C-150-600-35-70	35	70
	G-C-150-600-35-90	35	90

6.3 Results and Discussion

It was concluded in Chapter 5 that the measured strains for all specimens increase exponentially at some point in time, and this exponential behavior is interpreted as the onset of nonlinear behaviour due to tensile damage progression in the sample. The results in Chapter 5 demonstrated that strain measurement is a reliable indicator for fracture initiation in the case that fracture initiation could not be detected visually. Consequently, the strain at which this linear increase terminates, or the onset of nonlinear behaviour, is interpreted as an indication that cracking has initiated. Since the specimen is in an enclosed space, the controlled temperature chamber, the strain gauges served as a reliable tool to detect crack initiation.

To investigate the effect of various environmental conditions, the granite sample is first subjected to 25 °C, room temperature, as a base case. The time of cracking was identified by plotting

measured strains over time by also recording the SCDA heat of hydration. As shown in Figure 6.3, visual cracking is depicted with a thermal image camera to show cracking and the temperature of the rock. As can be seen, TFC is found to be at 4.5 hours and the MDT is 5.5 hours. As shown in Figure 6.4, strains begin to increase at 2 hours for SG2, SG3, SG4 and then followed by a decrease in strain at 3 hours and an exponential increase at SG1. This decrease in strain at 2 hours is attributed to the local stress relief due to cracking which is visually detected after 1.5 hours. The exponential behaviour depicted at SG1 indicates cracking will begin above the borehole and shortly after. As can be seen, 4 cracks are shown to propagate to the free surfaces of the specimen at 5.5 hours. The strains beyond 4 hours are not depicted as the intersection of cracks with the strain gauge caused damage to the gauges and readings are no longer deemed relevant. This corroborates with the trends in Chapter 5. The heat of hydration of SCDA shown in Figure 6.4, show with peak temperature 31.3 °C at 4.5 hours right when TFC occurs. The peak SCDA temperature could then serve as an indicator of when cracking occurs when visual observation is not possible. Another peak is observed at 2 hours before the TFC is observed right when the critical strain is detected indicating that fracturing initiation could have occurred deeper in the sample.



a)

b)

c)

Figure 6.3 G-C-150-600-25-30 a) t_0 b) TFC at $t_{4.5}$ c) MDT at $t_{5.5}$

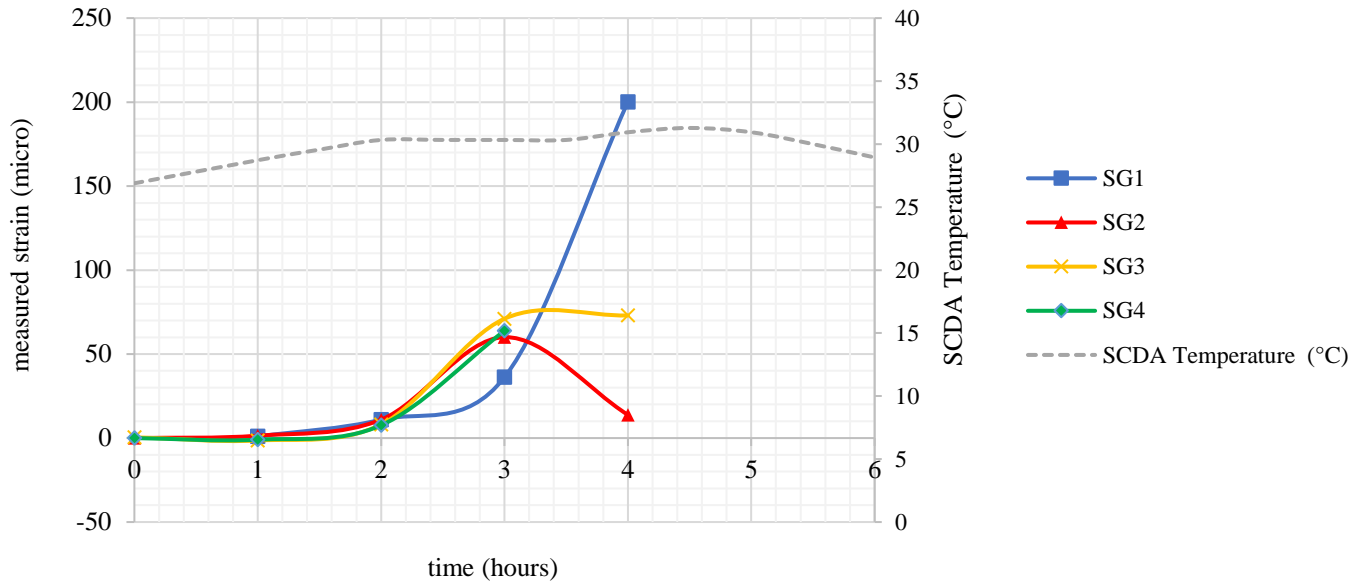


Figure 6.4 Measured strains and SCDA heat of hydration of specimen G-C-150-600-25-30

6.3.1 Effect of cold temperature

Most Canadian surface mining operations are found in Canada's north where cold temperature persists most of the year. Therefore, understanding the performance of SCDA in cold environment is important for rock breakage in surface mines. The effect of cold temperature is assessed by subjecting 3 samples to three temperatures namely -5°C , 5°C , and 10°C , while keeping the humidity constant at 30%.

Figure 6.5 shows specimen G-C-150-600- (-5)-30 at the start of the experiment (Fig, 6.5a), at TFC of 39 hours (Figure 6.5b) and at MDT of 45 hours (Figure 6.5c). An exponential strain increase is observed at 35 hours, i.e., 4 hours before cracking can be visually detected. As shown Figure 6.6, three temperature peaks are detected, however, the highest increase in SCDA temperature is at 40 hours with a temperature increase from -3°C to -2°C , at the point in which the TFC is detected an hour earlier. More samples are subjected to ambient cold conditions to identify the latter trend.

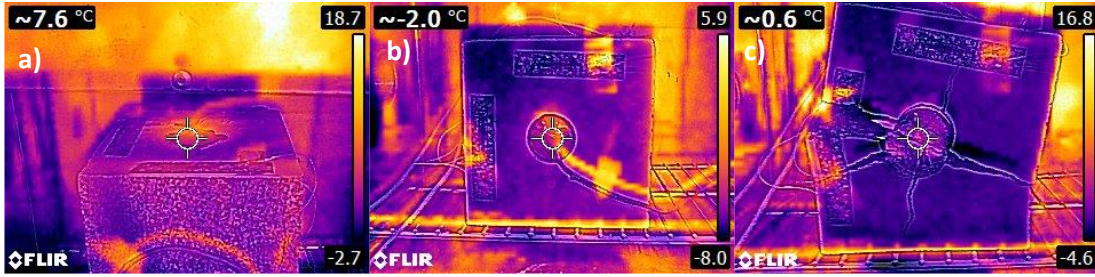


Figure 6.5 Sample G-C-150-600-(-5)-30 a) t_0 b) TFC at t_{39} c) MDT at t_{45}

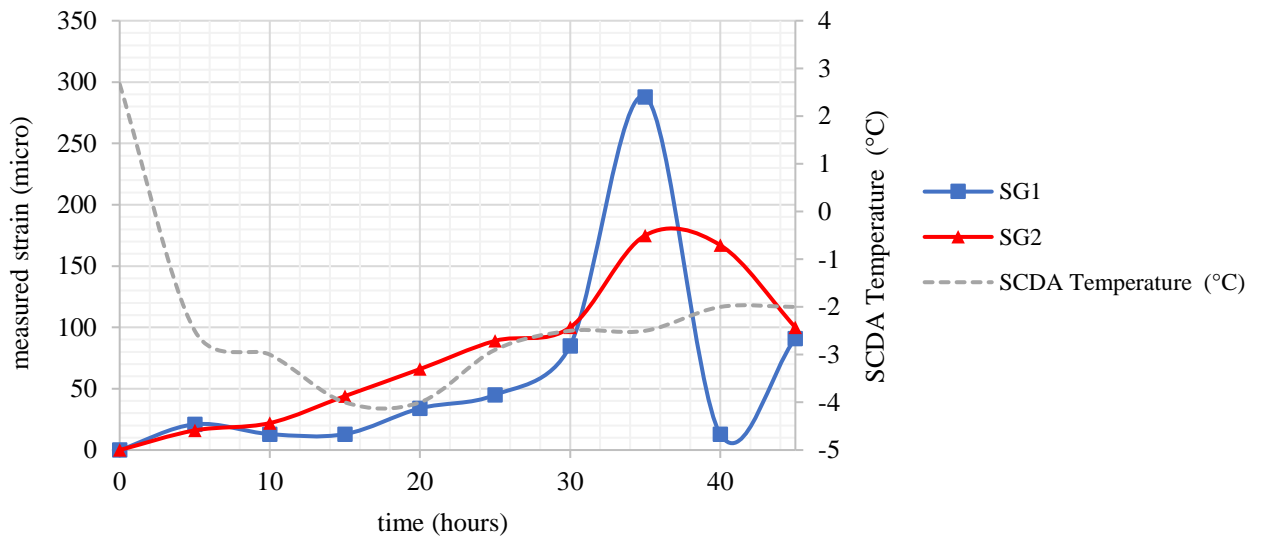


Figure 6.6 Measured strains and SCDA heat of hydration of specimen G-C-150-600-(-5)-30

As shown in Figure 6.7, once the ambient temperature is increased to 5°C , the TFC is significantly reduced to 18 hours visually and 22 hours of MDT. As can be seen in Figure 6.8, there are also three peaks in temperature in which the second peak appears 4 hours before the visual TFC is detected. The same trend is observed with the previous sample subjected to -5°C where the second peak in SCDA temperature is detected 9 hours before TFC. In addition, another peak is detected right at 22 hours when the block is considered broken, where the fractures have reached the free surfaces of the samples (MDT). Initially, the SCDA temperature is at 6.3°C and increases to 8.2°C

and 8.4°C at 14 hours and 22 hours respectively. The critical strain is also observed at 15 hours, 3 hours before cracks could be visually detected.

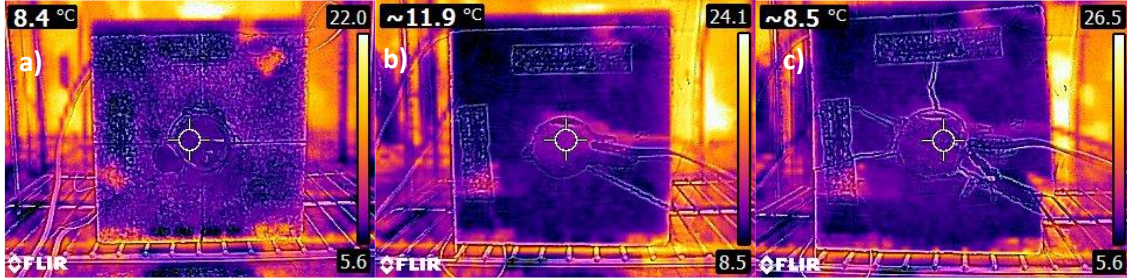


Figure 6.7 G-C-150-600-(5)-30 a) t_0 b) TFC at t_{18} c) MDT at t_{22}

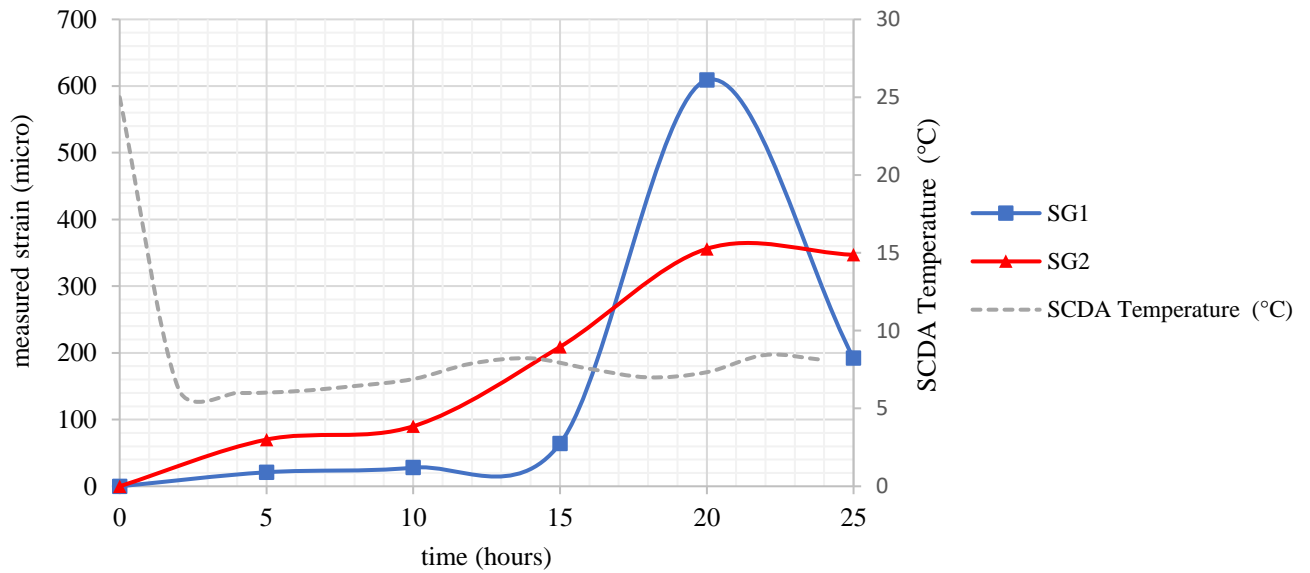


Figure 6.8 Measured strains and SCDA heat of hydration of specimen G-C-150-600-(5)-30

As shown in Figure 6.9, when the sample is subjected to 10°C, the TFC is decreased by 4 hours compared to the sample subjected to 5°C, and the MDT is also reduced by 4 hours. As can be seen in Figure 6.10, the measured strains for SG1 start to increase at 10 hours while SG2 also exponentially increases, however, the measurements are shortly cut off due to strain gauge damage. The same trend is observed for the SCDA temperature evolution. As can be seen, the

temperature increases at 10 hours, shortly before TFC is detected at 14 hours and again when the sample reaches its MDT.

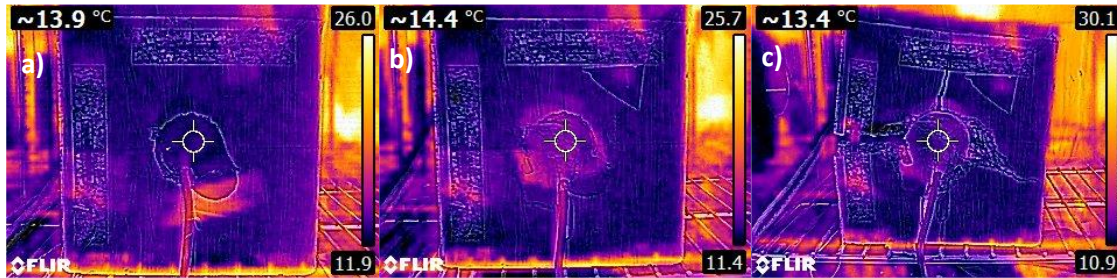


Figure 6.9 G-C-150-600-(5)-30 a) t_0 b) TFC at t_{14} c) MDT at t_{18}

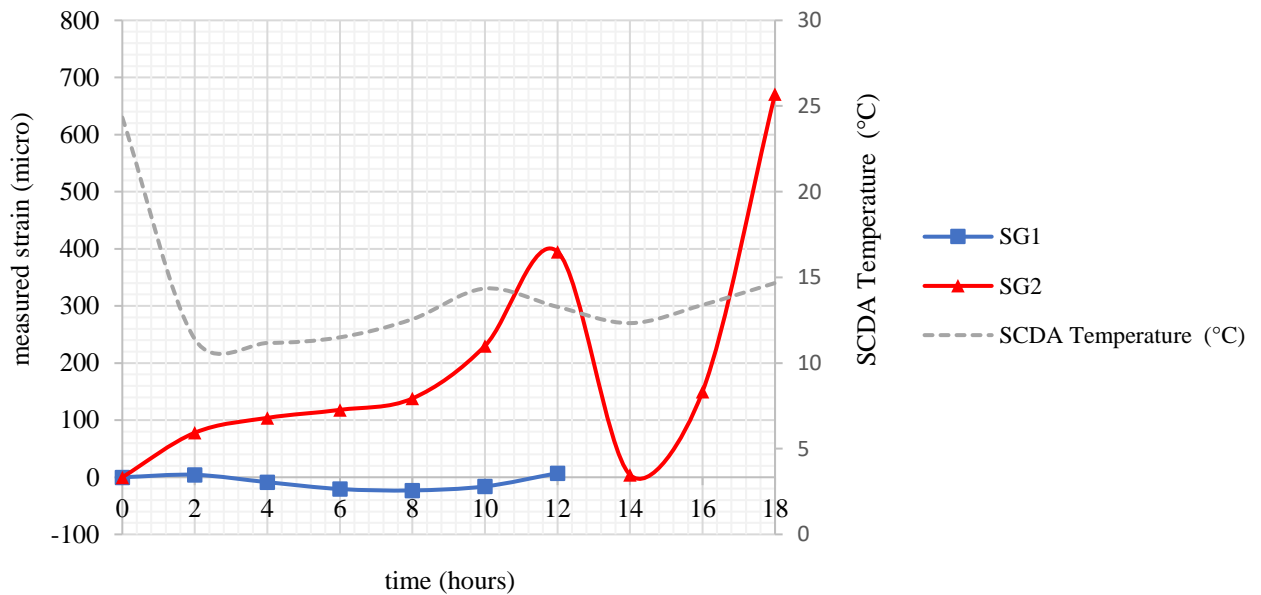


Figure 6.10 Measured strains and SCDA heat of hydration of specimen G-C-150-600-(5)-30

6.3.2 Effect of hot conditions

The effect of higher temperatures is then investigated. One sample is subjected 20°C to serve as a frame of reference to assess the effect of hotter temperatures on SCDA. It is shown that when the sample is subjected to 20°C, the TFC is at 6.75 hours and the MDT occurs shortly afterwards in

half an hour. Compared to the previous samples subjected to colder conditions (-5°C, 5°C, and 10°C) whereby the MDT is reached 4-9 hours after cracking has initiated, the MDT is reached faster following the TFC. It is also observed that there is only one peak in SCDA temperature at 24°C which happens at 5 hours; almost 2 hours before the TFC is visually detected. Being that the sample is subjected to higher ambient temperature, a clearer trend is observed between the measured strains and the SCDA hydration evolution. As shown in Figure 6.10, the SCDA temperature increases concurrently with the measured strains indicating that the SCDA is starting to generate calcium hydroxide crystals, which are the source of expansion of Betonamit.



Figure 6. 11 G-C-150-600-(20)-30 a) t_0 b) TFC at $t_{6.75}$ c) MDT at $t_{7.25}$

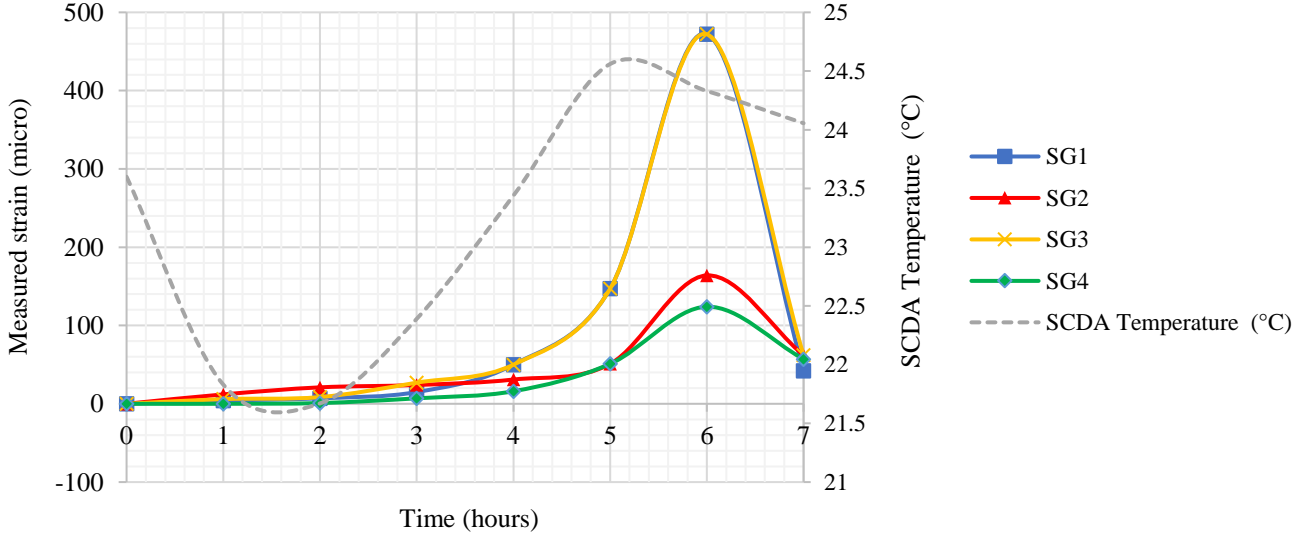


Figure 6.12 Measured strains and SCDA heat of hydration of specimen G-C-150-600-(20)-30

As shown in Figure 6.11, when the sample is subjected to 30°C the TFC is reduced to 3 hours and the MDT is reached half an hour later, the same time delay observed in the sample subjected to 20°C. As shown in Figure 6.12, that the temperature also concurrently increases with the measured strains with a peak temperature of 43°C when the MDT is reached.

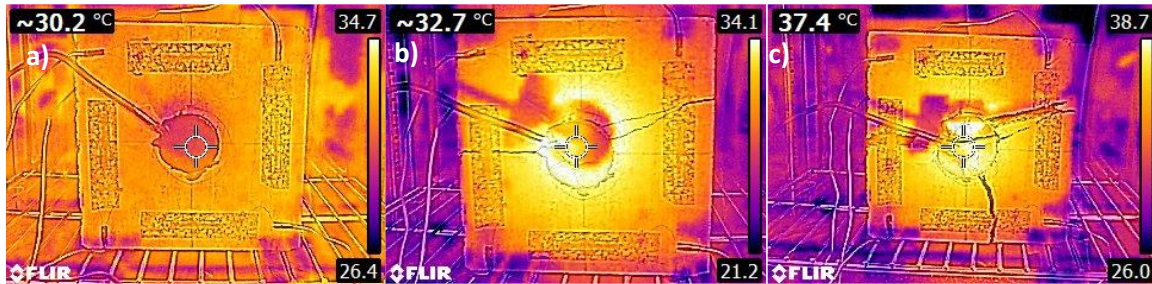


Figure 6.13 G-C-150-600-(20)-30 a) t_0 b) TFC at t_3 c) MDT at $t_{3.5}$

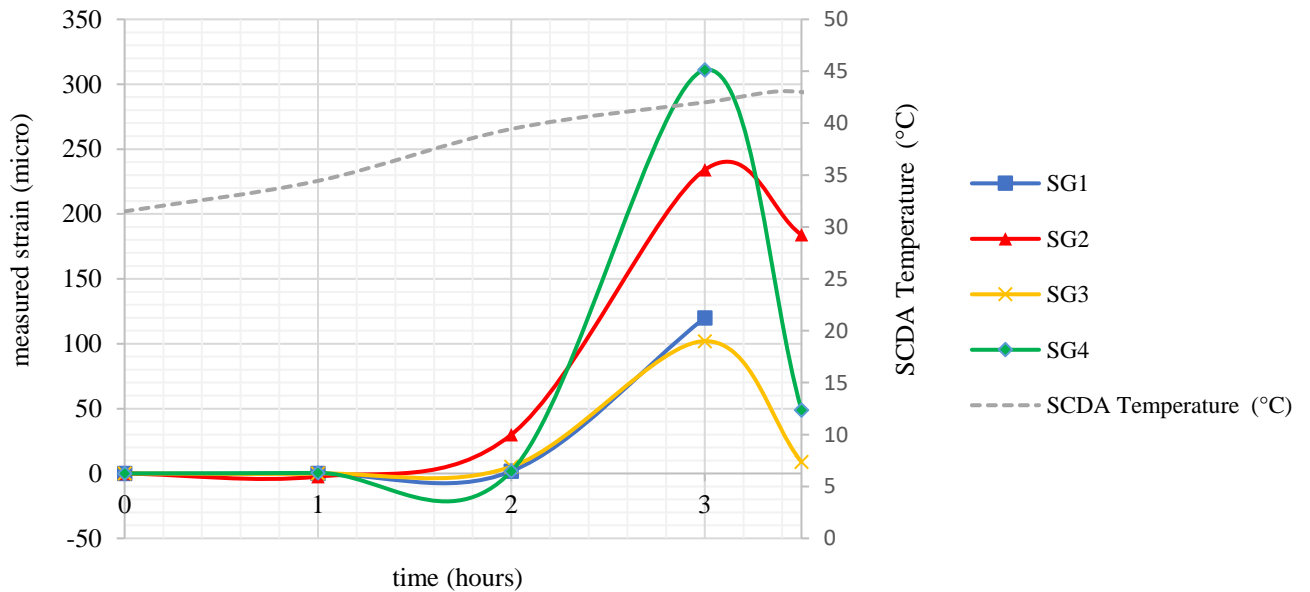


Figure 6.14 Measured strains and SCDA heat of hydration of specimen G-C-150-600-(30)-30

Lastly, subjecting the sample to a temperature of 40°C, the TFC occurs in less than an hour at 0.7 hours and MDT occurs an hour later (Refer to Figure 6.15).

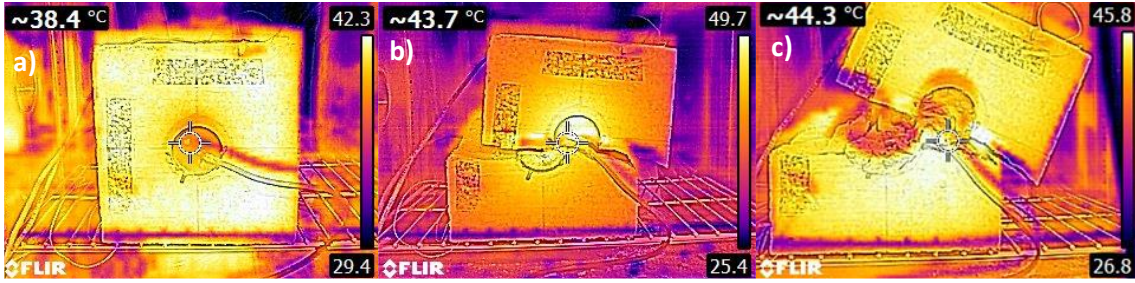


Figure 6.15 G-C-150-600-(40)-30 a) t_0 b) TFC at $t_{0.7}$ c) MDT at $t_{1.7}$

As shown in Figure 6.16, a higher SCDA temperature of 77°C is recorded at MDT. With that, it is shown that the peak SCDA heat of hydration is higher with higher ambient temperature. The same trend is observed with strains decreasing at 0.75 at SG2 and strain exponentially increasing at SG1 shortly after the TFC is observed.

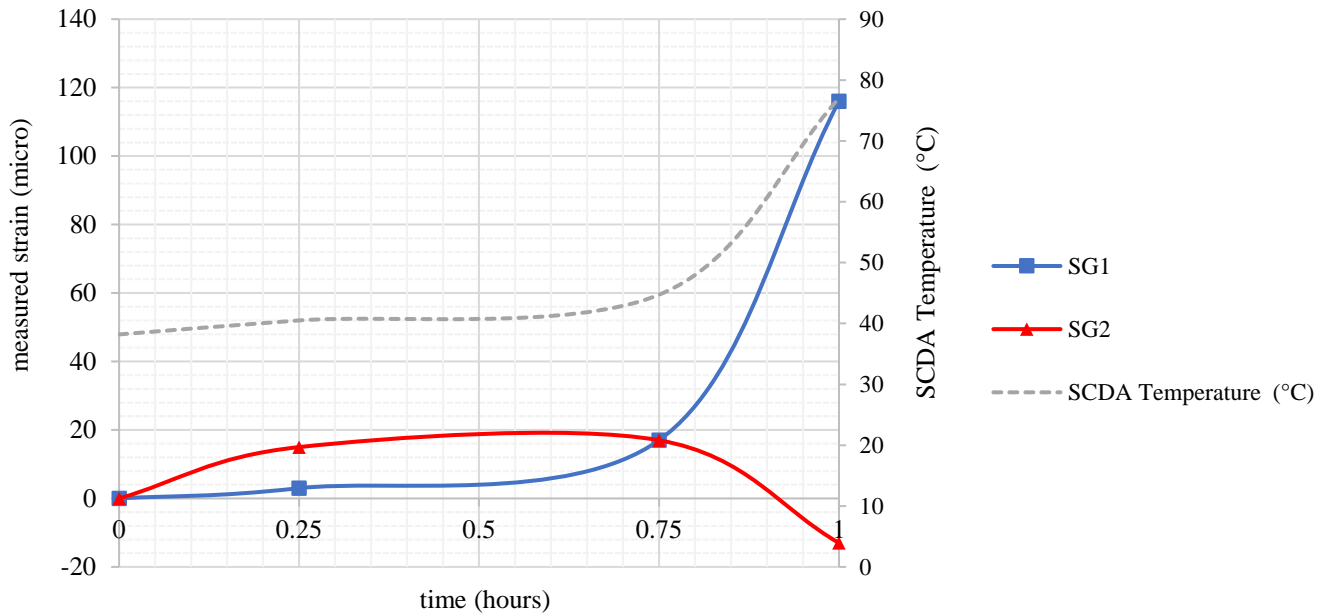


Figure 6.16 Measured strains and SCDA heat of hydration of specimen G-C-150-600-(40)-30

6.3.3 Effect of humid conditions

Investigating the effect of humidity on SCDA performance was deemed important as underground mines are known to encounter high humidity levels at depth. A range of humidity levels is investigated. Three samples were subjected to low, medium, and high humidity of 30%, 70%, 90% at an ambient temperature of 35°C. As shown in Figure 6.15, 6.17, and 6.19, all samples exhibit a TFC of 1.5 hours and MDT of 2 hours.

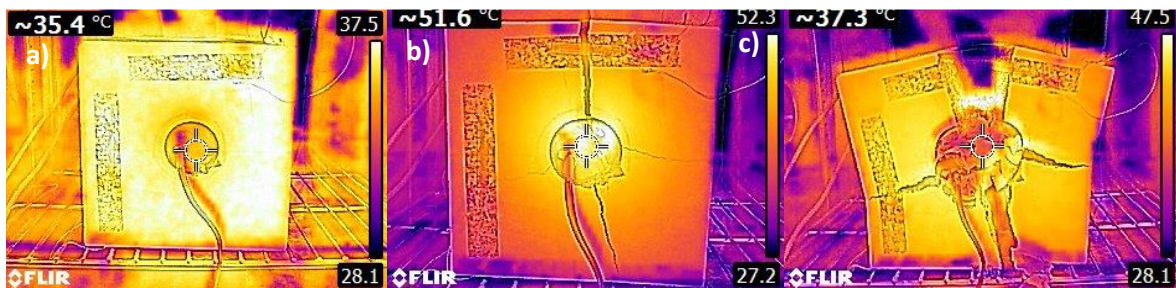


Figure 6.17 G-C-150-600-(35)-30 a) t_0 b) TFC at $t_{1.5}$ c) MDT at t_2

It can also be seen in Figures 6.18, 6.20, and 6.22 that the measured strain starts to show non-linearity after 1 hour where a TFC is observed half an hour later. It can be concluded that the humidity level does not have a significant effect on the TFC compared to the ambient temperature. The ambient temperature overrides the effect of humidity.

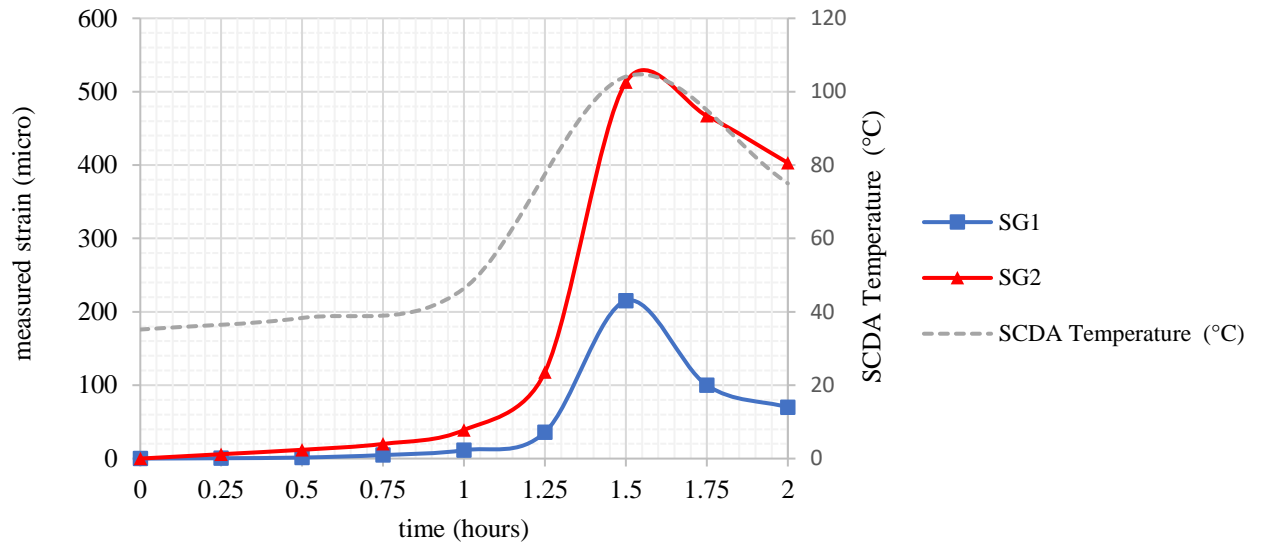


Figure 6.18 Measured strains and SCDA heat of hydration of specimen G-C-150-600-(35)-30

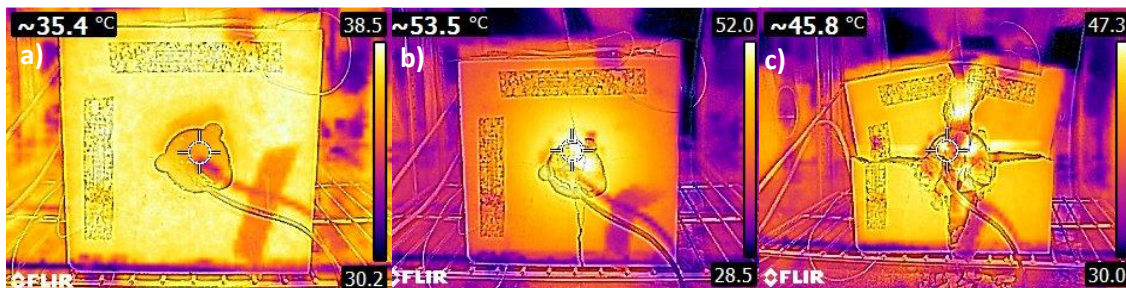


Figure 6.19 G-C-150-600-(35)-30 a) t_0 b) TFC at $t_{1.5}$ c) MDT at $t_{2.5}$

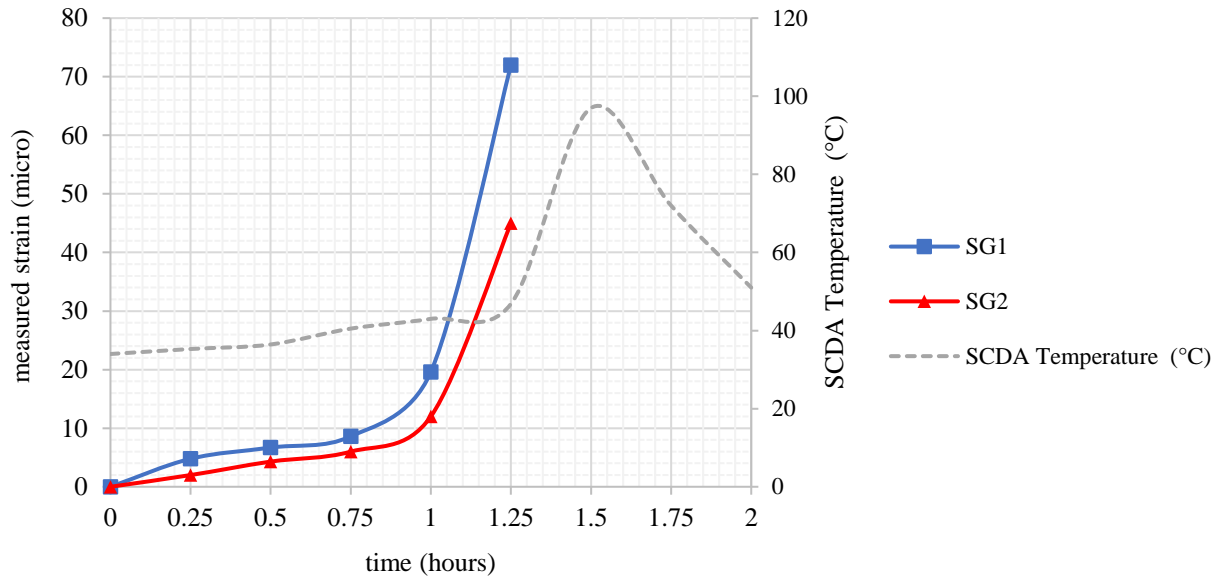


Figure 6.20 Measured strains and SCDA heat of hydration of specimen G-C-150-600-(35)-70

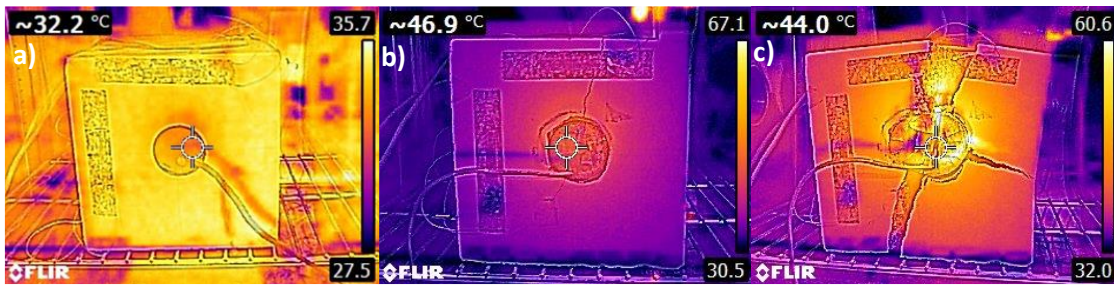


Figure 6.21 G-C-150-600-(35)-90 a) t_0 b) TFC at $t_{1.5}$ c) Time of Complete Fracturing t_2

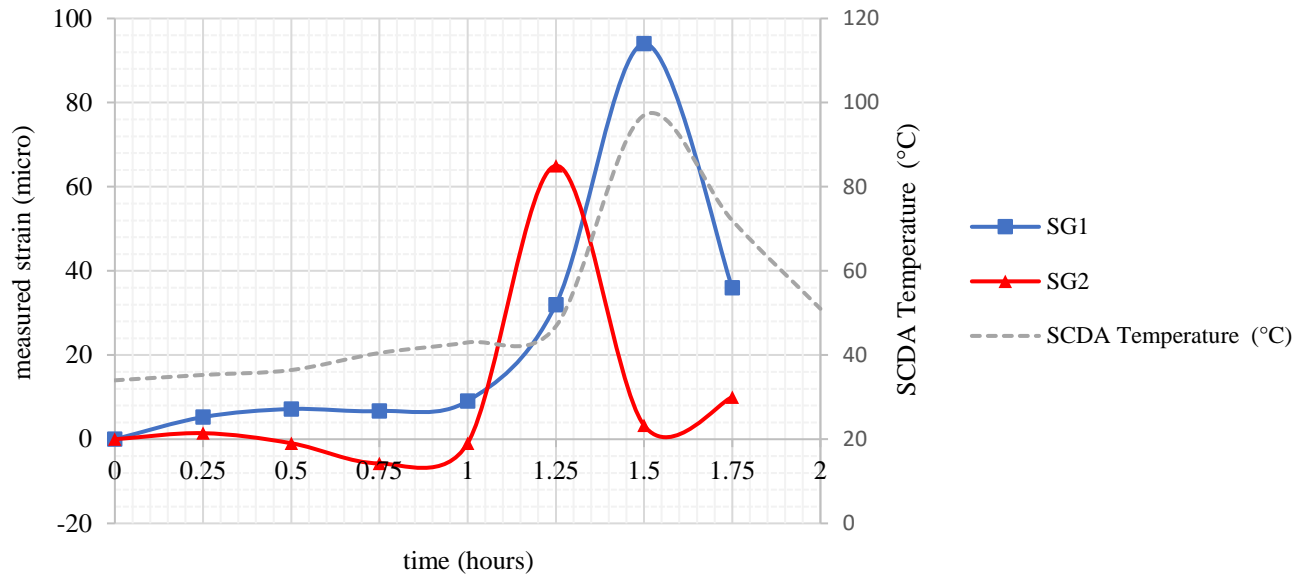


Figure 6.22 Measured strains and SCDA heat of hydration of specimen G-C-150-600-(35)-90

Table 6.2 Summary of Test Results

Effect of Temperature	Sample Configuration	TFC (hours)	MDT (hours)
Effect of Cold Conditions	G-C-150-600- (-5)-30	39	45
	G-C-150-600-5-30	18	22
	G-C-150-600-10-30	14	18
Effect of Hot Conditions	G-C-150-600-20-30	6.75	7.25
	G-C-150-600-25-30	4.5	5.5
	G-C-150-600-30-30	3	3.5
	G-C-150-600-40-30	0.7	1.7
Effect of Humid Conditions	G-C-150-600-35-30	1.5	2
	G-C-150-600-35-70	1.5	2
	G-C-150-600-35-90	1.5	2

A clear trend in TFC and MDT with respect to the ambient temperature is presented in Figure 6.23. As can be seen, the TFC and MDT significantly increase with decreasing temperature. This demonstrates that the performance of SCDA will vary depending on the mining depth where the ambient temperature increases with depth.

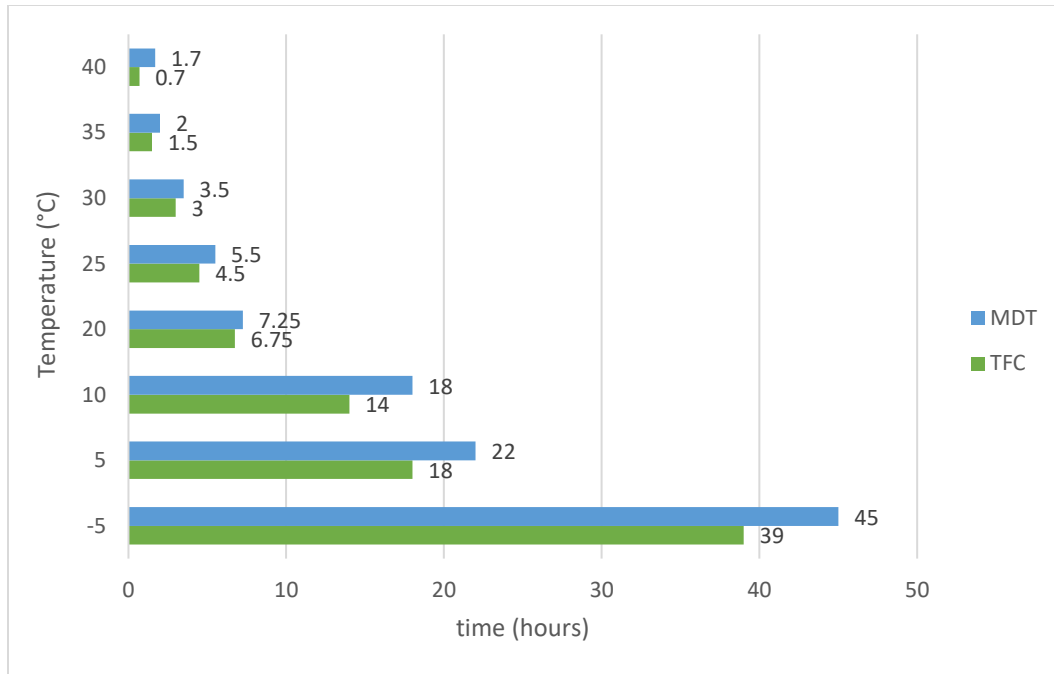


Figure 6.23 shows the summary TFC and MDT in different ambient conditions

6.4 Conclusions

In this chapter, the results of a series of experimental tests are reported to identify the effect of ambient temperature and humidity on SCDA. Stanstead granite specimens of 152.4 mm (6'') x 152.4 mm (6'') x 203.2 mm (8'') are used to test the influence of low to high temperature and humidity on the fracturing time with 38.1 mm (1.5'') SCDA holes. Time to fracture initiation is determined in terms of TFC and fracture completion is determined in terms of MDT from the time of mixing. It is shown that fracturing time decreases with increasing ambient temperature size. The TFC for a specimen subjected to cold temperature of -5° is 39 hours, compared to a specimen subjected to room temperature of 25°C , which exhibits a TFC of 4.5 hours. It is also observed that the heat of hydration of SCDA over time behaves differently in different conditions. Specimens subjected to colder temperatures such as -5°C , 5°C , and 10°C , show three peaks in SCDA temperature; one near the beginning of the test, one before the TFC is visually detected and one

when the MDT is reached. The highest peak in temperature, however, is shown to be when the specimen reaches its MDT. In warmer conditions, starting from 20°C, the evolution of the SCDA heat of hydration increases concurrently with the measured strains only one peak of hydration is detected shortly before the TFC is visually detected. Along with the strain measurements, which were already proven in Chapter 5 to be a reliable tool to detect the start of cracking, the SCDA heat of hydration can also be used as an indicator to detect the time of cracking in the cases where the fracture cannot be detected visually. Future work would involve investigating possible ways to reduce the TFC and MDT in colder conditions to render it a feasible method for rock fragmentation in surface mines during the winter.

Chapter 7: Field Applications

7.1 Introduction

In this chapter, field tests are conducted to test the performance of SCDA in real mining conditions. To begin, two large boulders were tested with SCDA: one on surface at Hoyle Pond mine and one underground at Éléonore mine site on Level 530. Following the boulder tests, two slash tests were performed underground at Éléonore mine site on Level 530. The goal of these tests is to assess SCDA effectiveness in real mining applications. The fragmentation of boulders with SCDA could be used to reduce the fragment size to enable mucking with a loader, whereas slashing with SCDA could be used at intersections to remove the underbreak to enable better traffic. It was concluded in Chapter 4 that the TFC decreases with borehole size under no loading conditions. The SCDA hole size was then selected based on the drill bit standards at the mine site and the largest size applicable for SCDA usage. At Hoyle Pond mine site, an SCDA hole size of 44.45 mm (1.75'') is selected while 50.8 mm (2'') SCDA hole is selected at Éléonore mine site. Based on previous findings in the literature, the appropriate spacing was used to design the hole pattern of the boulders with a spacing of 8Φ (unloaded conditions) (Gomez & Mura, 1984). As for the slash test, the L/Φ of 17.1-22.2 as estimated from Chapter 5 is used to design the spacing between holes. Some conservative modifications in spacing are made based on the ambient temperature, stress conditions, and based on the first tests performed on the first boulder test and second slash test.

7.2 Experimental Program

7.2.1 Hoyle Pond Mine Site (Surface)

The first part of investigating the performance of SCDA in large scale setting is testing its effectiveness on boulders. The dimensions of the first boulder (Greywacke) at Hoyle Pond mine site are 1 m (39'') x 0.64 m (25'') x 3 m (120'') (height x thickness x length) (Refer to Figure 7.1). As shown in Figure 7.2, the boulder was placed on surface and exposed to winter conditions with a rock temperature of 13.5°C. Based on the findings in Chapter 6, subjecting a small granite sample with a single 1.5'' SCDA hole in 10°C ambient conditions took 14 hours for the TFC to be visually detected compared to a sample subjected to a room temperature of 25°C with a significantly lower TFC of 4.5 hours. Based on proposed spacing between SCDA holes of 8Φ suggested by Gomez & Mura (1984), the spacing is modified by reducing the spacing to 4.5Φ to take into account the cold ambient temperature. The spacing based on 1.75'' SCDA holes for the first boulder was 8''. Eight holes were drilled with an average depth of 0.3 m. (Refer to Table 7.1 for further test specifications).



Figure 7.1 Greywacke boulder tested at Hoyle Pond mine site

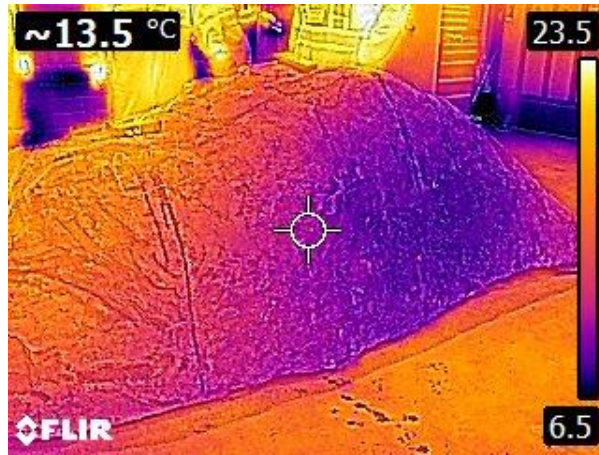


Figure 7.2 Rock Temperature Greywacke boulder at Hoyle Pond

7.2.2 Éléonore Mine Site (Underground)

7.2.2.1 Boulder Test

As shown in Figure 7.3, 3 different tests were conducted at Éléonore Mine Site at Level 530: the first test was conducted on a large boulder (Wacke) and two tests consisted of corner slashes (Wacke).

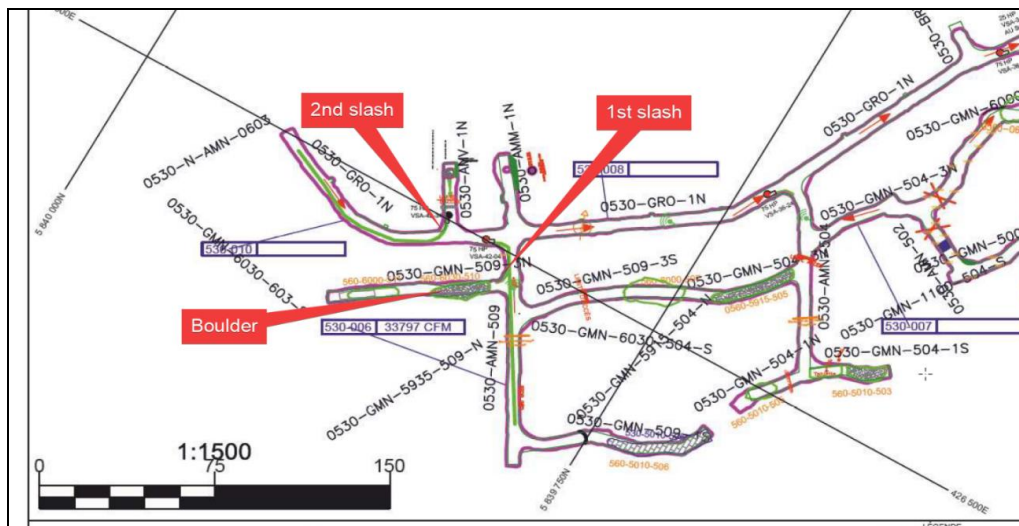


Figure 7.3 Plan view of Level 530 with locations of test performed at Éléonore Mine Site

The dimensions of the second boulder performed at Eléonore mine site are 1.12 m (44'') x 0.94 m (37'') x 3.8 m (148'') (height x thickness x length) (Refer to Figure 7.4). As shown in Figure 7.4, the boulder was also subjected to cold conditions with a rock temperature of 12.5°C



a) Front View

b) Top View

Figure 7.4 Wacke Boulder Test at Eléonore

Fig 7.4 Wacke Boulder Test at Eléonore

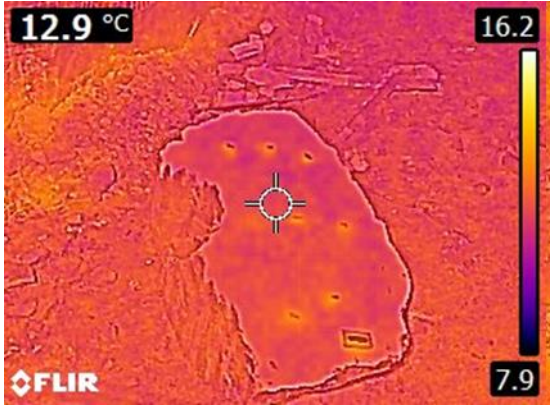
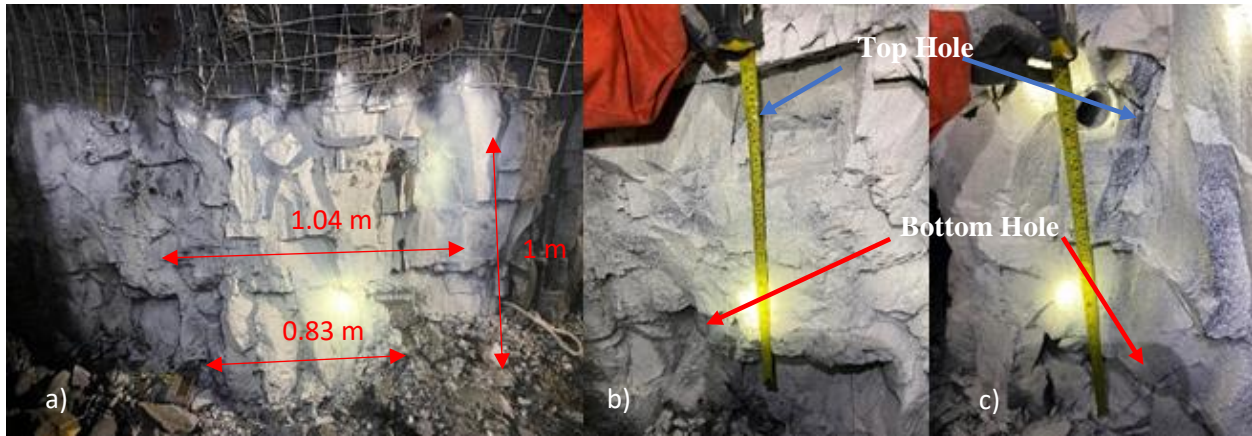


Figure 7.5 Rock Temperature of Boulder at Eléonore

The spacing of 4.5Φ is kept consistent from the previous boulder test at Hoyle Pond for the SCDA. Such that the SCDA holes are 2'', the spacing is calculated to be 9''. However, to optimize and reduce the quantity of SCDA used for such a large boulder, a spacing of 12'' is tested between SCDA holes in the rows and 32'' between SCDA holes in the columns. A total of 9 SCDA holes were drilled with average depth of 0.71 m.

7.2.2.1 Slash Test 1

The dimensions of the first slash test performed at Eléonore mine site are 1 m (39'') x 0.36-0.41 m (14-16'') x 0.83 to 1.04 m (33-41'') (height x thickness x length) (Refer to Figure 7.6). It was concluded in Chapter 4 that subjecting a sample under uniaxial stress accelerate the TFC. Based on the experimental results in Chapter 4, an L_F/Φ is estimated using Abaqus and was estimated to range between 17.1 and 22.2 under uniaxial conditions of 5MPa in an infinite medium. Such that the slash test was conducted 530 m deep, the uniaxial stress is calculated to be 14.2 MPa, a much higher stress than the small-scale tests performed in Chapter 4 which could also further reduce the TFC. As shown in Figure 7.7, the rock temperature of the slash was measured to be 12.5°C and as discussed previously, cold conditions could slow the TFC. Therefore, a lower L_F/Φ of 13 was used for the spacing between holes of the slash. Two 2'' holes were drilled 36-41 cm (14-16'') into the face with a spacing of 26'' with hole depth of 41'' (top hole) and 33'' (bottom hole).



a) Front View

b) Left side view

c) Right Side view

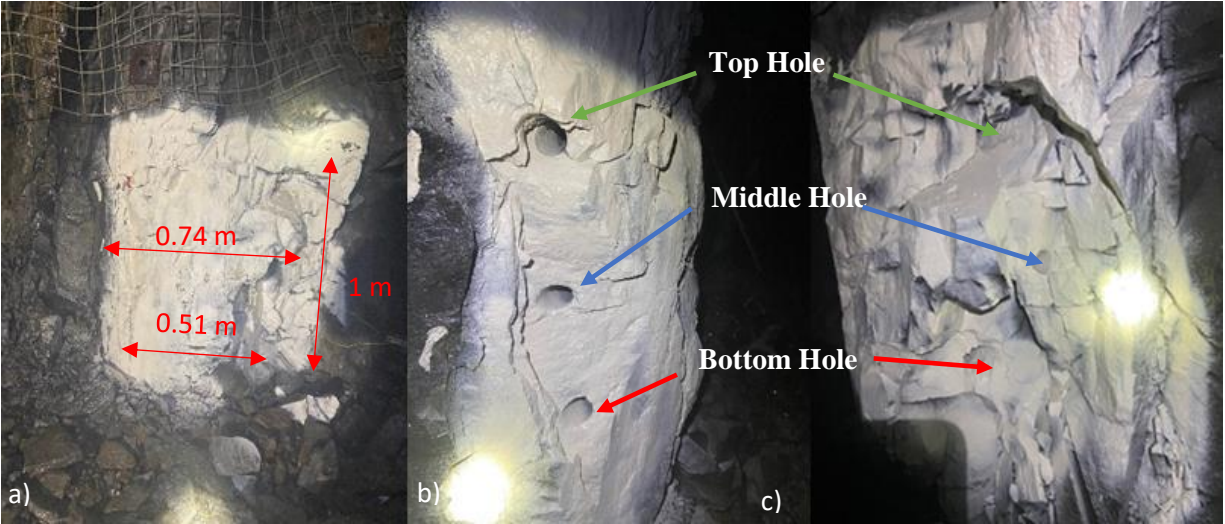
Figure 7.6 Slash Test #1 at Éléonore Mine Site



Figure 7.7 Rock temperature of Slash #1

7.2.2.2 Slash Test 2

The dimensions of the second slash test performed at Eléonore mine site are 1 m (39'') x 0.25-0.3 m (10-12'') x 0.51 to 0.74 m (20-29'') (height x thickness x length) (Refer to Figure 7.8). As shown in Figure 7.9, the rock was measured to be 13.5°C, similarly to the previous slash test. Due to minimal cracking from Slash 1, an additional SCDA hole is introduced with a spacing of 10-12''. The thickness of the slash is reduced from 14-16'' to 10-12'' to ensure cracking. Three 2'' holes were drilled with hole depth 29'', 20'' and 28'' for top, middle and bottom hole respectively (Refer to Figure 7.8).



a) Front View

b) Left side view

c) Right Side view of 3 SCDA holes

Figure 7.8 Slash Test #2 at Éléonore Mine Site

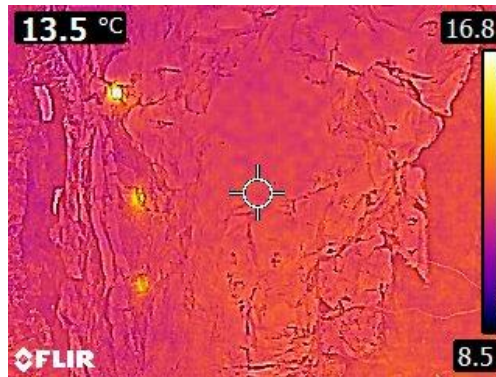


Figure 7.9 Rock Temperature of Slash #2

7.2.3 Loading of SCDA

Commercially available SCDA selected for this study is Betonamit. All SCDA grouts were mixed consistently for 2 minutes with a water to cement ratio of 0.2. For the boulders, the SCDA was directly poured into the borehole by gravity. For the slash tests, a cylindrical plastic cartridge with an O.D of 1.98” was used to horizontally load the SCDA (Refer to Figure 7.10).



Figure 7.10 Plastic Cartridge used for horizontal loading of slash tests

7.2.4 Monitoring Tools

To monitor the time of first crack (TFC), the following tools were used:

- a) A timelapse camera to visually detect the time of cracking
- b) Thermal logger to monitor the heat of hydration of SCDA

Table 7.1 shows a summary of the rock dimensions and rock properties for each test

Table 7. 1 Summary conditions for each test

Test Type	Mine Site Location	Rock Dimensions (inches)			Ambient Temperature (°C)	SCDA Hole Size (inches)	Rock Temperature (°C)	Rock Type	Tensile Strength (MPa)
		h ¹	t ²	l ³					
Boulder 1	Hoyle Pond	39	25	120	8-10	1.75"	13.5	Greywacke	-
Boulder 2	Éléonore	44	37	148	10	2"	12.9	Wacke	15 ^a
Slash 1	Éléonore	39	14-16	33-41	10	2"	12.5	Wacke	15 ^a
Slash 2	Éléonore	39	10-12	20-29	10	2"	13.5	Wacke	15 ^a

1: Height 2: Thickness 3: Length

a: Obtained from the geotechnical report provided by Éléonore Mine.

7.3 Results and Discussion

The TFC, MDT and SCDA heat of hydration are presented for each test.

7.3.1 Boulder Test at Hoyle Pond

The first boulder test was successfully fragmented with TFC of 13 hours and an MDT of 15 hours. As suggested in Chapter 6, the heat of hydration of SCDA in ambient cold temperature increase a few hours before the TFC is detected. The trend is also shown in Figure 7.13 with an increase in temperature at 8 hours, 5 hours before TFC is detected. It can also be seen that the SCDA temperature fluctuates during the testing time; this could be due to the change in temperature from loading (during the day) and testing throughout the night. As can be seen in Figure 7.11, the boulder fractures along the foliations in addition to fractures coalescing between the SCDA holes.



Figure 7.11 Fragmented Boulder at Hoyle Pond

As shown in Figure 7.12, the boulder is fragmented in 12 large pieces after nudged by a forklift.



Figure 7.12 Fragmented Boulder with forklift at Hoyle Pond

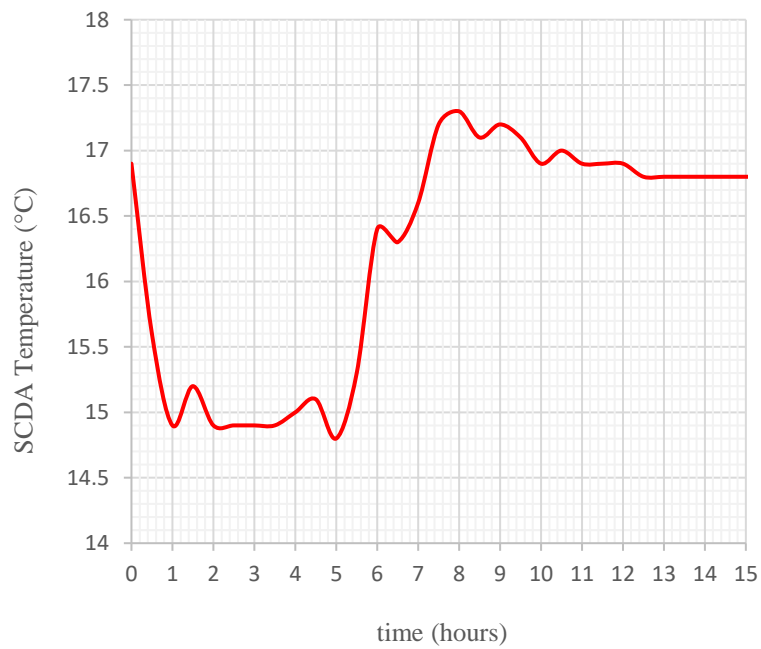


Figure 7.13 SCDA Temperature of SCDA for boulder test at Hoyle Pond

7.3.2 Boulder Test at Éléonore

The second boulder test was also successfully fragmented with TFC of 13 hours and an MDT of 21 hours. The increased time of MDT compared to the previous test may be attributed to the increased spacing of 32'' between SCDA hole in the columns. As shown in Figure 7.15, a peak SCDA temperature of 18°C is detected 9 hours, 4 hours before TFC is detected. Unlike the previous boulder test conducted at Hoyle Pond, the ambient temperature is kept consistent and therefore no significant fluctuation is detected in the evolution of heat of hydration of SCDA. As can be seen in Figure 7.14, the boulder fractures between SCDA holes in the rows (L_f of 12'') and propagate along the columns of SCDA holes (32''). It can also be seen that the fractures propagate all the way to the bottom of the boulder with a fracture length of 44''.

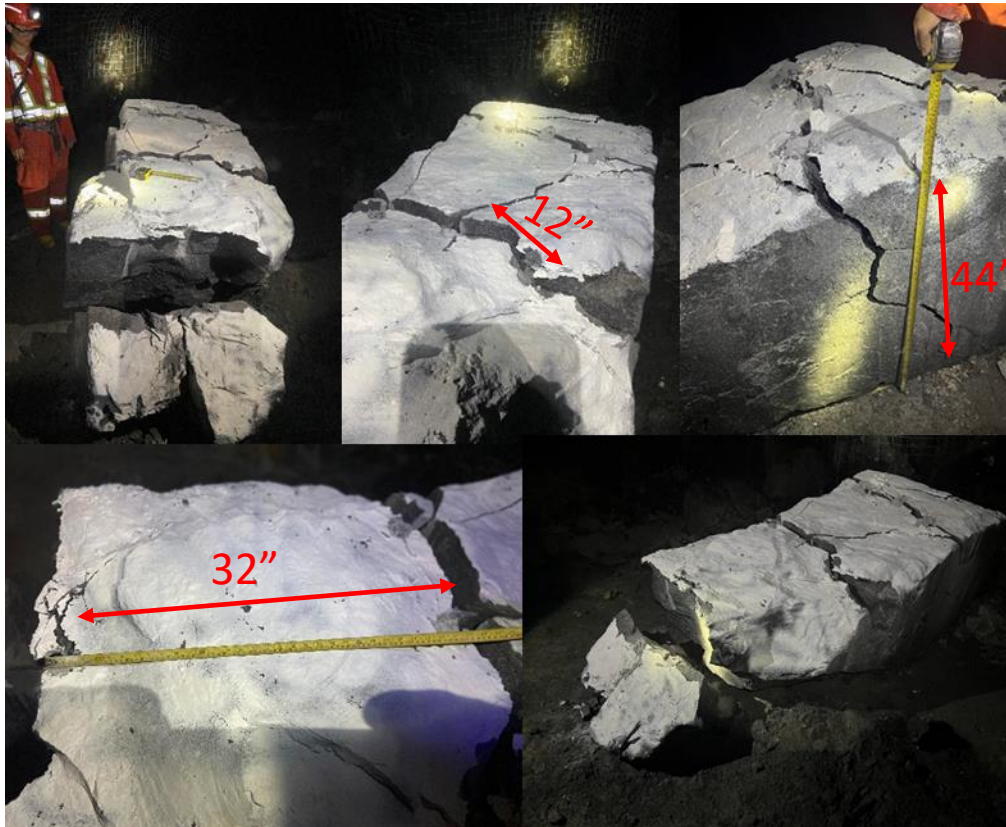


Figure 7.14 Fragmented Boulder at Éléonore

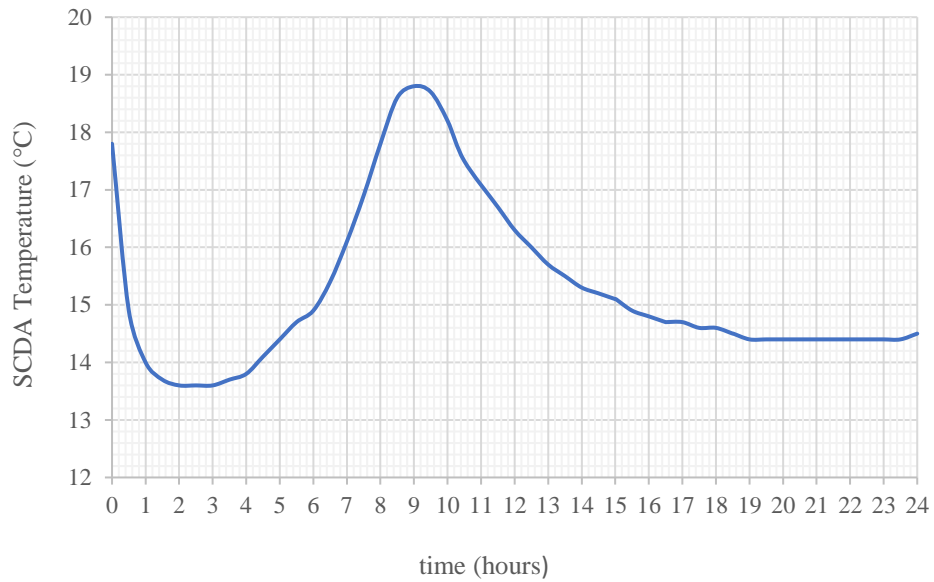


Figure 7.15 SCDA Temperature of SCDA for boulder test at Hoyle Pond

7.3.3 Slash Test #1 at Éléonore

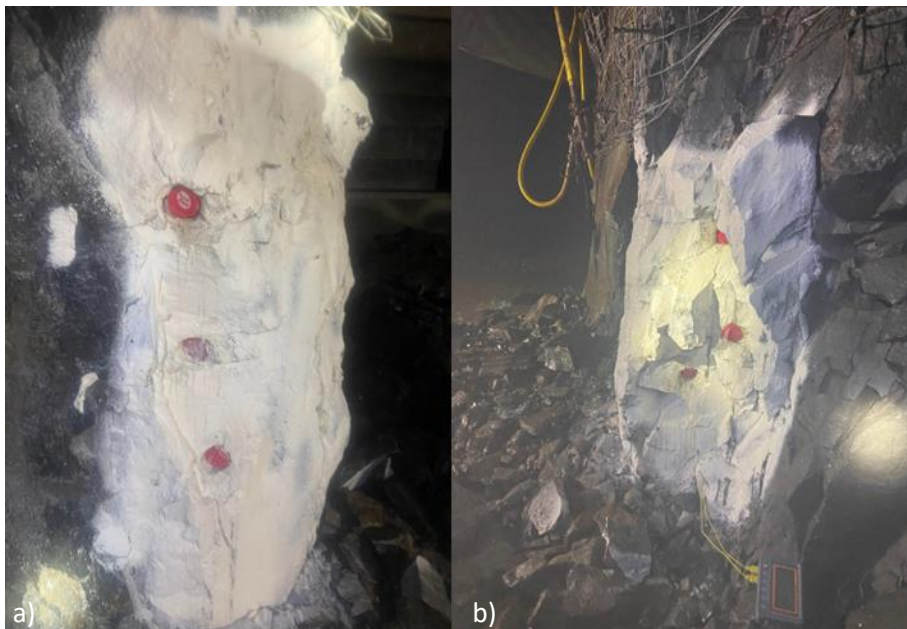
The first slash test was deemed unsuccessful. Only minimal cracking is detected after 48 hours at the bottom holes of the slash with a fracture length of 5- 6’’.



Figure 7.16 Minimal cracking around bottom left hole of Slash #1

7.3.4 Slash Test #2 at Éléonore

Since the previous slash test was unsuccessful with a spacing of 26'' between two SCDA holes, the second slash test introduces a third hole with closer SCDA hole spacing of 10- 12''. Below in Figure 7.17 shows the loaded corner slash with SCDA filled cartridges.



a) Left Side view

b) Right Side

Figure 7.17 Loaded Holes of Slash #2

Slash #2 was deemed successful with a visual TFC of 17 hours and MDT of 22 hours. As shown in Figure 7.17, cracking coalesces between SCDA holes vertically in the direction of the major directional stress. The same visual trend is observed to the small-scale test of granite samples subjected to 5 MPa of vertical stress in Chapter 4. A peak SCDA temperature is detected at 7.5 hours which indicate that cracking could have occurred earlier and could not be detected with the time-lapse camera. However, significant cracking in this case is of interest. As shown in Figure 7.18, the crack length between SCDA holes range 10 to 12". Although cracking is observed, it was not sufficient to remove the face. Using a scale bar, the slash corner was scaled 25-30 cm (10-12") deep into the face (Refer to Figure 7.20 for before and after scaling).



Figure 7.18 Cracking Coalescing between SCDA holes of Slash #2

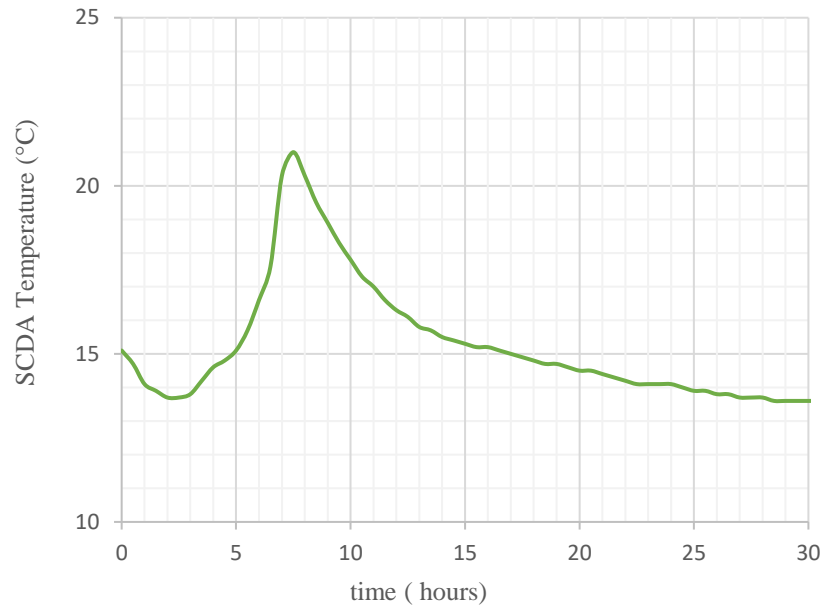


Fig 7.19 SCDA Temperature of SCDA for Slash #2



a) Before scaling

b) After scaling

Figure 7.20 Front View of Slash #2

7.4 Summary of Test Results

Table 7.2 provides a summary of the TFC and MDT for both the boulder and slash test. As can be seen, both boulders were successfully fragmented in similar times. However, more time is observed in the MDT of Boulder 2 as it was larger than Boulder 1. Slash 1 was deemed unsuccessful with minimal cracking after 48 hours, which may be attributed to too large of a spacing between holes. Slash 2 fragmented successfully with the introduction of an additional SCDA hole with closer spacing between SCDA holes.

Table 7.2 Summary of Test Results

Test	TFC (hours)	MDT (hours)
Boulder 1	13	15
Boulder 2	13	17
Slash 1	NA	NA
Slash 2	17	22

7.5 Conclusions

In this chapter, the results of a 4 field tests are reported to assess the effectiveness of SCDA to fragment large boulders and to excavate intersections (slashing). The dimensions of the first boulder (Greywacke) at Hoyle Pond mine site are 1 m (39'') x 0.64 m (25'') x 3 m (120'') (height x thickness x length). The boulder successfully fragmented with a TFC of 13 hours and MDT of 17 hours with an SCDA hole spacing of 8''. The dimensions of the second boulder performed at Eléonore mine site are 1.12 m (44'') x 0.94 m (37'') x 3.8 m (148'') (height x thickness x length). The boulder fragmented at similar times to the previous boulder with a TFC of 13 hours and MDT of 17 hours. The additional 2 hours to fully fragment the rock could be attributed to the larger spacing (12'' between SCDA holes in the rows and 32'' between SCDA holes in columns). The dimensions of the first slash test performed at Eléonore mine site are 1 m (39'') x 0.36-0.41 m

(14-16'') x 0.83 to 1.04 m (33-41'') (height x thickness x length). The first slash was unsuccessful with only minimal cracking after 48 hours. This could be due to large spacing between holes (26'') as well to large thickness of the rock (14-16''), which was not possible to test in laboratory. A second slash is done but by reducing the hole spacing to 10-12'' and reducing the thickness to 10-12''. The dimensions of the second test performed at Eléonore mine site are 1 m (39'') x 0.25-0.3 m (10-12'') x 0.51 to 0.74 m (20-29'') (height x thickness x length). The second slash test was deemed successful with a TFC 17 hours and MDT of 22 hours. Future work would involve more modeling work to estimate the spacing between SCDA holes in uniaxial conditions to take into account the thickness and length of the intersection. The field results from this investigation have demonstrated that the use of SCDA in underground mines to break boulders and slash the wall rock is feasible – with fragmentation results in less than 24 hours.

Chapter 8: Conclusions

8.1 Research Summary

The method of drilling and blasting with explosives is widely used in rock fragmentation applications in mining and civil industries for mine development, mining production, and underground construction such as tunnels and shafts. However, the use of explosives is associated with rigorous safety and environmental constraints as blasting creates toxic fumes, ground vibrations and dust. Due to these factors, there is a growing interest in transitioning from explosives-based rock fragmentation to methods without explosives, e.g., with Soundless, Explosive-Free Chemical Demolitions Agents. This thesis is part of a multi-phase project which aims to develop a sound methodology for rock fragmentation in underground mines. More specifically, it is the first phase of the project which focuses on laboratory tests to investigate and optimize the mechanical performance of SCDA in various conditions:

- A thorough critical review is conducted in Chapter 2 on various methods developed for rock fragmentation without explosives. Such methods include Thermal Fragmentation, Plasma Blasting, Controlled Foam Injection, Radial-Axial splitter, and Supercritical carbon dioxide. Each method has its advantages while also having its own limitations. Thermal fragmentation targets the extraction of narrow vein deposit; however, excessive heat is generated requiring additional ventilation. Plasma blasting has yet to be implemented but may only be limited to subsurface applications. The controlled foam injection technology is claimed to be environmentally friendly; however, the method is of dynamic nature which may result in flyrock and air blast. The radial-axial splitters are mechanical tools and

considered environmentally friendly but require a significant number of splitters to excavate a single mining face.

- The method of SCDA is then evaluated in detail and its merits over other methods. The use of SCDA has been explored by many researchers in the aim of optimizing its performance and possibly implementing the use of SCDA for applications other than the subsurface applications. Early literature focuses on optimizing the fragmentation of hard rock and concrete for surface applications and reports optimal hole patterns and spacing based on laboratory experiments under no loading conditions. More recently, there has been a renewed interest in the implementation of SCDA to other applications where high in-situ stress prevails such as its use in rock weakening in coal mines and for in-situ leaching. Current research is now dedicated to modelling crack patterns under different loading conditions with numerical modelling. Based on a thorough literature review on SCDA, the merits of SCDA are summarized as follows:

- (1) Reduced zone of influence around the tunnel excavation, thus having the potential to be implemented in shallow overburden projects near sensitive buildings and infrastructure
- (2) Reduced potential for ground water leakage
- (3) Noise reduction/elimination
- (4) Reduced occurrence of overbreak and strata collapse
- (5) Little or no nuisance to residents in the vicinity of the project.

From a practical perspective, it is shown that the proposed SCDA method has the most potential to become a viable alternative to blasting with explosives in underground mine drift advance applications. Such merits draw a high interest to many researchers to further

explore the use of SCDA in an underground setting. To validate such method for large-scale hard rock fragmentation in underground mines, some parameters were investigated and tested on the field.

- In Chapter 3, the expansive pressure generation of SCDA is quantified in different host conditions. The goal of this study was to better understand SCDA performance in hard rock. To do so, a classical analytical method for expansive pressure estimation in a thick-walled cylinder was used to estimate the expansive pressure with varying host medium rigidity- an aspect that has often been overlooked by previous research. By keeping the rigidity constant, the effect of borehole size is investigated for SCDA hole size of 25.4 mm (1”), 31.75 mm (1.25”), and 31.8mm (1.5”). The results show that the estimated peak expansive pressure is proportional with the borehole diameter. The 38.1 mm (1.5”) borehole exhibits a maximum pressure up of 60 MPa in only 6 hours and the 31.75 mm (1.25”) borehole shows a lower pressure 39.2 MPa in 6 hours but reaches a similar average maximum pressure of 55.4 MPa at 24 hours similar to the pressure of the 1.5” borehole at 24 hours exhibiting an ultimate pressure of 60 MPa. Specimen S-C-100-175-W exhibits a lower pressure of 16.9 MPa and 43 MPa in 6 hours and 24 hours respectively

It is also shown that when the host medium rigidity is increased, the estimated expansive pressure is reduced significantly. A high host rigidity of 13680000 MPa (S-C-150-420-S) generates significantly less pressure than a low rigidity host of 472222 MPa (S-C-150-275-S) at 24 hours which generated expansive pressures of 29.7MPa and 60 MPa respectively while a medium host rigidity of 1008889 MPa (S-C-150-340-S) generated pressures of 43.6 MPa.

- The practical implication of this finding is that the expansive SCDA peak pressure in hard rocks such as gabbro and norite (higher rigidity) commonly encountered in metal mines is likely to be less than that in sedimentary rocks such as limestone and mudstone (lower rigidity) commonly found in coal mines. The pressure obtained from the classical analytical method was also validated with direct measured of actual internal pressure. A series of tests employing direct pressure measurement using high-capacity pressure sensor was carried out while also monitoring the SCDA heat of hydration. The heat of hydration produced during the SCDA reaction was also measured throughout the testing period using thermocouples embedded in the SCDA. The results shows that a peak hydration heat of 50.8 °C was recorded at 5 hours for specimen with an I.D of 38.1 mm (1.5'') while a peak hydration of 39.9°C and 40.1°C was recorded at 5 hours for specimen with an I.D 25.4 mm (1.00'') and 31.75mm (1.25'') respectively. Based on the experimental results, higher heat generation corresponds to higher SCDA expansive pressure which is owed to the increased mass of SCDA relative to the surface area on which pressure is applied and through which heat is exchanged with the host medium. Using the high-capacity pressures sensors, pressures of 8 MPa, 55 MPa and 65 MPa are achieved in 6 hours for specimen S-C-100-175-W, S-C-125-210-S and S-C-150-275-S respectively (It is also shown that pressures of 56 MPa, 71 MPa and 83 MPa are achieved in 24 hours for specimen S-C-100-175-W, S-C-125-210-S and S-C-150-275-S respectively. The results show that the actual expansive peak pressure is consistently higher than the estimated peak pressure from the analytical model. A correction factor of α : 1.31 with $R^2 = 0.999$ is obtained. Finally, a new methodology based on iterative procedure was developed using axisymmetric finite element modelling and test results to derive the SCDA modulus of elasticity. Recognizing

the variation of pressure and elasticity with time, the focus is on the peak pressure and hence the peak modulus of elasticity. The methodology reveals that the modulus of elasticity of expansive cement at peak pressure is on average 8.2 GPa with a coefficient of variation of only 0.012. This result should prove useful in numerical modelling studies of SCDA hole pattern design in practical mining applications.

Since steel is highly conductive compared to rock, it is of critical importance to estimate the pressure in real conditions such as in rock where a much higher heat sink is present.

- In Chapter 4, the effect of SCDA is investigated in hard rock. The goal of the study was to perform a series of experiments on granite slabs (152.4 mm (6'') x 152.4 mm- 203.2 mm (6-8'') x 406.4 mm (16'')) with a single SCDA hole under load and no load to retrieve raw strain measurements up until fracture for future work and to be used as a basis of calibration. The influence of borehole size (25.4 mm (1''), 31.75 mm (1.25''), and 31.8 mm (1.5''), the same hole size tested in steel cylinder in Chapter 3, on the fracture time is investigated. It is shown that fracturing time decreases with increasing borehole size. The time of initial fracturing for a 38.1 mm (1.5'') borehole size is half of that of a 1'' filled SCDA hole. Moreover, the measured strains for all specimens increase exponentially at some point in time, and this exponential behavior is interpreted as tensile damage progression in the slab. The results demonstrate that strain measurement is a reliable tool for fracture initiation when this fracture initiation could not be detected visually. Another series of tests were performed to verify the influence of a uniaxial pressure of 5 MPa on the slab fracturing with SCDA. This goal of this part of study was to estimate the spacing of SCDA hole in uniaxial practical conditions. To do so, three tests with a single SCDA hole at 3 different locations were tested: 38.1 mm (1.5'') borehole size in the upper third

of the slab (G-SL2-150-600-UT-L), 1.75'' in the middle of the slab (G-SL2-175-700-M-L) and 1.75'' in the lower third of the slab (G-SL2-175-700-LT-L). SCDA expansion-initiated fracturing occurred as early as 7 hours for all tests. Specimens SL2-150-600-UT-L and G-SL2-175-700-M-L split after 10 hours, whereas specimen G-SL2-175-LT-L split after 12 hours. The effect of boundary conditions is also investigated by applying grease, MoS₂ at the top of granite slab only. It was shown that initial cracking propagates towards the greased end or the nearest boundary. Based on the experimental results, the fracture length to borehole diameter ratio L/Φ , was calculated to estimate the maximum allowable spacing between SCDA holes subjected to uniaxial stress. As each SCDA can generate a fracture length L_f , the spacing, S , between two SCDA holes is calculated as $S=2L_f/\Phi$. It is suggested that the spacing between SCDA boreholes be 12.8-14.6 Φ for practical applications involving uniaxial compression. Such higher borehole spacing suggestion for loaded samples than the 8 Φ for unloaded sample suggested by Gomez & Mura (1984) implied that uniaxial loading is beneficial for hard breakage with SCDA.

- However, due to the limited size of the tested blocks, it was not possible to delineate the full fracture length that would be generated under uniaxial loading condition in the field. In Chapter 5, the experimental results obtained in the previous chapter are used to develop and calibrate a numerical model in Abaqus using XFEM. The XFEM model is used to simulate crack propagation to its full natural limit and based on the calibrated model results, a new spacing between SCDA holes under uniaxial conditions is proposed.

- A higher borehole spacing is suggested from the numerical modeling compared to the loaded samples in Chapter 4 with a L_f/Φ of 17.1-22.2 Φ ; however, the lower ratio is attributable to the size limitation of the sample which could not account for further crack

propagation. A separate experiment is then conducted to determine the effect of hole shielding using the same instrumentation and modelling scheme. A comparison between a single SCDA hole specimen with a single SCDA hole with two shield holes specimens is assessed. Based on the experimental results, it was shown that the introduction of relief holes increased the MDT.

- Following the same modeling scheme as the single SCDA injected hole, it was found that the initialized SCDA stress ranges between 36 MPa and 39.5 MPa. It was also found that slabs are harder to split overall with the introduction of relief holes of 38.1 mm (1.5") and 50.8 mm (2") above and below a 25.4 mm (1") SCDA filled hole. Higher initialized SCDA stresses of 128-131 MPa are needed to split the slab with relief holes compared to an initialized SCDA stress of 85 MPa required to split a slab without the introduction of relief holes. These results indicate that the presence of relief holes in the direction of the major principal stress does not benefit crack propagation and in fact impedes faster crack growth. Based on both experimental and simulation results, the relief holes create a stress shadow which encompasses the SCDA hole.

- Another step in assessing the performance of SCDA in underground mines is investigating its effect under different ambient conditions such as high humidity and low to high temperatures to simulate a range of possible conditions in underground mines. In Chapter 6, a series of granite cubes of 152.4 mm x 152.4 mm x 203.2mm (6" x 6" x 8") with a single 38.1 mm (1.5") SCDA are placed in a controlled test chamber (Microclimate benchtop chamber, Model #: MCB (H)-1.2) and subjected to various humidity levels (30% 70%, 90%), hot conditions (30°C, 40°C) and cold conditions (-5°C, 5°C, 20°C). The TFC and MDT were determined with the use of 3 tools; strain measurements which were proven

to be a reliable indicator to detect time of fracturing in Chapter 4, a thermal logger to monitor the heat of hydration of SCDA and a thermal imager to periodically take photos during the testing period. It was shown that fracturing time decreases with increasing ambient temperature size. The TFC for a sample subjected to a cold temperature of -5° is 39 hours, compared to a sample subjected to room temperature of 25°C , which exhibits a TFC of 4.5 hours. It was also observed that the heat of hydration of SCDA over time behaves differently in different conditions. Samples subjected to colder temperatures such as -5°C , 5°C , and 10°C , show three peaks in SCDA temperature; one near the beginning of the test, one before the TFC is visually detected and one when the MDT is reached. The highest peak in temperature, however, is shown to be when the sample reaches its MDT. In warmer conditions, starting from 20°C , the evolution of the SCDA heat of hydration increases concurrently with the measured strains only one peak of hydration is detected shortly before the TFC is visually detected. Along with the strain measurements, which were already proven in Chapter 5 to be a reliable tool to detect the start of cracking, the SCDA heat of hydration can also be used as an indicator to detect the time of cracking in the cases where the fracture cannot be detected visually.

The long-term objective of this research program is to validate the use of SCDA for large-scale hard rock fragmentation in underground mines. The following summarizes the results obtained from real mining applications.

- Finally in Chapter 7, field tests were conducted at two mine sites: Hoyle Pond and Éléonore mine site. The goal of these tests was to assess SCDA effectiveness in real mining applications. The first set of tests included the fragmentation of large boulders with a series of SCDA holes while the second set of tests involve the excavation intersections (slashing).

The fragmentation of boulders with SCDA could be used to reduce the fragment size to enable mucking with a loader, whereas slashing with SCDA could be used at intersections to remove the underbreak to enable better traffic. The results of a 4 field tests are reported to assess the effectiveness of SCDA to fragment large boulders and to excavate intersections (slashing). 4 tests in total are reported: 2 large boulder and 2 slash tests. The dimensions of the first boulder (Greywacke) on surface Hoyle Pond mine site are 1 m (39'') x 0.64 m (25'') x 3 m (120'') (height x thickness x length). The boulder was subjected to 13.5°C indicating that a longer TFC would be detected as suggested in Chapter 6. Therefore a slight modification to the 8Φ is suggested by (Gomez & Mura ,1984) and is reduced to 4.5Φ to ensure a sufficient TFC. The boulder successfully fragmented with a TFC of 13 hours and MDT of 17 hours with an SCDA hole spacing of 8''. The dimensions of the second boulder performed at underground (Level 530) Eléonore mine site are 1.12 m (44'') x 0.94 m (37'') x 3.8 m (148'') (height x thickness x length). The boulder was subjected to similar cold conditions to the boulder performed at Hoyle Pond. However, based on the successful results of the previous boulder, the spacing between holes are increased between the SCDA holes in the rows (12'') and (32'') between the SCDA holes between the columns. The boulder fragmented at similar times to the previous boulder with a TFC of 13 hours and MDT of 17 hours. The additional 2 hours to fully fragment the rock could be attributed to the larger spacing (12'' between SCDA holes in the rows and 32'' between SCDA holes in columns). The dimensions of the first slash test performed at Eléonore mine site (Level 530) are 1 m (39'') x 0.36-0.41 m (14-16'') x 0.83 to 1.04 m (33-41'') (height x thickness x length). The first slash was unsuccessful with only minimal cracking after 48 hours. This could be due to large spacing between holes (26'') as well to

large thickness of the rock (14-16’), which was not possible to test in laboratory. A second slash is done but by reducing the hole spacing to 10-12’ and reducing the thickness to 10-12’ of the rock corner. The dimensions of the second test performed at Eléonore mine site (Level 530) are 1 m (39’’) x 0.25- 0.3 m (10-12’’) x 0.51 to 0.74 m (20-29’’) (height x thickness x length). The second slash test was deemed successful with a TFC 17 hours and MDT of 22 hours. The field results from this investigation have demonstrated that the use of SCDA in underground mines to break boulders and slash the wall rock is feasible – with fragmentation results in less than 24 hours.

Furthermore, the research undertaken in this thesis has prompted several research topics that could be further explored in future studies. The following is a list of suggestions for future research to expand on the work done in this study.

- This study employed prismatic rock specimens with limited dimensions up to 400 mm (16 inches). Testing the behaviour of SCDA with larger block size would help better understand the performance of SCDA in the rockmass.
- This study examined the mechanical performance of SCDA under uniaxial loading conditions and demonstrated its application at an underground mine. Future research could focus on the SCDA behaviour under biaxial loading conditions.
- This study reported on the SCDA performance for the breakage of underground mine boulders and in slashing applications. It would be interesting to investigate the use of SCDA for complete mining face advance such as a drift or ramp development.
- One possible mining application of SCDA is to break oversize blocks from large production blasts in surface mining operations. However, most Canadian surface mining operations are found in northern locations where the ambient temperature is below freezing

point most of the year. This could negatively impact the performance of SCDA. It would be interesting to explore how the SCDA performance could be enhanced in cold climate.

- While premature at this stage of the research, it would be useful to eventually carry out an economic evaluation of the SCDA method and compare it with the traditional drilling and blasting method.

8.2 Research Conclusions

The following conclusions can be drawn from the work reported in this thesis.

- A state-of-the-art literature review has revealed that SCDA has the greatest potential over other explosive-free-methods for practical applications of hard rock breakage.
- The thick-walled cylinder method for testing SCDA pressure has shown that while the generated pressure increases with the borehole diameter, larger host medium rigidity reduced the SCDA pressure.
- An axisymmetric FE model is developed and validated to predict SCDA pressure for a given cylinder geometry.
- Granite specimens with a single SCDA hole show that the TFC and MDT occur earlier when larger SCDA hole is employed and when the hole is closer to the greased end of the specimen.
- When the rock specimen is subjected to uniaxial stress of 5 MPa, fragmentation occurs earlier in terms of TFC and MDT.
- An XFEM model is developed and validated with experimental results under uniaxial load. It is then used to predict the longest possible fracture length in an infinite

medium. The optimum spacing between SCDA holes $L_F/\Phi = 17.1-22.2$ under uniaxial stress.

- The SCDA heat of hydration is dependent on the ambient temperature and its peak temperature serves as an indicator of significant cracking
- Granite specimens subjected to various temperature conditions show varying time of fracture (TFC and MDT significantly increases with decreasing temperature)
- Successful field tests were conducted on the fragmentation of boulders and excavation intersection of an intersection (slashing)

8.3 Contribution to original knowledge

This research has contributed to advancing the application of SCDA for rock fragmentation in hard rock mines. It has proven SCDA to be a feasible method for rock breakage in underground mines for both boulders and slashing applications. This work will set the stage to further develop the application of SCDA in hard rock mines. The specific contributions are:

- Provided a new and systematic methodological approach for the investigation of SCDA pressure evolution and the influence of borehole diameter and host medium rigidity.
- Conducted an extensive laboratory investigation into fracture initiation and propagation in Stanstead granite prismatic specimens due to SCDA while monitoring the time to first crack (TFC) and minimum demolition time (MDT).
- Examined the influence of uniaxial field stress on the performance of SCDA in terms of TFC and MDT.

- Developed and validated an XFEM model to establish the optimum spacing between SCDA holes in practical applications.
- Revealed the effect of temperature and humidity on the mechanical performance of SCDA with a view of application to underground mining.
- Successfully demonstrated the application of SCDA to two mining applications namely boulder fragmentation and slashing of excavation intersection.

References

- Arshadnejad S, Goshtasbi K, Aghazadeh J. A model to determine hole spacing in the rock fracture process by non-explosive expansion material. *Int J Miner Metall Mater* 18:509–514, 2011.
- Bentur A, Ish-Shalom M. Properties of type K expansive cement of pure components II. Proposed mechanism of ettringite formation and expansion in unrestrained paste of pure expansive component. *Cement and Concrete Research*, 4(5), 709–721, 1974.
- Cohen M.D. Modeling of expansive cements. *Cement and Concrete Research*, 13(4), 519–528, 1983.
- De Silva VR, Ranjith PG, Perera MS, Wu B. Artificial fracture stimulation of rock subjected to large isotropic confining stresses in saline environments: application in deep-sea gas hydrate recovery. *Natural resources research*. Apr;28(2):563-83.2019.
- Gambatese J.A. Controlled concrete demolition using expansive cracking agents. *J. Constr. Eng. Manag* 129,98-104, 2003.
- Habib K. M, Shnorhokian S, Mitri H. Evaluating the Application of Rock Breakage without Explosives in Underground Construction—A Critical Review of Chemical Demolition Agents. *Minerals*, 12(2), 220, 2022.
- Hanif M. Deformation Behaviour of Rock around a Borehole Filled with an Expansive Cement, *J. King Abdulaziz Univ. Sci.* 9. 93–107, 1997.
- Hanif M. Effective Use of Expansive Cement for the Deformation and Fracturing of Granite. *Gazi Univ J Sci* 20:1–5, 2010.

Harada T, Idemitsu T, Watanabe A, Takayama S. The Design Method for the Demolition of Concrete with Expansive Demolition Agents. In: Shah S.P., Swartz S.E. (eds) *Fracture of Concrete and Rock*. Springer, New York, NY, 1989, 47-57, 1989.

Hinze J, Brown J. Properties of Soundless Chemical Demolition Agents, *Constr. Eng. Manag.* 120 816–82,1994.

Laefer D.F, Ambrozevitch-Cooper N, Huynh M.P, Midgette J, Ceribasi S, Wortman J. Expansive fracture agent behaviour for concrete cracking, *Mag. Concr. Res.* 62 443–452,2010.

Silva RV D, Vidanage R, Pathegama Gamage R, Anne Perera MS. An alternative to conventional rock fragmentation methods using SCDA: a review. *Energies* 9.11: 958, 2016.

Silva RV D, Ranjith P.G, Perera M.S, Wu B, Wanniarachchi W,A. A low energy rock fragmentation technique for in-situ leaching. *Journal of Cleaner Production.* 2018a; 204:586-606.

Silva VR D, PG Ranjith, Perera MS, Wu B, Rathnaweera TD. A modified, hydrophobic soundless cracking demolition agent for non-explosive demolition and fracturing applications. *Process Safety and Environmental Protection.* Oct 1; 119:1-3, 2018b

Soeda HK. Fast-Acting Non-Explosive Demolition Agent, *Conf. Demolition Reuse Concr.* 231–241, 1994.

Tang S.B, Huang R.Q, Wang S.Y, Bao C.Y, Tang C.A. Study of the fracture process in heterogeneous materials around boreholes filled with expansion cement. *Int. J. Solids. Struct.* 112, 1–15, 2017.

Tang W, Zhai C, Xu J, Sun Y, Cong Y, Zheng Y. The influence of borehole arrangements of soundless cracking demolition agents (SCDAs) on weakening the hard rock. *Int. J. Min. Sci. Technol.* 31, 197–207, 2021.

Wang L, Duan K, Zhang Q, Li X, Jiang R. Study of the Dynamic Fracturing Process and Stress Shadowing Effect in Granite Sample with Two Holes Based on SCDA Fracturing Method. *Rock Mechanics and Rock Engineering.* 2022 Mar;55(3):1537-53.

Wang S, Mitri H, Li H, Li D, Wang Study of SCA-induced rock crack propagation under different stress conditions using a modified cohesive element method. *Advances in Civil Engineering*, 2018.

Zhai C, Xu J, Liu S, Qin L. Fracturing mechanism of coal-like rock specimens under the effect of non-explosive expansion. *International Journal of Rock Mechanics and Mining Sciences*, 103(February), 145–154, 2018.